Department of Civil Engineering DTU

Ane Mette Kjeldsen

Consolidation behavior of cement-based systems

Influence of inter-particle forces

PHD THESIS

BYG • DTU

Consolidation behavior of cement-based systems

Influence of inter-particle forces

Ane Mette Kjeldsen

Ph.D. Thesis

Department of Civil Engineering
Technical University of Denmark

2007

Consolidation behavior of cement-based systems
Influence of inter-particle forces

Printed by Eurographic A/S
Department of Civil Engineering
Technical University of Denmark
ISBN 97-8877-8772-077
ISSN 1601-2917

Preface

This thesis is submitted as a partial fulfilment of the requirements for the Danish Ph.d. degree. The thesis is divided into two parts. The first part introduces motivation and aim of the research. Furthermore, the main findings and conclusions of the research are presented here. The second part is a collection of five papers, reporting the research in more detail.

Acknowledgements

I would like to thank the following persons:

My main supervisor, Assoc. Prof. Mette Geiker for her support throughout the project, as well as my co-supervisors Professor Henrik Stang and Assoc. Prof. Kurt K. Hansen.

Dr. Lennart Bergström, Institute for Surface Chemistry (YKI) (now Stockholm University, Sweden) for the great amount of time and effort he spent to make my stay at YKI as professionally rewarding as it was.

Dr. Robert J. Flatt (SIKA technology, Switzerland) for his many invaluable inputs, suggestions and comments to the project.

All the people at YKI who assisted and helped me during my research stay, in particular Ph.d. Annika Kauppi (now at Sandvik Tooling, Sweden).

The project has benefitted greatly from results from the EC-financed research project "Design and function of novel polymeric admixtures for more durable high performance concrete". In this connection, the partners of the project are thanked for their readiness to help with providing materials and sharing information.

Abstract

The microstructure of concrete is of paramount importance for almost all performance aspects of the material. Therefore, the ability to model both initial and hydrated microstructure is a key to the subsequent understanding and prediction of many macroscopic properties of the material. Correct modelling of the initial microstructure requires knowledge of, among others, the forces acting on the constituent particles. In the hydrated state, the pore structure of a cement-based material is often assessed experimentally. However, the present methods are in no way perfect and there is a need for a robust method where both advantageous and drawbacks are well described. This thesis comprises theoretical and experimental investigations of the effect of inter-particle forces on the consolidation behavior of fresh cement-based materials. Furthermore, the basis for interpretation of results obtained through an experimental method for pore structure characterization is assessed.

A model material with surface properties similar to those of cement, magnesium oxide (MgO), was initially used to quantify inter-particle force changes by addition of different superplasticizers. The experiments were carried out by means of centrifugal consolidation and packing density profiles were obtained. Inter-particle forces were modified by the addition of different anionic comb-type superplasticizers in full surface coverage dosages. One of the superplasticizers was added in varying dosages to obtain sub-surface coverage. It was found that an increased length of the side chains of the adsorbed superplasticizers reduces the inter-particle bond strength and thus the yield stress, and results in an increased packing density. A relation between side chain length and inter-particle bond strength was determined. Furthermore, a linear relation was found between the obtained packing density of the centrifuged suspensions and the sub-surface coverage at low dosage. A quantitative link between the molecular structure and resulting adsorption thickness of the superplasticizers and the compression rheology behavior was established.

Following the quantification of inter-particle forces with a model material, combinations of cement and silica fume were investigated. The relevance of the forces acting on and between cement particles of 10 μm and silica fume particle of 100 nm, was evaluated and it was shown that the surface properties of silica fume particles in a cement-based suspension should be able to keep them from agglomerating with each other. It was also shown that cement-silica fume agglomeration occurs but may be resisted by the addition of a superplasticizer. The size and surface properties of cement may cause cement-cement agglomeration, the extend of which may be reduced by superplasticizer addition. Based on the inter-particle force calculations and considerations on geometrical packing, con-

ceptual packing and pore size models were proposed. The validity of the models was investigated experimentally by compressive consolidation experiments. The employed consolidation equipment enabled the simultaneous determination of flow through the material and obtained packing density. By modelling the consolidation process and using the Hagen-Poiseuille equation, a characteristic mean pore diameter was established for each of the studied systems. This approach enables the determination of initial permeability of cement-based systems. Experimental results verified the proposed conceptual packing model. The pore size model overall correlated with experiments, although some deviation was observed.

Assessment of the pore structure in a hardened cement-based material may be carried out experimentally. In this thesis, the basis for interpretation of results from the experimental technique, Low Temperature Calorimetry (LTC), was assessed in order to determine the possibilities and limitations of using LTC for characterization of the porosity of cement-based materials. Supercooling, general lack of equilibrium, bottle neck pores, and ions being expelled during freezing, were treated theoretically and evaluated experimentally using model materials. It was found that the measured temperature should be corrected for non-equilibrium between the sample and the reference block. Furthermore, corrections should be made for the effect on the freezing point depression of the varying ion concentration in the non-frozen part of the pore solution. Making use of the knowledge from the obtained results, it was proposed that LTC may be used for characterization of pore connectivity as well as pore size distribution.

Resumé

Betons mikrostruktur har stor indflydelse på næsten alle aspekter af materialets ydeevne. Derfor er evnen til at modellere både den initielle og den hydratiserede mikrostruktur nøglen til forståelse og forudsigelse af mange makroskopiske materialeegenskaber. En korrekt modellering af den initielle mikrostruktur kræver bl.a. kendskab til de kræfter der virker på partiklerne. I det hydratiserede materiale bliver porestrukturen ofte vurderet eksperimentelt. De eksisterende metoder er dog langt fra perfekte og der er behov for en solid metode, hvor både fordele og ulember er vel beskrevne. Denne afhandling indeholder teoretiske såvel som eksperimentelle undersøgelser af effekten af interpartikelkræfter på konsolideringsopførslen af friske cementbaserede materialer. Derudover er baggrunden for tolkning af resultater fra en eksperimentel metode til karakterisering af porestruktur, blevet vurderet.

Til at starte med blev et modelmateriale med overfladeegenskaber magen til cement, magnesium oxid (MgO), benyttet til at kvantificere ændringer i interpartikelkræfter. Dette blev gjort ved tilsætning af forskellige superplastificeringsstoffer. Eksperimenterne blev udført v.h.a. centrifugalkonsolidering af suspensioner og pakningsdensitet blev bestemt. Interpartikelkræfterne blev modificeret ved tilsætning af forskellige anioniske kam-formede superplastificeringsstoffer. Superplasten blev tilsat i mængder der sikrede fuld overfladedækning af partiklerne. Én af superplasterne blev tilsat i varierende doser, for at opnå delvis overfladedækning. Det blev fundet, at en øget længde af siderkæderne i den absorberede superplast, reducerer bindingsstyrken mellem partiklerne og dermed flydespændingen og resulterer i en øget pakningsdensitet. Der blev fundet en relation mellem længden af superplastens sidekæder og bindingsstyrken mellem partiklerne. Derudover blev der fundet en lineær relation mellem opnået pakningsdensitet og den absorberede superplasts overfladedækning ved lave doser. Der blev ydermere bestemt en kvantitativ forbindelse mellem molekylstrukturen af superplasten og suspensionernes rheologiske opførsel.

Efter kvantificeringen af interpartikelkræfter med modelmaterialet, blev kombinationer af cement og mikrosilika undersøgt. De relevante kræfter der påvirker cementpartikler på 10 μm og mikrosilikapartikler på 100 nm blev evalueret. Det blev vist at mikrosilikas overfladeegenskaber i en cementbaseret suspension skulle være i stand til at holde partiklerne dispergeret. Det blev også vist, at der sker agglomerering mellem cement og mikrosilika, men at denne agglomerering kan modvirkes ved tilsætning af en superplast. Cementpartiklernes størrelse og overfladeegenskaber kan give cement-cement agglomerering, men denne kan reduceres ved superplasttilsætning. Konceptuelle modeller for pakning og por-

estørrelse blev foreslået på basis af beregninger af interpartikelkræfter og overvejelser af geometrisk pakning. Gyldigheden af modellerne blev undersøgt eksperimentelt v.h.a. trykkonsolideringsforsøg. Det benyttede konsolideringsudstyr tillod samtidig bestemmelse af vandgennemstrømning og opnået pakningsdensitet. Ved at modellere konsolideringsprocessen og benytte Hagen-Poiseuille's ligning, var det muligt at bestemme en karakteristisk middelporediameter i materialerne. Denne fremgangsmåde muliggør bestemmelse af initial-permeabiliteten i cementbaserede materialer. Eksperimentelle resultater verificerede den konceptuelle pakningsmodel. På trods af små afvigelser blev der generelt fundet overensstemmelse mellem den konceptuelle porestørrelsesmodel og eksperimentelle resultater.

Vurdering af porestrukturen i hærdede cementbaserede materialer kan gøres eksperimentelt. In denne afhandling er basis for tolkningen af resultater fra den eksperimentelle metode, Lavtemperatur Kalorimetri (LTC) blevet vurderet. Dette blev gjort for at bedømme muligheder og begrænsninger ved at benytte LTC til karakterisering af porøsiteten af cementbaserede materialer. Underafkøling, mangel på temperaturligevægt, flaskehalsporer og ioner der udskilles under frysning blev behandlet teoretisk og evalueret eksperimentelt v.h.a. modelmaterialer. Det blev fundet, at den målte temperatur skal korrigeres for uligevægt mellem prøve og reference. Derudover bør der korrigeres for effekten af frysepunktssænkning fra de varierende ionkoncentrationer i den ikke-frosne del af materialet. Det blev foreslået at LTC kan benyttes til karakterisering af poresammenhæng samt porestørrelsesfordeling når viden fra de opnåede resultater bliver udnyttet.

Table of Contents

Additional work (not included in the thesis)

Kjeldsen, A.M.: Development of a geometrically based packing program in Matlab. The program is based on the model described in (de Larrard 1999). No manual is at present available.

Kjeldsen, A.M., Geiker, M. and Lindgreen, H.: *Porosity of cement-based materials with nano-sized layer silicates*, presentation at the European Congress on Advanced Materials and Processes (EUROMAT), September 1-5, Lausanne, Switzerland, 2003.

Kjeldsen, A.M., Geiker, M., Stang, H. and Hansen, K.K.:*Modelling the packing of cement-based materials*, in the proceedings of: 5th International PhD Symposium in Civil Engineering, June 16-19, Delft, The Netherlands, pp. 1329-1336, 2004.

Kjeldsen, A.M., Geiker, M., Stang, H. and Hansen, K.K.: *Modelling the initial packing of cement-based materials*, poster presentation at the conference on Cementitious Materials as model porous media: Nanostructure and Transport processes", July 17-22, Monte Verita, Switzerland, 2005.

Geiker, M., Bøhm, A. and Kjeldsen, A.M.: *On the effect of mixing on property development of cement-based materials*, in the proceedings of: Volume Changes in Hardening Concrete, August 20-23, Lyngby, Denmark, 2006.

Part I

Introduction and summary

Chapter 1

Introduction

1.1 Structure-property relations

Concrete is the most utilized building material in the world. At the same time, it is a highly complex material and a complete understanding of the structural behavior on the macro scale, requires a detailed understanding of the material behavior on the nano and micro scale. The connection between the material level and the structural level is illustrated in figure 1.1.

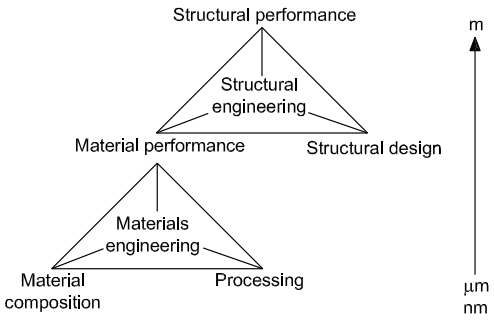

Figure 1.1 *Connection between micro- and macro properties of concrete. After (Geiker et al. 2005)*

On the nano and micro scale, the pore structure and homogeneity of the initial system is highly dependent on the properties of the constituent particles (e.g. size and shape), the mix composition, and the method of mixing. For instance, the addition of a sub-micron sized material, like silica fume, to a cement-based material may facilitate a decrease in porosity because the smaller silica fume grains can fit in the porosity between the larger cement grains. This effect is often prevalent in the so-called Interfacial Transition Zone (ITZ) between aggregate and paste. In this zone, the porosity is higher than in the bulk paste due, among other things, to poor packing of the cement grains in this area (Bentz & Stutzman 1994).

The effect of mixing on the homogeneity of cement paste was investigated by Yang and Jennings (Yang & Jennings 1995). They mixed cement pastes with a low speed paddle mixer and a high speed blender and found that when using the low speed mixer, the resulting paste contained cement agglomerates as large as mm-size, whereas the high speed blender eliminated these agglomerates. It was also found, that the addition of aggregates caused a grinding of the paste that produced results similar to using the high speed blender. Bøhm (Bøhm 2005) found, by epoxy impregnated thin section imaging, that gentle hand mixing of cement and silica fume left large silica fume agglomerates in the hydrated paste. These agglomerates were eliminated when using a high speed blender.

The addition of a sub-micron sized material to a cement-based material may also affect the microstructure through other mechanisms. The homogeneity of the hydrated product is on the microscopical level dependent on the number of nucleation sites and because sub-micron sized particles can act as nucleation agents, they may in this way further advance a more homogeneous and fine structure. At the same time some fine particles have pozzolanic properties causing a decrease in the total porosity as well as the connectivity of the larger pores.

Durability, e.g. with regards to freeze-thaw action, can to a large extend be traced back to porosity and pore structure. Furthermore, it is widely recognized that the pore structure, i.e. the pore sizes and connectivity, controls the resistance to transport of harmful substances like chlorides, sulphates, etc. The formation of cracks during hydration, or later as a result of some chemical reaction or mechanical action, also holds vast responsibility for increased concrete permeability, diffusivity, loss of strength, and subsequent degradation. The formation and effect of cracks however, will not be treated in the present thesis. In figure 1.2, selected factors affecting the initial and hydrating stages of cement-based materials are shown.

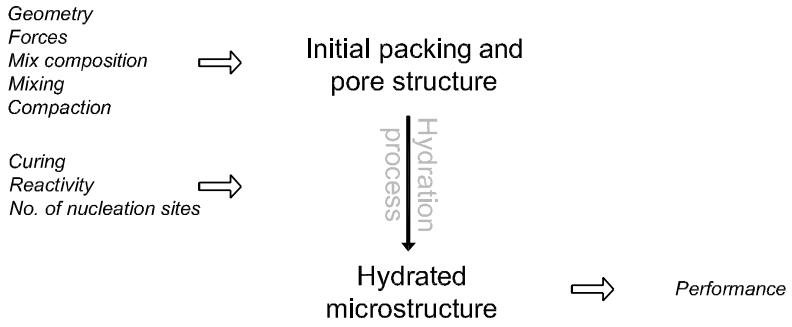

Figure 1.2 *Flow diagram of the stages in material and property development. Selected factors affecting each stage are shown.*

As the microstructure is of paramount importance for almost all performance aspects of the resulting material, the ability to predict property development by the correct mod-

elling of both initial and hydrated microstructure is a key to the subsequent understanding of many macroscopic properties of the material. This will enable the design of a concrete material with given properties and ultimately by-pass the trial-and-error proportioning that is still, to some extend, necessary today.

1.1.1 Structure-property models

A number of different models accounting for e.g. hydration development, are currently available (cf. (Bentz 1997), (van Breugel 1997), (Pignat et al. 2005), (Stroeven & Stroeven 2001), (Maekawa et al. 1999)).

An example of a pixel-based model (developed at The National Institute of Standards and Technology (NIST)) is the CEMHYD3D model (cf.(Bentz 1997)). The pixel approach allows for representation of several phases, sizes and shapes of grains. However, features below the pixel size are not possible to model, thus creating a lower boundary for the modelling. Modelling is initiated by placing all the particles randomly from largest to smallest, in a box. The user has the option to create a specified number of flocs prior to hydration, by moving all particles one pixel to a random side. If this causes the particle to touch another particle, they become agglomerated. This approach requires that the user has an outstanding knowledge of the particles tendencies to agglomerate. The model allows for determination of degree of hydration along with numerous properties like strength and chloride diffusivity.

The model, *Integrated Particle Kinetics Model* (IPKM) currently being developed at Ecole Polytechnique Fédérale de Lausanne (EPFL) (cf. (Pignat et al. 2005)) is an example of a spherical model that does not have the problem of minimum resolution. However, it is inherently unable to model other shapes than spherical. As with CEMHYD3D, the IPKM places all the particles in a box from largest to smallest and let them hydrate. The model allows for determination of e.g. permeability of the hydrated particle network.

The aim of the models available today is to predict the development of hydration in the form of microstructural development and structure-property relationships. Until now, the focus has mainly been on the hydration process, thus placing less focus on the formation of the initial stage and the placement of particles. As this initial placement of particles is the basis for the hydration development, it seems that an important step has been somewhat neglected.

1.2 Initial particle packing

1.2.1 Packing models

A number of geometrically based analytical packing models have been developed for optimization of the aggregate skeleton in concrete. Binary mixtures were e.g. dealt with by Aïm and Goff (Aïm & Goff 1967), while a ternary model was suggested by Toufar, Klose and Born (Toufar et al. 1976). In 1986, Stovall and co-workers (Stovall et al. 1986) presented their linear packing model, which accounted for multiple particle sizes. The

model was later expanded by de Larrard to include compressibility of the aggregates by means of a given compaction process (de Larrard 1999)).

Increasingly, packing models are being applied for optimization of the concrete binder as well as the aggregate skeleton. However, as all the models mentioned are based on geometrical considerations, they fail to comprehend the effects of inter-particle forces that may cause agglomeration of a number of the particles.

1.2.2 Effect of inter-particle forces

In larger grain size populations like aggregates, inter-particle forces are negligible while they on nano and micro scale can be determining for the overall particle behavior. The reason for this is that while external forces scale with the square of the particle size, a, the inter-particle forces, like the van der Waals force, scale with the particle size, as shown below.

$$\begin{aligned} F_{ext} &\propto a^2 \\ F_{int} &\propto a \end{aligned}$$

This means that the relative importance of the inter-particle force will increase, as the particle size decreases. Several attempts have been made to include the effect of inter-particle forces in packing models. One approach is to indirectly include inter-particle force effects by using an experimentally established packing density for each component, cf. (Glavind & Stang 1992). A completely different approach is offered by Yu and co-workers (Yu et al. 2003), who employ discrete dynamic simulation to investigate the packing of fine particles. An example of their results is shown in figure 1.3, where the van der Waals force have been taken into consideration. This approach simulates the packing of mono sized fine particles and nicely illustrates the increasing effect of inter-particle forces with decreasing particle sizes. However, the computational time of such modelling is long and will increase if expanded to several particle sizes.

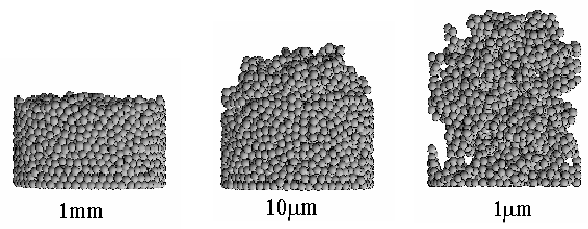

Figure 1.3 *Discrete dynamic simulation of mono-sized spheres with different sizes, from (Yang & Yu 2005).*

The use of sub-micron sized materials in cement-based materials may reduce porosity by filling out the space between packed cement grains. The principle is shown in figure 1.4

(left). This size of the added particles, as well as the size of the smallest cement particles, make them highly disposed to agglomeration due to attractive inter-particle forces and this may result in some undesired agglomeration, cf. figure 1.4 (right), and thus ultimately counteract the aim of the sub-micron particle addition. The effect of this agglomeration may be an increased water demand to maintain workability, due to large amounts of water being trapped in the agglomerates.

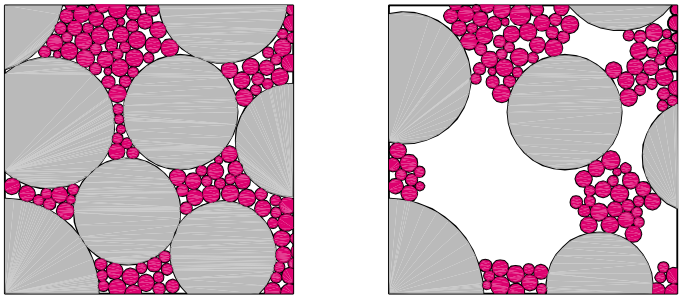

Figure 1.4 *Schematic drawing of the effect of sub-micron sized materials. Left: Desired action, right: expected action due to attractive inter-particle forces.*

Accommodating the workability in concretes with sub-micron sized materials have spurred the development of superplasticizers. The superplasticizers absorb onto the particles preventing or reducing agglomeration while reducing the water demand by freeing water trapped in the agglomerates. In connection with this, the macroscopic response on rheological properties on fresh concrete has also undergone a drastic change by reducing yield stress of the mix (Wallevik 2002), (Flatt 2004*b*). This has turned the focus towards inter-particle forces and their effect on agglomeration and yield stress of the suspensions. Much work is currently being carried out in order to quantify the effect of superplasticizers on cement-based systems. Schober and Mäder (Schober & Mäder 2003) found that the spread of cement-paste dispersed with various comb-type copolymers varied linearly with the adsorbed amount of polymer. In (Flatt & Houst 2001) the adsorption mechanism of superplasticizers added directly with the mixing water compared to delayed addition, was treated. They found that direct addition could result in an AFm phase that was highly intercalated with superplasticizer and that large amounts of superplasticizer this way was consumed uselessly in the AFm phase. Also, compatibility aspects between superplasticizers and cement is a major concern. Yamada and Hanehara (Yamada & Hanehara 2001) found that in the case of comb-type copolymers, adsorption and workability was decreased by the addition of sulphates. This was interpreted as sulphates competing with the polymer for adsorption sites. Thus, it seems there is a need for a basic understanding of the stabilizing mechanisms of comb-type superplasticizers, in order to understand the effects on the rheology of cement-based suspensions.

1.3 Characterization of microstructure

In order to experimentally determine the effects of the mix composition on the hydrated pore structure, there is a need for reliable experimental methods for determining pore size distribution and pore connectivity (e.g. in terms of permeability). Through the years, numerous experimental methods, both direct and indirect, have been developed for this purpose, a number of which are listed in table 1.1. The direct methods visualize the micro structure (and thus the pore structure), while the indirect measure a given property of the material and interpret this property with regards to pore structure.

Table 1.1 *Selected methods for porosity determination*

Direct	**Indirect**
Atomic Force Microscopy	Mercury Intrusion Porosimetry
(Environmental) Scanning	Nitrogen sorption
Electron Microscopy	Water sorption
	Suction
	H^1-Nuclear Magnetic Resonance
	Low Temperature Calorimetry

Each method have strong as well as weak points. For instance, Mercury Intrusion Porosimetry (MIP) and nitrogen sorption require complete drying of the material which has been proven to alter the microstructure of cement-based materials, cf. (Bager & Sellevold 1986*b*), (Moukwa & Aitcin 1988). Water sorption gradually dries the material and the samples may take months to reach equilibrium, thereby allowing the material to continue hydrating during the measurements. Suction is carried out on saturated samples, but is quite time consuming. N^1-Nuclear Magnetic Resonance (NMR) may be carried out on saturated samples and measures only water filled porosity. However, the method is still in its infancy and not all aspects of the method are fully investigated. Some direct methods, like Environmental Scanning Electron Microscopy (ESEM) and Atomic Force Microscopy (AFM) can be carried out under humid conditions, thereby mitigating drying damage. However, whereas the resolution of ESEM is not high enough to image sub-micron sized pores, AFM image sections so small that they are not representative of the bulk material.

The method Low Temperature Calorimetry (LTC) can be carried out on virgin (never dried) samples and tests can be completed within hours. LTC utilizes that water in pores freezes at a lower temperature than free water. Bentz (Bentz 2004) used the LTC technique to obtain knowledge on the pore connectivity of the hydrated material. At the Technical University of Denmark, the method has been used to investigate, among others, the effect of drying on cement-based materials, cf. (Bager & Sellevold 1986*a*) and (Bager & Sellevold 1986*b*) as well as to determine pore size distributions in porous materials, cf. (Villadsen 1992). However, the freezing of saline solutions in an ill-defined pore system is a complicated matter and can at present not be fully described. Therefore, interpretation of LTC-results comes with a number of assumptions and an assessment of the validity of

these assumptions will improve the basis for pore structure characterization.

1.4 Overview of the thesis

The thesis is divided into two parts. This first part consists of an introductory chapter (chapter 1) where the project background and aim is explained. Furthermore, an overview of the papers is given. Chapters 2-4 summarize the research with emphasis on the major findings, while the closing chapter (chapter 5) gives the overall conclusions along with recommendations for future work.

The second part of this thesis is a collection of five papers describing the research in detail. The papers are not presented in chronological order, but in an order that aims to give the reader a coherent picture of the research.

1.4.1 Aim

It is the intent of the thesis, through theoretical considerations, as well as experimental testing, to:

1. quantify the effect of inter-particle forces on the consolidation behavior of fresh cement-based materials
2. develop a conceptual model for the packing and pore size of fresh cement-based materials, based on considerations of geometry and inter-particle forces
3. evaluate the basis for interpretation of results from the experimental technique, Low Temperature Calorimetry (LTC), in order to improve the assessment of the pore structure of hardened cement-based materials

The project is seen as an important step towards linking structure-property models to packing models and in turn enable a reliable prediction of property development of any given concrete matrix composition. Furthermore, a correct evaluation of the LTC-results will enable the assessment of e.g. percolated pore space and pore sizes in hardened cement-based materials.

1.4.2 Approach

The theory of inter-particle forces in cement-based materials is described and used to assess particle interactions in the fresh material. The investigation of the effect of superplasticizer addition on cement-based materials is carried out using different consolidation techniques. Consolidation techniques exploits, rather than suffers from the fact that dispersed or weakly flocculated suspensions have a tendency to sediment. Furthermore, the technique is highly sensitive to alterations in the stability of the suspension and is therefore applicable in the current study.

A model material with surface properties similar to those of cement, magnesium oxide (MgO), is initially used in the experiments to quantify inter-particle force changes by

addition of different superplasticizers. These experiments are carried out using centrifugal consolidation. Calculations of inter-particle forces and considerations on the molecular structure of the adsorbed superplasticizers are used to relate experimental results to theory. Subsequently, cement and silica fume interactions are evaluated theoretically and conceptual models for packing and pore size are proposed. The effect of a single type superplasticizer on the packing behavior of combinations of cement and silica fume is evaluated experimentally by compressive consolidation, allowing for rapid completion of the experiments. Modelling the flow through the material during consolidation is used to determine characteristic pore sizes in the material.

The basis for interpretation of LTC-results is evaluated through theory and experiments. The theory of freezing mechanisms in water and saline solutions in the bulk as well as in pores is described. The theory is evaluated experimentally by means of an inert model material with mono sized pores. The material is saturated with either water or water with 10% NaCl allowing for investigation of the combined action of pores and a saline solution with a well defined phase diagram. The implications for cement-based materials are described.

1.4.3 Scope

In the following, the papers on which the thesis is based, are briefly described. The order of the papers follows the outline of the thesis, rather than the chronological order in which they were produced. *Paper I - IV* all concern the effect of inter-particle forces on cement-based or model cement systems, with regards to consolidation behavior. *Paper V* concerns evaluation of the experimental method, LTC, for pore structure characterization.

Paper I concerns the effect of superplasticizers on the centrifugal consolidation behavior of magnesium oxide suspensions. The superplasticizers used adsorb onto the MgO surface and infer a steric repulsion that reduces the degree of flocculation. The packing density profiles of the particulate cakes have been measured and the maximum packing density of the consolidated particle network is related to the calculated inter-particle force. The implications of this simple compression rheological method for evaluating the stabilizing mechanism of superplasticizers are discussed.

Paper II expands on the experimental results from paper I. Additional results are presented and the compression rheology behavior is related to the estimated thickness of the adsorbed superplasticizers and a scaling analysis is used to quantitatively assess the importance of the length of the side-chains grafted on the polymer, on the magnitude of the inter-particle bond strength.

In *Paper III* the implications of the use of silica fume, are considered. On the basis of inter-particle and shear force calculations, calculations on maximum agglomerate size present after the combined action of superplasticizers and shear are carried out. Qualitative experimental results indicate that external shear affects the particle size distribution of MgO as well as silica fume, whereas the addition of superplasticizers affects only the

smallest particles in MgO and thus primarily acts as water reducers.

In *Paper IV*, calculations of inter-particle forces in fresh cement-silica fume suspensions is carried out and in combination with considerations on geometrical packing, conceptual models for packing and pore size are proposed. To determine the validity of the models, cement-based suspensions with varying additions of silica fume, and with and without superplasticizer are studied experimentally by compressive consolidation. The employed consolidation equipment enables the simultaneous determination of flow through the material and obtained packing density. Modelling the consolidation process makes it possible to determine a characteristic mean pore diameter in the studied systems and shows, as expected, a significant effect of addition of silica fume as well as superplasticizer.

In *Paper V* the effect of selected factors and phenomena on Low Temperature Calorimetry (LTC) results is investigated, in order to determine the possibilities and limitations of using LTC for characterization of the porosity of cement-based materials. It is proposed that the connectivity of pores, e.g. in cement-based materials, may be characterized based on cooling curves, whereas the pore size distribution may be characterized based on the heating curve.

Chapter 2

Centrifugal consolidation - Model suspensions

The aim of the consolidation investigations has been to reach a fundamental understanding of the stabilization mechanism of comb-type superplasticizers. To avoid any hydration mechanisms perturbing the experiments, a model material, magnesium oxide (MgO), was used for all the investigations described in the present chapter. In what follows, an overview of the work, as well as major results and conclusions are summarized. For a more complete review of the work, the reader is referred to the appended *Paper I* and *Paper II*.

2.1 Introduction

Superplasticizers are able to reduce the porosity of the hardened concrete by allowing the fresh material to become workable with less water. Increasing demands on workability, high strength and enhanced durability spurred the development of new types of synthetic superplasticizers with improved performance ((Sakai & Daimon 1997), (Uchikawa et al. 1997)). These new generation superplasticizers are comb-type copolymers with an anionic backbone, commonly having carboxylic and/or sulphonate groups that can render the polymer a negative charge, and uncharged poly (ethylene oxide (PEO))- based chains of variable length grafted onto the anionic backbone at regular intervals.

In the present chapter, the rheological behavior is related to the conformation of the adsorbed superplasticizers. Inert suspensions of MgO in an ionic solution is used as a model system for cement. A range of comb-type superplasticizers with a systematic variation in the length of the grafted polyethylene oxide side chains is used and the study is performed by centrifugal consolidation, also known as compressive rheology.

The maximum packing density, γ_m, is strongly dependent on the particle size distribution and the particle size. A broad particle size distribution usually results in a higher value of γ_m because the small particles can fit into the voids between the large particles. However, while the geometric packing rules are useful when dealing with coarse particles in concrete, like aggregates, the situation becomes more difficult when dealing with the

smallest fraction of cement and fine particle additions like silica fume. The inter-particle forces and thus the colloidal stability of the suspension have a profound influence on the packing of fine particles. If the particles in suspension are instable they will stick upon first contact and thus not be able to rearrange during consolidation. Colloidally stable suspensions, characterized by a repulsive inter-particle force of sufficient range and magnitude to keep the particle dispersed, usually facilitate a homogeneous mixing of powders. Due to this, the particle packing is usually not as efficient in an originally flocculated (instable) suspension as in an originally dispersed (stable) suspension (see figure 2.1).

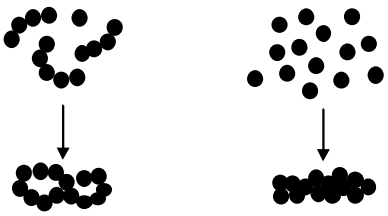

Figure 2.1 *Consolidation behavior of flocculated (left) and dispersed (right) suspensions.*

2.2 Experimental

Materials

Magnesium oxide (MgO) was chosen for this study, because it mimics the surface properties of cement in a high pH solution. Upon mixing with water it undergoes an initial hydration to $Mg(OH)_2$ but the reaction essentially stops after 30 minutes and offers stable conditions for about 3.5 hours, before further conversion takes place (Perche 2004).

The hydration reactions that occur when cement is mixed with water create a supersaturated solution at a very high ionic strength of mainly Ca^{2+}, SO_4^{2-}, K^+, and Na^+ at a high pH $\approx$ 12-13. Because of this, it was chosen to work with an ionic solution that mimics the aqueous phase of the cement suspensions. The artificial pore solution is composed of 2.07 g/L of $CaSO_4 \cdot 2H_2O$, 12.5 g/L of Na_2SO_4 and 2.92 g/L of NaOH and has an ionic strength of 0.415 M, and a pH of 12.8. In what follows, it is referred to as the *YS* (the composition was initially suggested by Dr. Yves Houst, EPFL).

Six different comb-type superplasticizers (noted PC 1-4 and A-B) were used in the study. All the polymers are composed of a polymethacrylic (PMA) backbone and grafted side chains of polyethylene glycol (PEG) and the length of the backbone and the grafted side chains have been systematically varied. The polymers PC1-4 were used in an EC-project called "Design and function of novel polymeric admixtures for more durable high performance concrete" and some details of these polymers have been published ((Schober & Mäder 2003), (Perche 2004), (Perche et al. 2003), (Kauppi et al. 2003)). The polymers A

and B were synthesized especially for this study. In figure 2.2, schematic drawings of the polymers are shown.

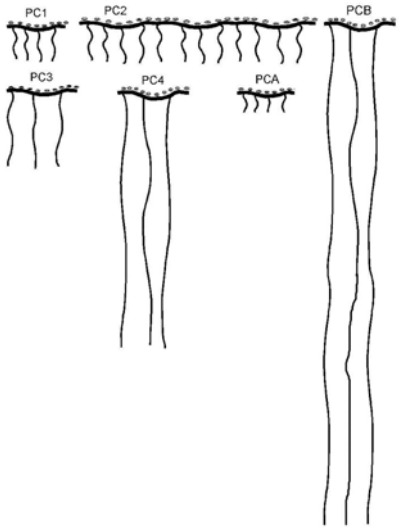

Figure 2.2 *Schematic illustration of the molecular structure comb-type copolymers with a negatively charged polycarboxylate backbone with grafted polyethyleneoxide side chains of different length.*

Method

MgO-suspensions at solids concentration of 20 vol% were prepared by mixing the MgO powder with the electrolyte solution YS. The suspension was treated with ultrasound for 5 minutes and left with magnetic stirring for 30 minutes. Afterwards, superplasticizer was added and the solution was again left with magnetic stirring for 30 minutes. The superplasticizers were added in amounts of 6 mg superplasticizer/g of the MgO powder, which ensured that the MgO surface was saturated by the polymer. One set of experiments was also performed at sub-monolayer coverage where the polymer PC 1 was added at a lower dosage; 0.41, 0.98, 2.00 and 4.00 mg superplasticizer/g powder, respectively.

The suspensions were centrifuged at 400 rpm for approximately 3 hours. The centrifugation was terminated when the consolidation process had reached steady state, as determined from the variation in the cake height during centrifugation. The consolidation cake was cut into slices of a thickness of 2-3 mm following a modification of the procedure described by Meeten (Meeten 1993). The water content, and thus the packing density of the slices, was determined by measuring the weight loss after drying at 105°C.

2.3 Full surface coverage superplasticizer

Figure 2.3 shows that the addition of comb-type superplasticizers to the MgO suspensions has a significant effect on the packing density profiles. All the suspensions displayed a compressible behavior with an increasing packing density towards the bottom of the centrifuge tube (increasing distance from the rotor center). This behavior is typical for flocculated particle networks since a fully stable suspension is expected to display an essentially incompressible consolidation behavior ((Bergström 2001), (Bergström et al. 1992)). The MgO suspension without addition of any superplasticizer forms a particle network that attains a low packing density in the applied centrifugal force field (figure 2.3). This implies that the compressive yield stress is high and that the maximum stress that is applied at the bottom of the cake at a rotational speed of 400 rpm (approximately 6 kPa) only consolidates the MgO particle network to a packing density of $\gamma \approx 0.36$. Additions of superplasticizers result in an increase of the packing density at the bottom of the tubes, $\gamma \approx 0.43$-0.50, which shows that adsorption of the comb-type superplasticizers significantly reduces the compressive yield stress of these particle networks. The addition

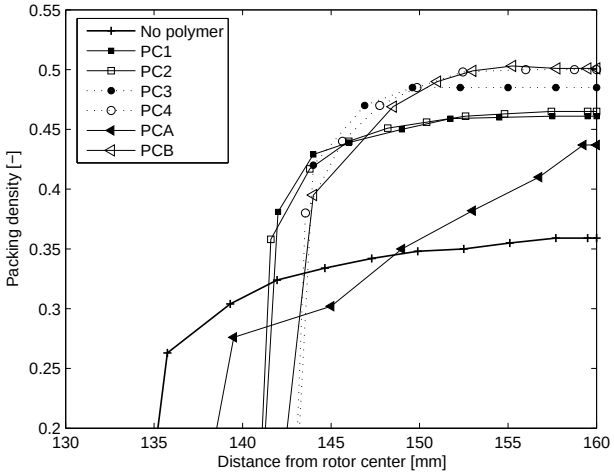

Figure 2.3 *Packing density profiles at steady state for MgO suspensions with different comb-type superplasticizers added. The suspensions were centrifuged at 400 rpm for 3 hours.*

of superplasticizers yielded a "milky" supernatant containing a small concentration of very fine particles. The MgO suspension without any addition superplasticizer addition resulted in the formation of a clear supernatant after centrifugal consolidation, which is typical for a strongly flocculated suspension. This suggests that at least a fraction of the MgO particles are stabilized by the addition of the superplasticizers.

By means of de Gennes scaling laws (de Gennes 1987), the layer thickness, δ of the

adsorbed comb-type superplasticizers layer can be estimated from a simple expression for a so-called mushroom conformation of the PEO side chains (side chains are coiled in a mushroom shape):

$$\delta = L_{PEO} P^{3/5} \tag{2.1}$$

Where L_{PEO} is the length of the ethylene oxide [-CH2-CH2-O-] segment and P is the number of segments in the chain.

Figure 2.4 shows that the maximum packing density of the consolidated particle networks scales with the inverse of the estimated layer thickness. The simple relation clearly corroborates the importance of the grafted PEO-side chains in imparting a steric repulsion that controls the consolidation of the particle network.

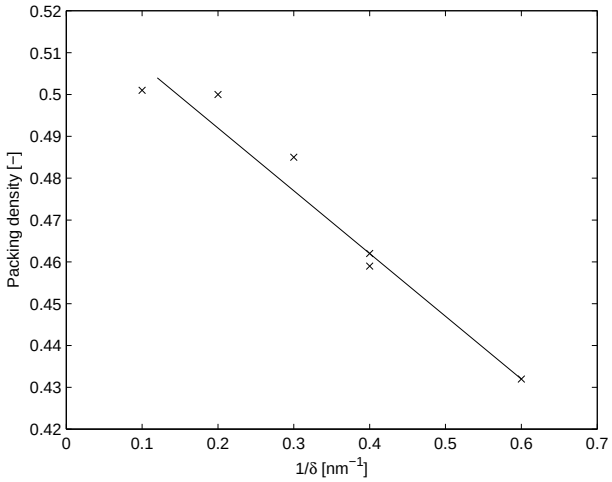

Figure 2.4 *The highest attained packing density after centrifugation at 400 rpm, as a function of the inverse of the estimated adsorbed layer thickness,* $1/\delta$.

2.4 Sub-surface coverage superplasticizer

Superplasticizers are commonly added to cementitious systems at very low dosages, much below the amounts needed for full surface coverage. Figure 2.5 shows how the consolidation behavior varies with the amount of added PC1 comb-type superplasticizer. All the suspensions display a compressible behavior with an increasing packing density towards the bottom of the centrifuge tube (increasing distance from the rotor center). Increasing the addition of PC1 results in an increase in the packing density at the bottom of the

tubes. This suggests that an increase in the surface coverage reduces the compressive yield stress.

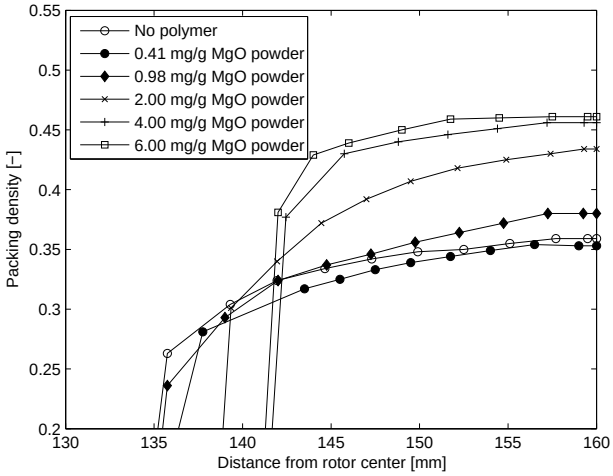

Figure 2.5 *Packing density profiles at steady state for MgO suspensions that have been centrifuged at 400 rpm for 3 hours with various amounts of the superplasticizer PC1 added.*

At low superplasticizer dosages, a linear behavior was found between dosage and obtained maximum packing density. Higher dosages, close to the saturation dosage, yields a more complicated situation and was not quantified. The low-dosage connection suggests that sub-monolayer surface coverage relates to a thinner "efficient" layer thickness, compared to full surface coverage.

2.5 Scaling relation

The total inter-particle force between two particles consists of a summation of several contributions, i.e. the van der Waals force, the double layer force and the polymer induced steric force.

The van der Waals force between two particles of equal radius a, and material (1) acting across a medium (2) can be approximated by ((Flatt 2004*a*), (Pedersen 1998)):

$$F_{vdW} \approx -A_{12} f_{retardation} \frac{dH}{dh} \tag{2.2}$$

where A_{12} is the Hamaker constant (see (Bergström 1997)), $f_{retardation}$ is a retardation factor that incorporates the retardation of the dipole interaction over large distances (Russel

et al. 1989), H is a geometrical factor dependant on the shape of the interacting particles (see (Bergström et al. 1992)) and h is the separation distance.

The double layer force can be described by (Flatt 1999):

$$F_{Electrostatic} = -2\varepsilon_0\varepsilon_r a\pi\psi_0^2 \cdot \frac{\kappa e^{-\kappa h}}{1+e^{-\kappa h}} \tag{2.3}$$

where ε_0 is the permittivity of vacuum, ε_r is the relative permittivity of the medium, ψ_0 is the surface potential of the particle and κ is the inverse of the so-called Debye-length.

The polymer induced steric force can be described by this simplified expression ((Flatt 1999), (Bergström et al. 1992)):

$$F_{Steric} = 2\pi a \cdot \frac{\gamma_2^2}{\overline{V}_3} k_B T(\frac{1}{2} - \chi)(h - 2\delta) \tag{2.4}$$

where γ_2 is the solids volume fraction of chains in the adsorbed layer, V_3 is the partial molecular volume of the medium, χ is the polymer segment-solvent interaction parameter and δ is the thickness of the steric layer.

Figure 2.6 shows the decline of the van der Waals force as a function of separation distance, along with the effect of different steric layer thicknesses on the maximum attractive force.

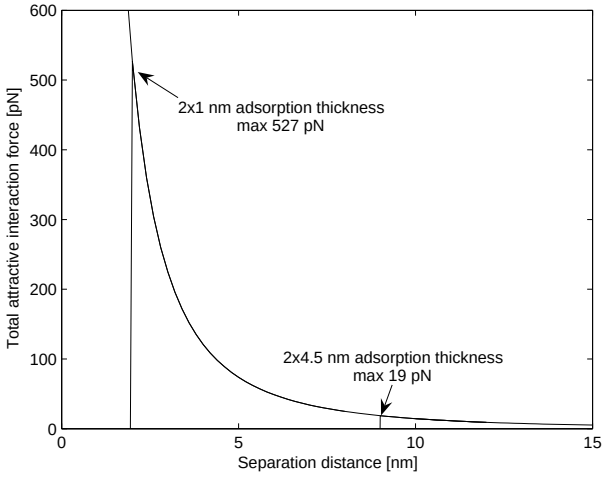

Figure 2.6 *The calculated inter-particle force for MgO particles with radius of 1325 nm.*

Using a scaling approach, it is possible to link the consolidation behavior of the polymer coated networks to the magnitude of the inter-particle forces. The adsorbed layer thickness estimated from the de Gennes theory is now used.

At close separation distances, equation (2.2) simplifies to

$$F_{vdW} \approx -A_{12}\frac{a}{12h^2} \tag{2.5}$$

Due to, among other things, the high ionic strength characterizing these systems, the electrostatic double layer force is ignored and the maximum inter-particle force can be estimated from the van der Waals interaction at separation distances twice the layer thickness. Furthermore, for the scaling approach it suffices to write

$$F^*_{max} \propto \delta^{-2} \tag{2.6}$$

The compressive yield stress of a particle network, P_y can be written as a product of a packing density function $f(\gamma)$ and maximum attractive inter-particle force F_{max}:

$$P_y \approx f(\gamma)F_{max} \tag{2.7}$$

The use of the same amount of MgO powder in all the experiments means that the values of P_y are essentially identical at the bottom of the centrifuged particle networks for all samples. Hence, under the condition of constant P_y, it is possible to obtain a scaling between F_{max} and $f(\gamma)$,

$$F_{max} \propto \frac{1}{f(\gamma)} \tag{2.8}$$

The simple form of $f(\gamma) = \frac{\gamma^3}{\gamma_{max}-\gamma}$ has been used, and the resulting relation between obtained packing density and adsorbed layer thickness is shown in figure 2.7.

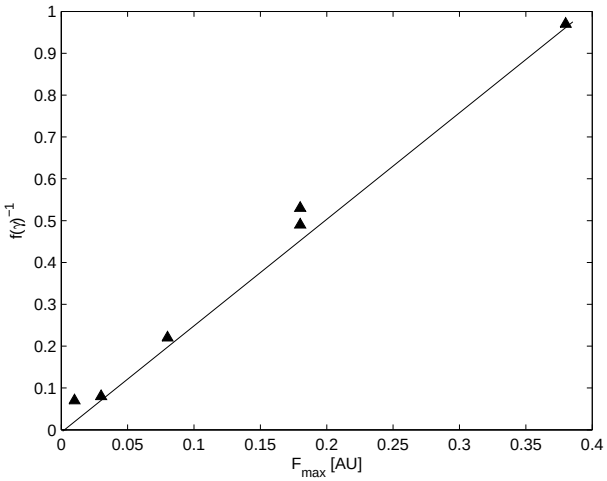

Figure 2.7 *The inverse of the assumed packing density function* $f(\gamma) \approx \frac{\gamma^3}{\gamma_{max}-\gamma}$ *versus the estimated maximum attractive interparticle force,* F_{max}*. The points relate to the values for highest attained packing density after centrifugation at 400 rpm, and the* F_{max} *in arbitrary units (AU) calculated from the estimated layer thickness of the specific superplasticizer.*

Attempts were made to expand the scaling approach to the sub-surface coverage systems. The main problem of doing this consists in determining an average maximum inter-particle force. A simple *ad-hoc* approach was employed, consisting of determining the average inter-particle force by a weighed average of the layer thickness of the superplasticizer covered surfaces. The approach yielded a reasonable correlation between packing density and estimated maximum inter-particle force, but must be viewed as demonstration of a potential expansion of the scaling approach, rather than a definitive result. A further description of the approach is given in *Paper II*.

Chapter 3

Compressive consolidation - Cement-based suspensions

The aim of this part of the research was to develop a conceptual model for the packing and pore size of fresh cement-based materials, based on considerations of geometry and inter-particle forces. Furthermore, compressive consolidation experiments on cement and silica fume was used to determine the validity of the model. In the following, an overview of the work, as well as major results and conclusions are summarized. For a more complete review, the reader is referred to the appended *Paper III* and *Paper IV*.

3.1 Introduction

The previous centrifugal consolidation results showed a good correlation between inter-particle forces and consolidation behavior. In the current chapter, the use of the cement model material is replaced by cement. Furthermore, in order to quantify the effect of sub-micron sized particles, silica fume is added to the mix. As the use of cement poses the problem of hydration, an alternative method, i.e. compressive consolidation, is chosen to determine consolidation behavior. The employed equipment enabled rapid determination of flow through the material and obtained packing density, thus avoiding excessive hydration. Modelling the consolidation process and combining with measured flow, enabled calculation of a characteristic mean pore diameter in each material combination.

3.2 Experimental

Materials
The cement used was a Portland BASIS® cement delivered in 25 kg bags, from Aalborg Portland A/S. This type of cement contains 14% limestone filler. The silica fume was an Elkem Microsilica®. Superplasticizer (PC4) and artificial pore solution (YS) were the same as used on the model material. Both PC4 and YS have been described in the previous chapter.

Methods
Powders were initially mixed together with a spatular. The YS was added to the mix

and stirred by hand. The suspension was ultrasonicated for 3 minutes after which superplasticizer was added and the mix was subjected to 1 minute of ultrasonic treatment. Superplasticizer was added in an amount of 6 mg/g of the cement. The water/powder ratio was varied to obtain a workable paste in each experiment.

The test equipment comprises a steel tube, a steel piston, a filter, and a steel base. A schematic drawing is shown in figure 3.1. The tube has small holes penetrating the tube wall at the level of the filter, thus permitting water to drain from the filter. The piston is a cylindrical bar which fits into the tube.

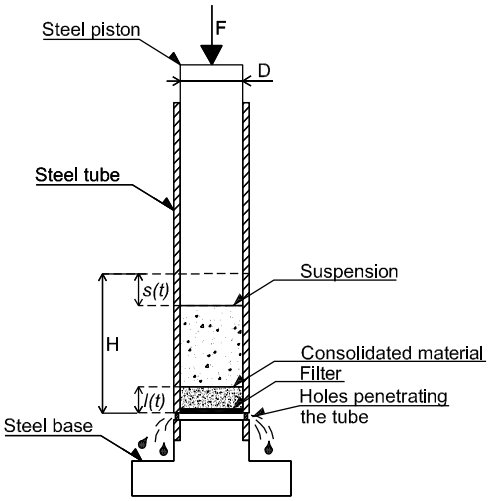

Figure 3.1 *Schematic representation of the equipment for compressive consolidation tests*

The suspension was poured into the tube and closed off with the piston. The arrangement was placed in a universal testing machine and the piston was exposed to a constant load, F, corresponding to a uniformly distributed pressure of 2 and 4 MPa, respectively. Corresponding values of load, deformation and time were recorded.

When the piston is loaded, water flows from the suspension through the filter (at the bottom) and a consolidation process develops. The consolidation will start at the level of the filter (at the bottom of the tube) and advance to the top. The height of the consolidated material (the "cake") is termed *l(t)*, while the deformation is termed *s(t)*. The initial suspension height prior to loading is H. When full consolidation is achieved, deformation will come to a rest, and the test is terminated. After termination, the consolidated material was removed from the tube, weighed, dried at 105°C, and weighed again, thereby determining the porosity, ϕ and resulting packing density, $\gamma = 1 - \phi$, of the material.

3.3 Particle forces

As described in the previous chapter, the dominating inter-particle forces in cement and concrete are the van der Waals force, the electrostatic double-layer force, and the steric (polymer induced) force.

The zeta-potential of cement in a high ionic strength, high pH solution is very low (around $\pm$ 5 mV) and does not give rise to a very pronounced electrostatic force. Thus, for cement suspensions, the electrostatic force between the particles can be ignored. Oppositely, the zeta-potential of silica fume particles, suspended in this media is very high (around -50 mV) giving rise to a repulsive force between the silica fume particles and thus counteracting the van der Waals force effect.

The action of the superplasticizer used in the current study is mainly to absorb onto the cement particles in a specific layer thickness and thus create a steric barrier, preventing the particles from coming into close contact. In (Flatt et al. 1998), the zeta-potential of silica fume in a suspension of 0.01 M NaOH was measured with and without the addition of superplasticizers. The similar zeta-potentials obtained with and without superplasticizer addition indicate that the superplasticizer does not adsorb onto silica fume particles. This is supported by the fact that an anionic superplasticizer should not be able to adsorb onto the highly negatively charged silica fume particles. Particle size distribution measurements of silica fume suspended in YS with and without PC4 addition are shown in figure 3.2. The similar particle size distributions obtained with and without superplasticizer addition corroborates with theory.

The presence of the so-called solvation force, stemming from the orientation of the polar water molecules near a surface, will prevent all particles immersed in water, from physical contact. The solvation force is active for approximately 1-3 layers of water molecules, i.e. about 0.3 - 0.9 nm.

Besides the solvation force, a number of external factors may assist in keeping particles separated, like gravity, Brownian motion, and shear force. Small colloids undergo Brownian motion because they are bombarded by solvent molecules. It is the kinetic energy of the solvent molecule that causes them to move. Because the kinetic energy of the molecules is the same regardless of particle size, smaller particles will exhibit the effect more pronounced than larger ones. Silica fume will be affected by Brownian motion, whereas cement will be unaffected. On the other hand, cement is sensitive to gravity and shear force. In the current experiments, shear is induced by the consolidation force and will therefore henceforth be referred to as the consolidation force.

Based on the above, determining the resulting force between cement (C) and silica fume (SF) particles may be able to determine with which particle interactions, agglomeration is more likely to occur. In equations (3.1)-(3.3) the inter-particle forces that are deemed relevant in each case are listed. It is assumed that the principle of superposition can be applied:

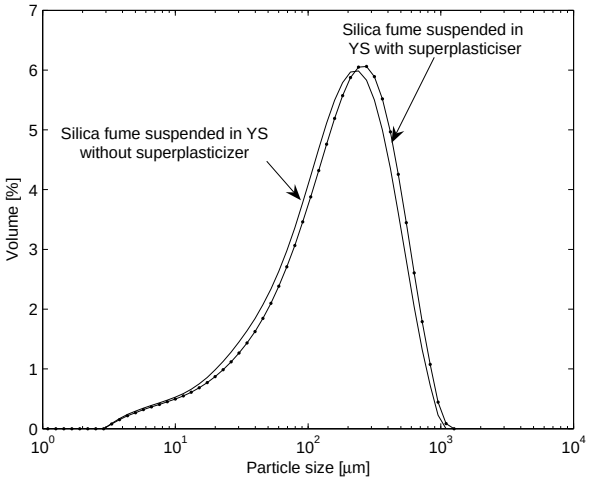

Figure 3.2 *Particle size distribution of silica fume with and without superplasticizer addition.*

$$F_{i(C-C)} \approx F_{vdW} + F_{Solvation} + F_{Steric} \tag{3.1}$$
$$F_{i(SF-SF)} \approx F_{vdW} + F_{Electrostatic} + F_{Solvation} \tag{3.2}$$
$$F_{i(C-SF)} \approx F_{vdW} + F_{Electrostatic} + F_{Solvation}(on\ SF) + F_{Steric}(on\ C) \tag{3.3}$$

Also the effect (and thus relevance) of external forces acting, is determined by the particle size:

$$F_{ex(C-C)} \approx F_{Consolidation} + F_{Gravity} \tag{3.4}$$
$$F_{ex(SF-SF)} \approx F_{Brownian} \tag{3.5}$$
$$F_{ex(C-SF)} \approx F_{Consolidation}(on\ C) + F_{Gravity}(on\ C) + F_{Brownian}(on\ SF) \tag{3.6}$$

Assuming the size of cement to be 10μm and that of silica fume to be 100 nm, calculations of the particle interactions with and without superplasticizer are carried out. A solvation layer of 0.3 nm and a steric layer of 6 nm are assumed. The result is shown in figure 3.3. The maximum gravitational force has a magnitude of $\sim$ 10 pN for cement sized particles, while the Brownian force has a magnitude of about $\sim 10^{-1}$ pN for silica fume sized particles. These are indicated by the horizontal dotted lines.

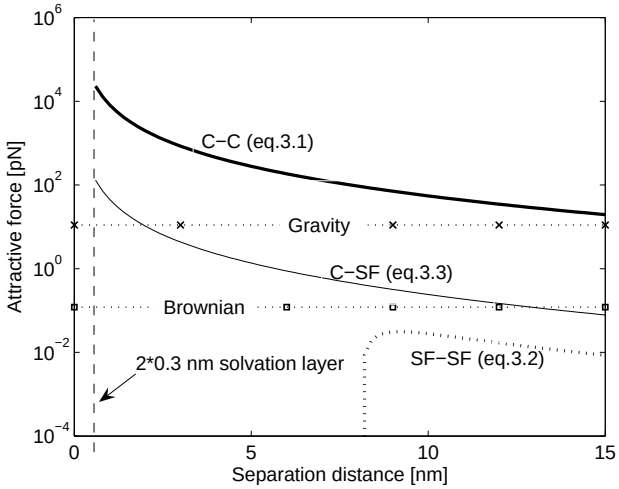

(a) Inter-particle force interaction without superplasticizer addition.

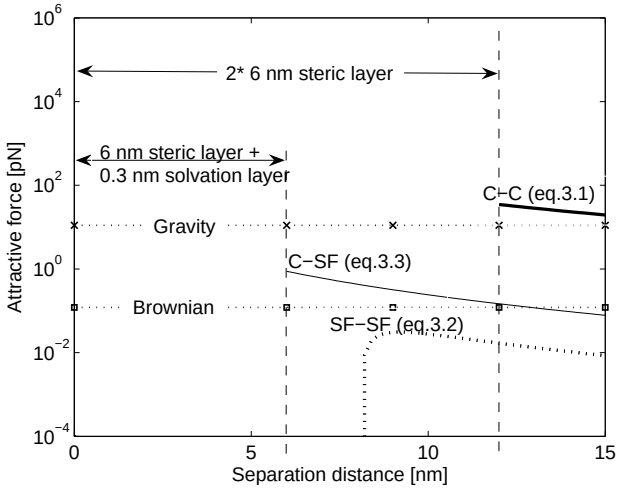

(b) Inter-particle force interaction with superplasticizer addition.

Figure 3.3 *Inter-particle force interaction with and without superplasticizer addition between two cement grains (C-C), a cement and a silica fume grain (C-SF), and two silica fume grains (SF-SF).*

From this comparison between force magnitudes, it may be deducted that Brownian motion will be able to keep the silica fume particles dispersed at all times. As it is commonly perceived that silica fume is highly agglomerated it is worth noting that while silica fume actually *is* a highly agglomerated material, this is not due to attractive inter-particle forces. Instead, the nature of the production process tends to fuse a large number of silica fume particle together, creating larger clusters (Diamond 2003), many of which are able to be broken by ultrasonic treatment. Particle size distribution measurements of silica fume suspended in YS and either gently mixed or ultrasound-treated, are shown in figure 3.4

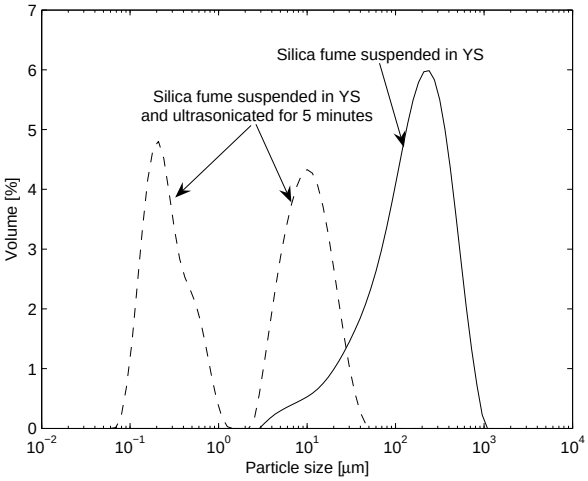

Figure 3.4 *Particle size distribution of silica fume gently mixed with YS or mixed with YS and ultrasound treated.*

The mean particle size of silica fume is given by the supplier as being well below 0.5 μm (webpage Elkem 2005), but it seems that the mean particle size as supplied is quite a bit larger than that. The application of ultrasonic treatment does seem to break a large number of the agglomerates, but not all.

The comparison in figure 3.3 also showed that silica fume and cement are likely to agglomerate, but that this agglomeration may be resisted by the addition of superplasticizer. Furthermore, due to the large size of the cement grains, they will be most affected by the consolidation force. Further elaboration of figure 3.3 can be found in *Paper IV*.

3.4 Packing characteristics

Based on the packing theory developed by de Larrard (de Larrard 1999) and the considerations on inter-particle forces, a conceptual model is proposed. In figure 3.5, a model

where no consolidation force is applied is shown.

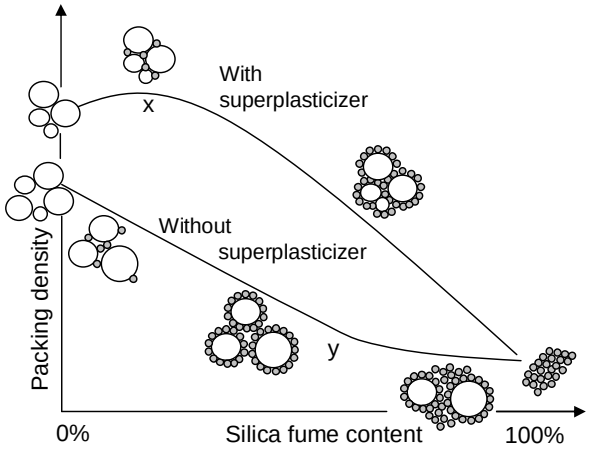

Figure 3.5 *Conceptual packing model where inter-particle forces have been included.*

In the top curve, superplasticizer has been added, screening the attractive forces between cement and silica fume. The top curve will therefore resemble that of a geometrically based packing model. The packing density will increase when silica fume is added, until the point, x, where the silica fume just fills the cement porosity. After this, the packing density will be reduced until it reaches the packing density of silica fume alone. In the bottom curve, it is assumed that silica fume and cement will agglomerate with each other when silica fume is added. This will cause the immediate decrease of packing density. The subsequent linear section represents the situations where all silica fume is agglomerated in some way to the cement particles. The last section succeeding the point, y, represents the situation where there is an excess of free silica fume, prohibited from agglomerating to any cement-particles, because the existing agglomerates are now so large, that they are influenced by external dispersive forces.

Applying consolidation force to the mix will result in increased packing densities, because more attractive inter-particle forces may be overcome and each cement-silica fume mix will have a characteristic packing density, achievable by application of a given consolidation force.

Selected experimental results are shown in figure 3.6. The fact that same packing density is obtained in the pure cement suspension with and without superplasticizer addition is due to the consolidation force exceeding the attractive inter-particle forces between this size particles. In fact, an estimate showed that the consolidation pressure should be below 0.0001 MPa to avoid compression of the pure cement suspensions to similar packing

densities. An increasing consolidation force will ultimately yield similar packing densities for all particle combinations with or without the addition of superplasticizers.

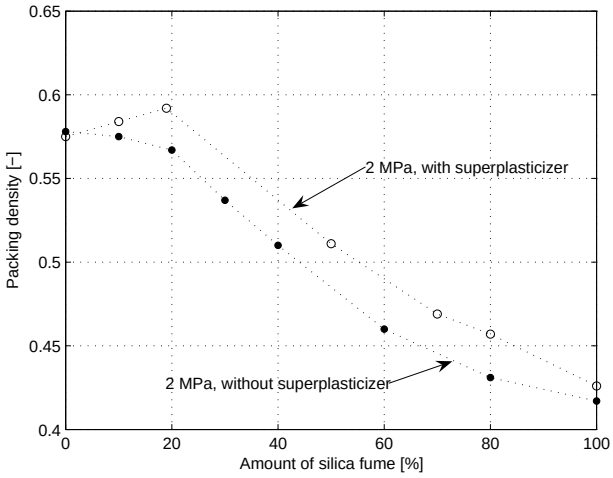

Figure 3.6 *Experimental packing results obtained from the consolidation experiments.*

3.5 Pore characteristics

From the conceptual packing model, it is now possible to specify an expected pore size model. The situation without consolidation is considered. When superplasticizer has been added, purely geometrical packing rules apply: Prior to the point, x, where silica fume just fills the porosity between the cement grains, the characteristic pore size may be linearly decreasing from the characteristic pore size of cement to the characteristic pore size of silica fume. After this point, the characteristic pore size of silica fume should be governing. When no superplasticizer has been added, and the attractive inter-particle forces play a role in the resulting packing, the characteristic pore size will be continuously decreasing from that of the cement to that of the silica fume, until the point, y, where the silica fume does not agglomerate further to cement. The principle is shown in figure 3.7. To examine the validity of the pore size model, the consolidation process was modelled. Using Darcy's law for laminar flow in a tube and assuming that the volume of flow at a specific time is proportional to the increase in the amount of solidified material, the consolidation process can be modelled. Combining this result with the Hagen-Poiseuille equation and considerations of a pore size distribution function, yields an expression for a characteristic mean pore diameter, $\overline{x_c}$:

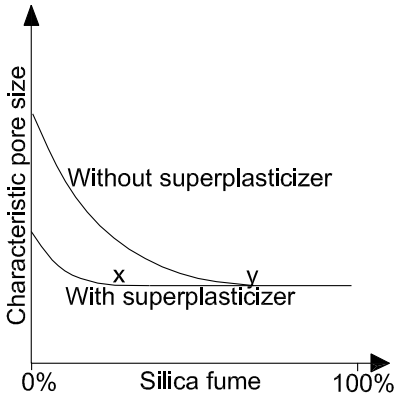

Figure 3.7 *The conceptual characteristic pore size model.*

$$\overline{x_c} = 4\tau\sqrt{\frac{\mu SC}{p\phi L}} \tag{3.7}$$

where τ is a factor accounting for the tortuosity of the system (arbitrarily chosen as 2), μ is the viscosity of the liquid, S is the total deformation of the suspension after consolidation, p is the pressure drop from top to bottom, ϕ is the porosity of the consolidated cake, and L is the height of the cake. C is a constant, specific for each consolidation process. By plotting square of the deformation against time, C can be determined as the slope of the resulting linear curve. An example is shown in figure 3.8.

For a viscosity of water at 20°C of $1.002 \cdot 10^{-3}$ Pa· s and the constant loads applied at the top of the piston, corresponding to a uniformly distributed pressure, p, of 2 and 4 MPa, the characteristic mean pore diameter could be calculated. The result is shown in figure 3.9.

Rough estimates on simple lattice packing of monosized spheres showed that this pore size range seemed realistic. The result seems to correlate well to the conceptual pore size model. However, considering the packing results and the applied consolidation force, it was expected that the same pore size be obtained in the pure cement suspension with and without superplasticizer addition. Furthermore, the general decrease in pore size, when superplasticizer was added, was unexpected. Subsequent measurements on the liquid showed no significant change in the viscosity due to the addition of the superplasticizer and the change can at present not be accounted for.

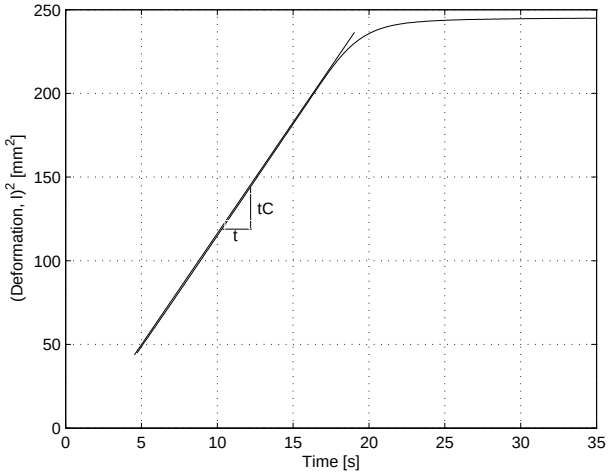

Figure 3.8 *Example of curve for determination of* C. *A 2 MPa load is applied to the suspension, consisting of 90% cement and 10% silica fume.*

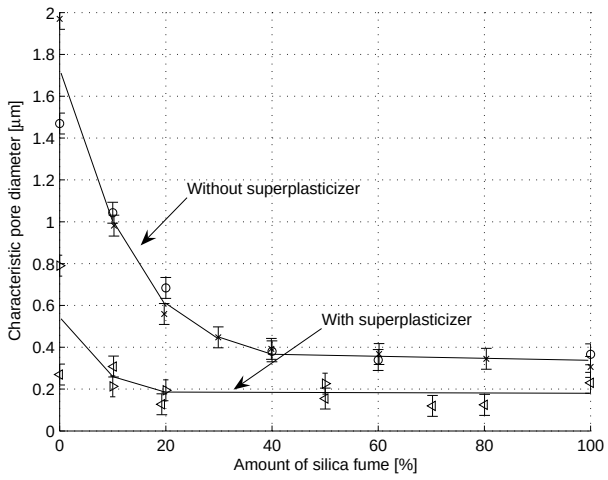

Figure 3.9 *Calculated characteristic pore diameters. Results from both 2 MPa (◁, ×) and 4 MPa (○, ▷) pressure measurements are shown. Errorbars indicate a standard deviation of 0.03 µm*

Chapter 4

Evaluation of a cryo-calorimetric method

The aim of this part of the study has been to evaluate the feasibility of using the method Low Temperature Calorimetry (LTC) for pore structure characterization of porous materials. In the following, an overview of the major findings and conclusions are presented. For further elaboration, the reader is referred to *Paper V*.

4.1 Introduction

Characterization of the porosity is an important tool in connection with both design and investigation of cement-based materials. A number of methods, both direct and indirect, are used for this purpose. Low temperature (micro) calorimetry (LTC) (also called differential scanning calorimetry (DSC), cryoporometry, and thermoporometry) is one of the indirect methods. The method has been used since the late 1970'ties.

The principle of LTC is based on 1) the freezing of liquid is an exothermic process (and melting of ice is an endothermic process) and 2) at subfreezing temperatures a solid meniscus exists, whose curvature lowers the free energy of the pore liquid and induces a freezing point depression. When performing LTC, heat flow to and from a saturated porous material is measured during controlled cooling and heating, typically between 20°C and -55°C. From the resulting heat flow curves, the amount of ice formed or melted at a given temperature can be calculated. This information may be used to estimate threshold pore sizes or the pore size distribution in the material by means of the Gibbs-Thomson equation. Determination of pore size distribution from freezing point depression has been dealt with by e.g. Fagerlund (Fagerlund 1973).

Reasons for using LTC are, among others, that the method can be performed on virgin (not dried) samples and compared to water desorption is fast, i.e. can be used on young samples. However, the use of LTC and the Gibbs-Thomson equation for quantification of pore size (distribution) is based on several questionable assumptions (see e.g. (Fagerlund 1973), (Sellevold & Bager 1980)).

The study concerns an investigation of the effect of selected factors and phenomena on LTC results. These are; super-cooling, transport of liquid during freezing, dissolved ions, and thermal non-equilibrium between reference block and sample. For this purpose LTC has been undertaken on simple model materials.

4.2 Experimental

Materials
As a model material, a silica (SilicaV432) from Grace Davison, Germany, was selected. According to producer specifications, the silica contains mono sized pores with a diameter of 14 nm. Three liquids were used to saturate the silica; distilled water, distilled water with 10 weight-% NaCl and the artificial pore solution, YS, described in chapter 2.

Method
LTC was undertaken, on the saturated material, in a Low Temperature Calvet Micro Calorimeter. The calorimeter is described in e.g. (Fontenay & Sellevold 1980), (Bager 1984). Temperature cycles were made between +20°C and -50°C. As nucleation agent, silver iodide was sprinkled onto each sample prior to cooling. An overview of the experiments are shown in table 4.1.

Table 4.1 *Material combinations and cooling/heating rates*

	H_2O			H_2O+ 10% NaCl	Artificial pore solution
Rate	-1.2°C/h +1.2°C/h	-3.3°C/h +4.1°C/h	-15°C/h +15°C/h	-3.3°C/h +4.1°C/h	-3.3°C/h +4.1°C/h
pure liquid	x	x	-	x	x
saturated porous silica	x	x	x	x	

4.3 Freezing of solutions

When the temperature rises just above 0°C, ice will start to melt, but for ice to form from pure water, the temperature must drop to about -30°C (Weeks & Ackley 1986). This phenomenon is called supercooling and is caused by the lack of nucleation sites. In most cases, the supercooling of water is fairly small due to the presence of impurities facilitating nucleation. Especially silver iodide or any biological material are good nucleation agents. The measured heat flow from bulk water as a function of temperature is shown in figure 4.1 for different cooling and melting gradients. As seen, even the lowest freezing gradient induced supercooling, though a nucleation agent was used. Increasing the cooling rate caused a slightly larger supercooling. Melting began between 0.3°C and 1.5°C from the freezing point of bulk water. Furthermore, as melting takes time and the temperature continuously changes in the calorimeter, equilibrium is not obtained and some of the ice apparently melts at higher temperatures.

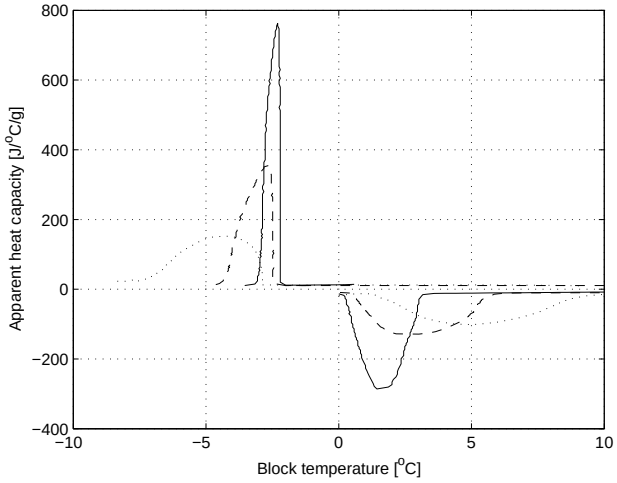

Figure 4.1 *Heat flow from bulk water (given as apparent heat capacity) as a function of block temperature. Cooling and heating rates:- ± 1.2°C/h, - - ± 3.3°C/h, ·· ± 15°C/h*

If ions are present in the water, the freezing point is depressed below that of pure water. The freezing point depression can be estimated based on a combination of Raoults law and the Clapeyron equation (Castellan 1970). Furthermore, during freezing of a salt solution, ice formation will cause an increased salinity of the remaining solution due to ions being expelled from the ice front, see e.g. (Weeks & Ackley 1986), (Wang et al. 1996). The amount of ice to be formed as a function of temperature can be estimated based on phase diagrams, if available.

The heat flow curves for the 10 weight-% NaCl solution are shown in figure 4.2. For comparison, the heat flow curves for pure water are also shown.

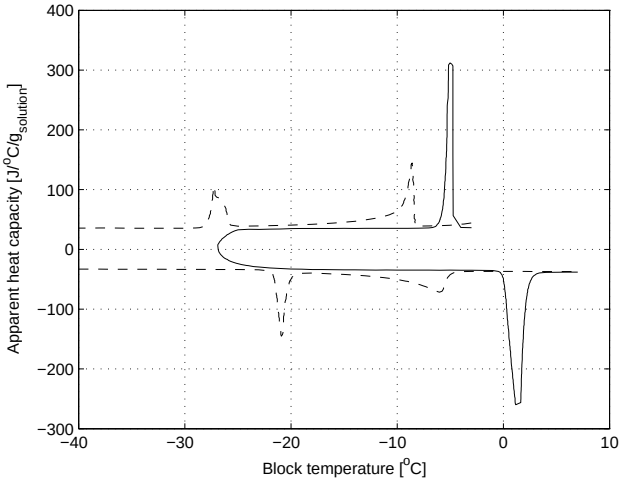

Figure 4.2 *Heat flow (given as apparent heat capacity) as a function of block temperature. − Bulk water and −− 10 weight-% NaCl solution. Cooling and heating rates -3.3°C/h and +4.1°C/h.*

According to the phase diagram for NaCl and water, a 10% aqueous sodium chloride solution will start to freeze around -8°C. With decreasing temperature the salinity of increases in the remaining solution from 10% to about 22%, when the temperature reaches -21°C. If the temperature is decreased beyond this point $NaCl{\cdot}2H_2O$ will precipitate.

Ice formation has been calculated from the phase diagram and a comparison with the ice formed and melted in the experiment is shown in figure 4.3. There seem to be some discrepancies between measured and calculated ice formation. For the heating part, non-equilibrium is again determining for the temperature at which melting actually ends. For the cooling part, the main discrepancy is the lowering of the last freezing peak by about 5°C, compared to what was expected. This discrepancy may be explained by either 1) a form of supercooling; in this case due to the fact that a nucleus resembling the shape of the salt crystal is missing, or 2) the small pockets of brine encapsulated in the pure water ice acting as small pores and causing an additional freezing point depression (Nestle 2005). Considering these effects, the calculated and the measured may be correlated.

Experiments with the less concentrated artificial pore solution, YS, showed the existence of three peaks. However, since no phase diagram is available for this system, it is not possible to calculate expected phase transformation temperatures. One point that could be observed, was that melting began around -3°C. This indicates that even in this dilute solution, the ions cause a measurable melting point depression.

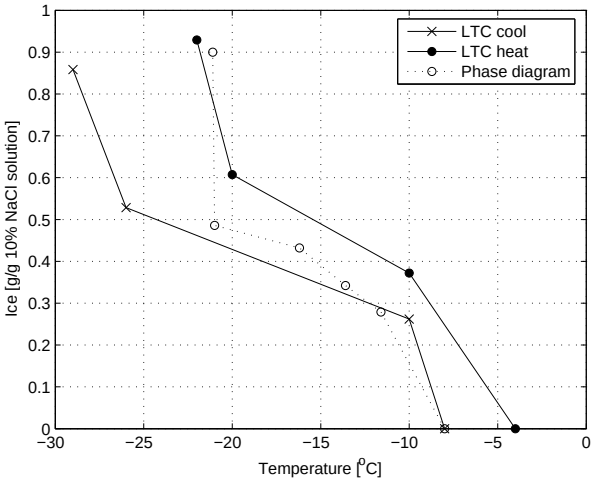

Figure 4.3 *Estimated (from phase diagram) and measured (from LTC) ice formation during cooling and heating of the 10 weight-% NaCl solution.*

4.4 Effect of pores

According to Feldman (Feldman 1970) a solid meniscus exists between liquid and ice in capillary condensed liquids at subfreezing temperatures. The curvature of the meniscus lowers the free energy of the pore liquid and induces a freezing point depression. This effect can be quantified by use of the Gibbs-Thomson equation (see e.g. (Tombari et al. 2005)). The equation describes the connection between the so-called Kelvin radius of the pore, r_K [m], and the freezing point depression, $T = T - T_0$;

$$r_K = -\frac{2 \cdot M \cdot \sigma_{l-s}}{\Delta H_{fus} \cdot \rho_l \cdot ln\left(\frac{T}{T_0}\right)} \tag{4.1}$$

where M is molar mass of the liquid [kg/mole], σ_{l-s} is the interfacial energy between liquid and solid [N/m], ΔH_{fus} is the heat of fusion [J/mole], ρ_l is the density of the liquid [kg/m^3], and T_0 and T are the freezing temperature of the bulk liquid and the pore liquid [K]. The heat of fusion, density of water, and interfacial energy of water are all temperature dependant. A description of the dependency can be found in *Paper V*.

Figure 4.4 shows the effect of cooling and heating rate on the heat flow during cooling and heating for the porous model material saturated with distilled water. Two peaks are present in each curve. The first peak is due to freezing of the bulk water, which is present between the particles. The second represents freezing of the water in the pores. The temperature at peak maximum is assumed to reflect the mean pore size. Based on the

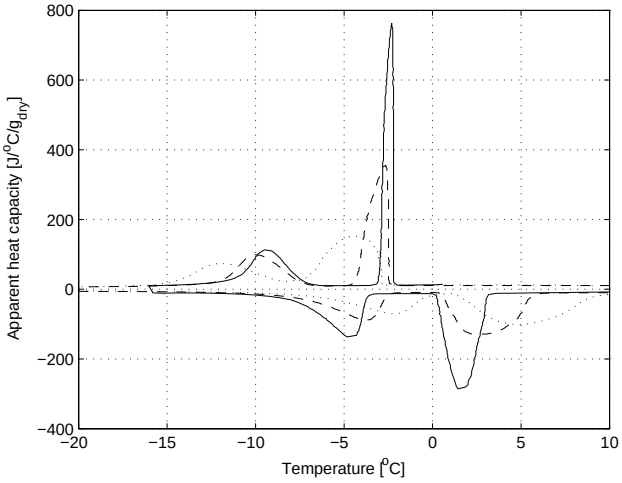

Figure 4.4 *Heat flow (given as apparent heat capacity) as a function of temperature. Silica and water. - ± 1.2°C/h, - - -3.3°C/h, +4.1°C/h, and · · ± 15°C/h.*

observed difference between the melting temperature of bulk water in equilibrium (0°C) and the measured melting peak maximum, the melting temperature at peak maximum of the pore water can be corrected, facilitating similar peak melting temperatures at all three heating temperature rates.

To investigate if any water transport takes place from the pores to the bulk during freezing and melting, calculations were carried out on the amount of ice formed in the bulk liquid and in the pore liquid. The calculations showed that only limited water transport was taking place at all cooling and heating rates.

Considering the combined effect of pores and saline solution, four peaks should now be visible, representing 1) a peak for the bulk liquid, 2) a peak for precipitation of $NaCl{\cdot}2H_2O$, 3) a peak for initiation of freezing within the pores, and 4) a peak for the precipitation of salt within the pores. Experimental results showed only three visible peaks but it is assumed that the expected peak 2) and 3) are superimposed. This assumption corresponds well to calculations of the temperature regions at which the peaks should occur.

4.5 Freezing of cement-based materials

When cement reacts with water, the resulting pore sizes are manifold and the pore liquid contains a number of different ions. In addition, bulk liquid may be present on the surface of the sample. Dissolved ions present in a cement paste pore liquid will in general cause an initial freezing point depression at 1 to 2°C. However, as mentioned previously, the

concentration of ions, and thus the freezing point depression, increases with ice formation. This effect complicates the assessment of results from LTC on porous materials with ill-defined pore liquids.

Freezing is initiated by addition of a nucleation agent on the surface, and freezing will therefore propagate through the material from the surface. For cement-based materials, where larger pores are likely to be connected to the surface through smaller pores, the propagation of ice from the surface causes ice formation to take place at intervals. Upon reaching the temperature corresponding to the freezing point of the liquid in the small pore, ice will almost simultaneously form throughout all the larger pores connected through this pore. In figure 4.5 an example of a hydrated cement-paste is shown.

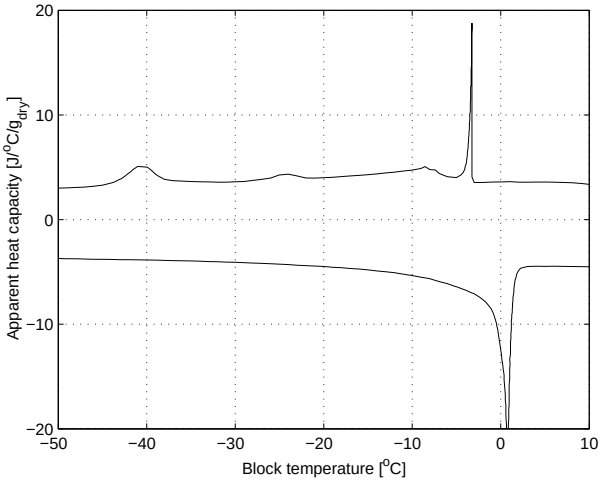

Figure 4.5 *Heat flow (given as apparent heat capacity) as a function of temperature. Cement paste, w/c=0.5 after 75 days of hydration at* $15°C$ *(Kjeldsen 2003).*

Especially the melting curve seem to reflect the manyfold pore sizes in the material, by melting gradually taking place. The peaks on the freezing curve confirm the presence of characteristic pore sizes in the hardened material.

Based on the above it seems that pore connectivity may be characterized based on freezing curves whereas the pore size distribution may be characterized using the melting curves. Cooling should be undertaken at high rate to limit migration of water to the surface, while heating should be undertaken at low rate to limit non-equilibrium. On the basis of melting point data, as a function of temperature gradient, an empirical equation was developed:

$$T_{Corr} = 1.7 \left(\frac{\Delta T}{\Delta t} \right)^{0.35} \tag{4.2}$$

The use of the Gibbs-Thomson equation for pore size determinations was found to be feasible, when corrections for non-equilibrium are made using equation (4.2).

Chapter 5

Conclusions

The effect of inter-particle forces on the consolidation behavior of fresh cement-based materials was quantified. The quantification was based on combined theoretical and experimental investigations of magnesium oxide (MgO) as a model cement material and cement and silica fume. Furthermore, the applicability of Low Temperature Calorimetry (LTC) for pore structure characterization was evaluated. The phenomena occurring during freezing were described theoretically and evaluated by experimental investigations of model materials.

MgO was used as a model cement material to avoid any hydration mechanisms perturbing the results. The model material was investigated by means of centrifugal consolidation, also known as compression rheology, and packing density profiles were obtained. The effect of inter-particle forces was investigated by addition of comb-type superplasticizers with different molecular structures and in varying dosages. Based on assumptions of polymer absorption conformation, a relation between adsorbed layer thickness and obtained packing density was established. It was found, that an increased length of the side chains of the adsorbed superplasticizers reduces the inter-particle bond strength, and thus the yield stress and results in an increased packing density. This is consistent with an increase in the range of the polymer-induced steric repulsion. Compression rheology studies at different dosages of one superplasticizer suggested that a reduction in the surface coverage increases the compressive yield stress. A linear relation was found between the obtained packing density of the centrifuged suspensions and the surface coverage at low dosage. A quantitative link between the molecular structure and resulting adsorption thickness of the superplasticizers, and the compressive rheological behavior was established.

Following the quantification of the effect inter-particle forces on a model material, combinations of cement and silica fume was investigated with and without superplasticizer addition. Assuming the particle size of cement to be 10 μm and that of silica fume to be 100 nm, the relevance of the forces acting on and between these particles was evaluated. It was found that in a cement-based suspension, anionic superplasticizers are prevented from adsorbing onto the negatively charged silica fume particles. Nevertheless, the surface properties of the silica fume should be able to keep them from agglomerating with each other. Any existing agglomeration may be ascribed to fusion of the silica fume particles

during the production stage. It was also shown that there may be extensive cement-silica fume agglomeration. However, the addition of an anionic comb-type superplasticizer inferring a repulsive steric layer around each cement particle may prevent this. The size and surface properties of cement may cause cement-cement agglomeration, the extend of which may be reduced but not removed, by superplasticizer addition. Based on the inter-particle force calculations and considerations on geometrical packing, conceptual packing and pore size models were proposed. The validity of the models was investigated by compressive consolidation experiments on combinations of cement and silica fume with and without superplasticizer addition. The employed consolidation equipment enabled the simultaneous determination of flow through the material and obtained packing density. Subsequent modelling of the consolidation process and use of the Hagen-Poiseuille equation made it possible to determine a characteristic mean pore diameter in the studied systems. This method may be used to evaluate transport characteristics in fresh cement-based systems. The experimental results verified the proposed conceptual packing model. The pore size model overall correlated with experiments, although some deviation was observed.

Finally, the effect of selected factors and phenomena on Low Temperature Calorimetry (LTC) results was investigated in order to determine the possibilities and limitations of using LTC for characterization of the porosity of cement-based materials. The principle of LTC is based on the fact that water in pores freezes at a lower temperature than free water. LTC was carried out on a model material with mono-sized pores and different aqueous solutions. It was shown that supercooling, general lack of equilibrium, bottle neck pores, and ions being expelled during freezing, make assessment of heat flow curves from heating and cooling of cement-based materials a delicate matter. Nevertheless, it was proposed that LTC may be used for characterization of pore connectivity based on cooling curves, and pore size distribution, based on the heating curve. The measured temperature was proposed corrected for non-equilibrium between the sample and the reference block. Furthermore, it was showed that corrections should be made for the effect on the freezing point depression of the varying ionic concentration in the non-frozen part of the pore solution.

The first part of the project has resulted in a comprehensive understanding of the effect of inter-particle forces on cement-based materials. The inter-particle forces have been quantified theoretically as well as experimentally, and it has been shown that it is necessary to implement them in packing and pore size models in order to account for possible agglomeration of particles. This will facilitate an accurate description of the initial microstructure of a cement-based material and by use of structure-property models, in turn enable the reliable design of concrete materials with given properties.

As a results of the second part of the project, the evaluation of the method for pore structure characterization (LTC) will enable a more reliable assessment of the pore structure of hardened cement-based materials. The method may especially assist in the characterization of the materials with regards to percolated pore space and existence of pores with sizes that may mitigate or facilitate the transport of harmful substances.

5.1 Recommendations for future work

In *Paper II*, an attempt was made to establish a quantitative link between the molecular structure of the employed superplasticizers and the compression rheology behavior of the model system, at sub-surface coverage. However, a more robust description of the average inter-particle force at sub-surface coverage is needed.

The conceptual model proposed in *Paper IV* should be implemented in an existing structure-property model, so that the initial particle interactions may be modelled correctly. One of the challenges in doing so is to avoid or minimize the extensive computational time, calculations of particle-particle interactions could cause.

As discussed in *Paper V*, possible effects of cracking during freezing and thawing should be considered. This could for instance be done by examining epoxy-impregnated thin sections of the model material after an LTC-cycle. The directional solidification technique employed in (Wang et al. 1996) where the solid/liquid interface in a saturated pore can be monitored continuously during freezing, could also be beneficial, in order to determine at which time possible cracking occurs.

Bibliography

Aïm, R. & Goff, P. (1967), 'Effet de paroi dans les empilements dsordonns de sphres et application la porosit de mlanges binaires', *Powder Technology* **1**, 281–290.

Bager, D. (1984), Ice formation in hardened cement paste, Technical Report 141/84, Technical University of Denmark.

Bager, D. & Sellevold, E. (1986*a*), 'Ice formation in hardened cement paste, part i - room temperature cured pastes', *Cement and Concrete Research* **16**.

Bager, D. & Sellevold, E. (1986*b*), 'Ice formation in hardened cement paste, part ii - drying and resaturation on room temperature cured pastes with variable moisture contents', *Cement and Concrete Research* **16**.

Bentz, D. P. (1997), 'Three-dimensional computer simulation of cement hydration and microstructure development', *American Ceramic Cociety* **80**(1), 3–21.

Bentz, D. P. (2004), 'Capillary porosity depercolation/repercolation in hydrating cement pastes via low temperature calorimetry measurements and cemhyd3d modeling', *Submitted to Cement and Concrete Research* .

Bentz, D. & Stutzman, P. (1994), 'Evolution of porosity and calcium hydroxide in laboratory concretes containing silica fume', *Cement and concrete research* **24**.

Bergström, L. (1997), 'Hamaker constants in inorganic materials', *Advances in Colloid and Interface Science* **70**, 125–169.

Bergström, L. (2001), *Handbook of Applied Surface and Colloidal Chemistry*, John Wiley and Sons, Ltd., chapter Colloidal Processing of ceramics.

Bergström, L., Schilling, C. & Aksay, I. (1992), 'Consolidation behavior of flocculated alumina suspensions', *J.Am.Ceram.Soc.* **75**(12), 3305–3314.

Bøhm, A. (2005), Effekt af blandeintensitet på cement-baserede materialer, Master's thesis, Technical University of Denmark, Dept. of Civil Engineering. In danish.

Castellan, G. (1970), *Physical Chemistry*, Addison-Wesley Publishing Company.

de Gennes, P. (1987), 'Polymers at an interface; a simplified view', *Adv. in Colloid and Interface Science* **27**, 189–209.

de Larrard, F. (1999), *Concrete Mixture Proportioning - A Scientific Approach*, Modern Concrete Technology, E&FN SPON.

Diamond, S. (2003), Densified silica fume - it is what you think it is?, *in* 'Proceedings of Advances in Cement and Concrete', Copper Mountain, Colerado, USA, pp. 233–248.

Fagerlund, G. (1973), 'Determination of pore-size distribution from freezing-point depression', *Materials and Structures* **33**(6), 215–225.

Feldman, R. (1970), 'Length change-adsorption relations for the water-porous glass system to $-40°c$', *Canad. J. of Chem.* **48**, 287–297.

Flatt, R. & Houst, Y. (2001), 'A simplified view on chemical effects perturbing the action of superplasticizers', *Cement and Concrete Research* **31**, 1169–1176.

Flatt, R., Houst, Y., Bowen, P., Hofmann, H., Widmer, J., Sulser, U., Maeder, U. & Burge, T. (1998), Effects of superplasticizers in highly alkaline model suspensions containing silica fume, *in* 'Sixth CANMET/ACI international conference on Fly ash, Silica fume, slag and natural pozzolans in concrete', Vol. 2, American Concrete Institute, Farmington Hill, Mi, USA, pp. 911–930.

Flatt, R. J. (1999), Interparticle Forces and Superplastisizers in Cement Suspensions, PhD thesis, Ecole Polytechnique Federale Lausanne.

Flatt, R. J. (2004*a*), 'Dispersion forces in cement suspensions', *Cem Concr Research* **34**, 399–408.

Flatt, R. J. (2004*b*), 'Towards a prediction of superplasticized concrete rheology', *Materials and Structures* **37**, 289–300.

Fontenay, le sage de, C. & Sellevold, E. (1980), Ice formation in hardened cement pastes - i. mature water-saturated pastes, *in* 'Durability of Building Materials and Components', ASTM STP 691, pp. 425–454.

Glavind, M. & Stang, H. (1992), A geometrical packing model as a basis for composing cement paste containing clay for high strength conrete, *in* A. Brandt & I. Marshall, eds, 'Brittle Matrix Composites 3', pp. 508–518.

Kauppi, A., Banfill, P., Bowen, P., Galmiche, L., Houst, Y., Lafuma, F., Mder, U., Perche, F., Petersen, B., Reknes, K., Schober, I., Siebold, A. & Swift, D. (2003), Improved superplasticizers for high performance concrete, *in* 'Proc. 11th ICCC', Tech book International, New Delhi, India, Durban, pp. 528–537.

Kjeldsen, A. (2003), The effect of layer silicates and silica fume on the micro-porosity of cement-based materials, Master's thesis, Technical University of Denmark, Dept. of Civil Engineering.

Maekawa, K., Chaube, R. & Kishi, T. (1999), *Modeling of Concrete Performance*, E&FN SPON.

Meeten, G. (1993), 'A dissection method for analyzing filtercakes', *Chemical Engeneering Science* **48**(13), 2391–2398.

Moukwa, M. & Aitcin, P.-C. (1988), 'Effect of drying on cement pastes pore structure as determined by mercury porosimetry', *Cement and Concrete Research* **18**.

Nestle, N. (2005), Private communication. TU Damstadt, Germany.

Pedersen, H. (1998), Particle Interactions: An AFM Study of Colloidal Systems, PhD thesis, The Technical University of Denmark.

Perche, F. (2004), Adsorption de polycarboxylates et de lignosulfonates sur poudre modle et ciments, Phd-thesis no 3041, EPFL, Lausanne, Switzerland.

Perche, F., Houst, Y., Bowen, P. & Hofmann, H. (2003), Adsorption of lignosulfonates and polycarboxylates - depletion and electroacoustic methods, *in* V. Malhotra, ed., 'Proc. 7th CANMET/ACI International Conference on Superplasticizers and Other Chemical Admixtures in Concrete', Vol. Supplementary papers, Berlin, Germany, pp. 1–15.

Pignat, C., Navi, P. & Scrivener, K. (2005), 'Simulation of cement-paste microstructure hydration, porespace characterization and permeability determination', *Materials and Structures* **38**, 459–466.

Russel, W., Saville, D. & Schowalter, W. (1989), *Colloidal Dispersions*, Cambridge University Press.

Sakai, E. & Daimon, M. (1997), Dispersion mechanisms of alite stabilized by superplasticizers containing polyethylene oxide graft chains, *in* V. Malhotra, ed., 'Proceedings of the 5th Canmet/ACI International Conference on Superplasticizers and Other Chemical Admixtures in Concrete', number SP-173, American Concrete Institute, Detroit, pp. 187–202.

Schober, I. & Mäder, U. (2003), Compatibility of polycarboxylate superplasticizers with cement and cementitious blends, *in* V. Malhotra, ed., 'Proc. 7th Canmet/ACI Int. Conf. on Superplasticizers and Other Chemical Admixtures in Concrete', number SP-217, American Concrete Institute, Farmington Hills, pp. 453–448.

Sellevold, E. & Bager, D. (1980), Low temperature calorimetry as a pore structure probe, *in* '7th International Congress on the Chemistry of Cement', Vol. 4, Paris.

Stovall, T., De Larrard, F. & Buil, M. (1986), 'Linear packing density model for grain mixtures', *Powder Technology* **48**(1-12).

Stroeven, P. & Stroeven, M. (2001), 'Space approach to concrete's space structure and it's mechanical properties', *HERON* **46**(4), 265–289.

Tombari, E., Salvetti, G., Farrari, G., & Johari, G. (2005), 'Thermodynamic functions of water and ice confined to 2 nm radius pores', *Chemical Physics* **122**.

Toufar, W., Born, M. & Klose, E. (1976), 'Beitrag zur optimierung de packingsdichte polydisperser krniger systeme', Freiberger Forschungsheft A 558.

Uchikawa, H., Hanehara, S. & Sawaki, D. (1997), 'The role of steric repulsive force in the dispersion of cement particles in fresh paste prepared with organic admixtures', *Cem and Concr Res* **27**(1), 37–50.

van Breugel, C. (1997), *HYMOSTRUC - Simulation of hydration and formation of structure in hardening cement-based materials*, second edn, Delft University Press.

Villadsen, J. (1992), Pore structure in cement-based materials, Technical Report 277, Technical University of Denmark.

Wallevik, O. (2002), Rheology of cement suspensions, Technical report, The Icelandig Building Research Institute, 112 Keldnahold, Iceland.

Wang, K., Monteiro, P., Rubinsky, B. & Arav, A. (1996), 'Microscopic study of ice propagation in concrete', *ACI Matr. Jour.* **4**(93), 370–377.

webpage Elkem (2005), www.materials.elkem.com.

Weeks, W. & Ackley, S. (1986), *The Geophysics of Sea Ice*, NATO ASI Series, New York, chapter The growth structure and properties of sea ice, pp. 9–164.

Yamada, K. & Hanehara, S. (2001), 'Interaction mechanism of cement and superplasticizers - the roles of polymer adsorption and ionic conditions of aqueous phase', *Concrete Science and Engineering* **3**, 135–145.

Yang, M. & Jennings, H. (1995), 'Influences of mixing methods on the microstructure and rheological behavior of cement paste', *Advances in Cement Based Materials* **2**, 70–78.

Yang, R. & Yu, A. (2005), 'Dynamic simulation of the packing of fine particles'. www.simpas.unsw.edu.au/pmp/results/advancedmodelling/fine_particle_dem.

Yu, A., Liu, L., Zhang, Z., Yang, R. & Zou, R. (2003), 'Computer simulation of the packing of particles', *Int. J. Materials and Product Techology* **19**, 324–336. Nos 3/4.

Part II

Appended papers

Paper I

Centrifugal Consolidation of MgO-Suspensions - The Influence of Superplasticizers on Particle Packing

Kjeldsen, A.M., Bergström, L. and Geiker, M.
Paper in the proceedings of: *Nordic Rheology Conference, Reykjavik, Iceland, pp. 31-39, 2004.*

Centrifugal Consolidation of MgO-Suspensions - The Influence of Superplasticizers on Particle Packing

Ane M. Kjeldsen*, Lennart Bergström**, and Mette Geiker*

*Department of Civil Engineering, Technical University of Denmark DK-2800 Kgs. Lyngby, Denmark, e-mail: amk@byg.dtu.dk

**Institute for Surface Chemistry, YKI, Box 5607, SE-114 86, Stockholm, Sweden.

Paper in the proceedings of: Nordic Rheology Conference, Reykjavik, Iceland, pp. 31-39, 2004

Abstract

The effect of superplasticizers on the centrifugal consolidation behaviour of magnesia suspensions has been studied. The superplasticizers adsorb onto the MgO surface and infer a steric repulsion that reduces the degree of flocculation. The packing density profiles of the particulate cakes have been measured and the maximum packing density of the consolidated particle network is related to the inter-particle force. The implications of this simple compression rheological method for evaluating the stabilizing mechanism of superplasticizers are discussed.

1 Introduction

The durability of concrete is promoted by a low porosity of the binder, which is related to the packing of the particles and the following hydration reactions. However, the placement of concrete is facilitated by a high water content that improves the flowability. The maximum packing density, γ_m, is strongly dependent on the particle size distribution and the particle size. A broad particle size distribution usually results in a higher value of γ_m because the small particles can fit into the voids between the large particles. However, while the geometric packing rules are useful when dealing with coarse particles in concrete, like stones, the situation becomes more difficult when dealing with the smallest fraction of cement and sand and fine particle additions like silica fume. The inter-particle forces and thus the colloidal stability of the suspension have a profound influence on the packing of fine particles. If the particles in suspension are flocculated they will stick upon first contact and thus not be able to rearrange during consolidation. Colloidally stable suspensions, characterized by a repulsive inter-particle force of sufficient range and magnitude to keep the particle dispersed, usually facilitate a homogeneous mixing of powders. Due to this, the particle packing is usually not as efficient in an originally flocculated suspension as in an originally dispersed suspension (see figure 1). However, it can be easier to obtain

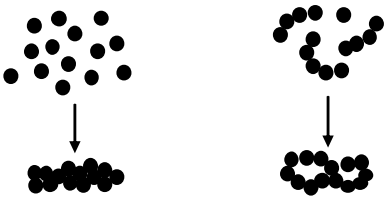

Figure 1: Consolidation behavior of dispersed and flocculated suspensions.

a uniform mass distribution throughout the consolidated cake of a flocculated suspension, whereas a stable suspension, with its net repulsive force, will have a tendency to segregate during consolidation because the denser particles will settle first (Chang et al. 1991).

This study deals with the effect of superplasticizers on the consolidation behaviour of MgO suspensions. Polycarboxylate polymers with a similar backbone but different lengths of the grafted ethylene oxide side chains have been adsorbed onto the MgO particles and the density of the particle network was determined after centrifugation. The inter-particle forces of this relatively non-reactive model system for cement were estimated by applying realistic theoretical models and using prior knowledge on the thickness of the adsorbed polymers. It was found that strongly attractive interactions result in a compressible particle network that resists consolidation while a more weakly flocculated particle network only displays a small density gradient.

2 Theory

2.1 Inter-particle forces

The dominating inter-particle forces in cement and concrete are the van der Waals, double-layer (electrostatic), and steric (polymer induced) forces. The *van der Waals* force, which is always attractive between like materials, arises from the interaction of atomic and molecular electric dipoles whose orientations are correlated so they attract each other. The van der Waals force between two particles of equal radius a and material (1) acting across a medium (2) can be approximated by ((Flatt 1999), (Pedersen 1998)):

$$F_{vdW} \approx -A_{12} f_{retardation} \frac{dH}{dh} \tag{1}$$

where A_{12} is the so-called Hamaker constant, $f_{retardation}$ is a retardation factor that incorporates the retardation of the dipole interaction over large distances, H is a geometrical factor dependant on the shape of the interacting particles and h is the separation distance. The Hamaker constant is given by ((Bergström 1997)):

$$A_{12} = \frac{3}{2} k_B T \sum_{m=1}^{\infty}{}' \sum_{s=1}^{\infty} \frac{1}{s^3} \left[\frac{\varepsilon_2(i\xi_m) - \varepsilon_1(i\xi_m)}{\varepsilon_2(i\xi_m) + \varepsilon_1(i\xi_m)} \right]^{2s} \tag{2}$$

where $\varepsilon(i\xi)$ is the dielectric response function of the material and medium, respectively. The determination of the dielectric response function for different materials and water has been described by (Flatt 1999) and (Bergström 1997) and will not be discussed further here. $f_{retardation}$ is given by:

$$f_{retardation} = \left(1 + \left(\frac{n_2 \sqrt{n_1^2 + n_2^2}}{4\sqrt{2}} \frac{h\pi\omega_{UV}}{c} \right)^{\frac{3}{2}} \right)^{-\frac{2}{3}} \tag{3}$$

where n represents the refractive indices of material and medium, c is the speed of light in vacuum and ω_{UV} is a characteristic frequency in the ultraviolet range. For two spheres, dH/dh is given by (Bergström et al. 1992):

$$\frac{dH}{dh} = \frac{4a^2 D}{6} \left[\frac{1}{(D^2 - 4a^2)^2} + \frac{1}{D^4} - \frac{2}{(D^2 - 4a^2)D^2} \right] \tag{4}$$

Where $D = 2a + h$ is the distance between the particle centers.
Immersing an inorganic particle in an aqueous solution usually results in the build-up of a charge at the solid-liquid interface. Ions of opposite charge (counterions) are attracted to the charged interface and form a diffuse ion "cloud" adjacent to the charged particle surface. The *double layer force* between two charged particles is related to the osmotic pressure created by an increase in the ion-concentration of the overlapping ion "clouds". The double layer force can be described by (Flatt 1999):

$$F_{Electrostatic} = -2\varepsilon_0 \varepsilon_r a\pi\psi_0^2 \cdot \frac{\kappa e^{-\kappa h}}{1 + e^{-\kappa h}} \tag{5}$$

where ε_0 is the permittivity of vacuum, ε_r is the relative permittivity of the medium, Ψ_0 is the surface potential of the particle and κ is the inverse of the so-called Debye-length. The Debye-length is a measure of the thickness of the double-layer, which determines the range of the double layer interaction and is given by (Hunter 1993):

$$1/\kappa = \sqrt{\frac{\varepsilon_0 \varepsilon_r k_B T}{2e^2 N_A I}} \tag{6}$$

where e is the charge of an electron, N_A is Avogadros constant and I is the ionic strength of the electrolyte. The range of the double layer interaction is controlled by the valency and concentration of ions in solution while the magnitude is controlled by the charge density of the particle.
It is also possible that a repulsive interaction can develop between two particles at close proximity due to an orientation of the molecules in the polar liquid, usually water. This effect is called the *solvation force*. For oxidized surfaces, the dominating interaction between the water molecules and the surface groups will probably be hydrogen bonding. The range of the solvation force has been reported to vary from 3 Å (one water molecule layer) up to 50 Å depending on the material, ionic strength and pH ((Butt 1991), (Raviv & Klein 2002), (Vigil et al. 1994)). There is a lack of theoretical models that go beyond a phenomenalistic description and the solvation force will therefore not be included in the calculations.
The adsorption of surfactants and polymers onto the particle surface can induce a polymer-induced interaction that can be both attractive and repulsive. The interpenetration of the polymer layers upon the close approach of two particles covered with adsorbed polymers gives rise to a repulsive interaction, the so-called steric repulsion. The net interaction of a colloidal system will either be repulsive (fully stabilized) or weakly attractive (partly stabilized) depending on the range of the steric repulsion and the van der Waals attraction. The interaction between two spheres having adsorbed polymers on the surface can be described by this simplified expression((Flatt 1999), (Bergström et al. 1992)):

$$F_{Steric} = 2\pi a \cdot \frac{\gamma_2^2}{\overline{V}_3} k_B T (\frac{1}{2} - \chi)(h - 2\delta) \tag{7}$$

where γ_2 is the solids volume fraction of chains in the adsorbed layer, V_3 is the partial molecular volume of the medium, χ is the polymer segment-solvent interaction parameter and δ is the thickness of the steric layer.
The total interaction force can then be determined by summing up all the contributions:

$$F_{total} = F_{vdw} + F_{Electrostatic} + F_{Steric} \tag{8}$$

3 Experimental

3.1 Materials

The reactivity of cement particles makes it difficult to perform experimental studies that can provide a fundamental understanding of the stabilisation mechanisms and the rheological properties of the fresh paste. It is not only the surface properties of the cement particles that change continuously with time. The hydration reactions that occur when cement is mixed with water create a supersaturated solution at a very high ionic strength of mainly Ca^{2+}, SO_4^{2-}, K^+, and Na^+ at a high pH $\approx$ 12-13. Previous work by (Flatt et al. 2003) has shown that MgO is a relatively un-reactive material that mimics the surface properties of cement, e.g. an isoelectric point (iep) at pH 12.4. Recent work has shown (Flatt et al. 2003), that MgO displays an inert period for about 3.5 hours following an initial 30 minutes reaction. The MgO used in this project has a particle size distribution (PSD) as shown in figure 2. For comparison, the PSD of a mix of ordinary Portland cement and 5 mass-% silica fume is also shown. Ordinary Portland cement has a relatively broad PSD ranging from 1 μm-100 μm while the commonly added pozzolanic filler material silica fume, has a PSD ranging from around 0.06 μm to around 1 μm. Hence, the MgO used in this study displays a significantly more narrow PSD than the cement-silica fume mix. This is motivated by the need to have a relatively well-defined average particle size for the calculations of the inter-particle forces.

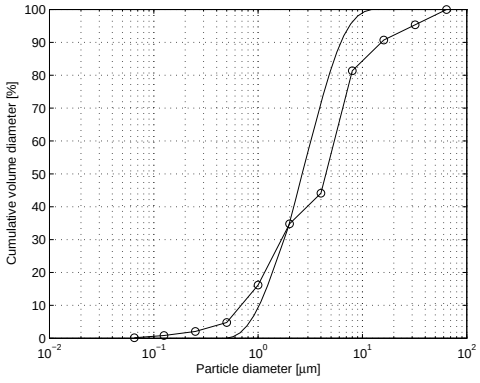

Figure 2: The particle size distributions of MgO (-) and a mix of 95 weight-% Ordinary Portland cement and 5 weight-% silica fume ($\circ$)

As the electrolyte, a concentrated salt solution with an ionic strength of 0.415 M has been used (table 1).

Table 1: Composition of the electrolyte solution.

Salt	$CaSO_4 \cdot 2H_2O$	Na_2SO_4	NaOH
g/L	2.0658	12.4960	2.9167

Four different modified anionic acrylic ester type polymers have been used in this study (PCP1, PCP2, PCP3, and PCP4). These novel types of superplasticizers mainly differ with respect to the length of the grafted ethylene oxide chains. The adsorption isotherms of these polymers and the thickness of the adsorbed layer has been determined previously (D8 2003) (see table 2).

3.2 Methods

The suspensions were centrifuged in a Mistral 2000 Small Capacity Bench centrifuge using polyallomer centrifuge tubes with the dimension ø25mm and length 89 mm. The tubes are round-bottomed and have been filled with an epoxy/lead ball mix to obtain a flat bottom, to create an even radial stress on the suspension and the resulting cake. To determine the time of equilibrium (when no further consolidation occurs) the height of the resultant cake was monitored during centrifugation.
Particle size distributions were determined by means of a Malvern Mastersizer 2000, Model APA2000 using a refractive index for MgO of 1.735 and zero light absorption.

3.3 Experimental procedure

Suspensions with a solids concentration of 20 volume-% were made in 60 mL batches in 150mL beakers. After mixing the MgO powder with the salt solution (see 1), the suspension was ultrasonicated in an ultrasonic bath for 5 minutes and then left with magnetic stirring for 30 minutes. The polymers were added and the suspension was again ultrasonicated for 5 minutes and then equilibrated for 30 minutes under magnetic stirring. Approximately 2 $\times$ 30 g of each suspension were transferred from the beaker into two weighed and marked tubes and centrifuged at 400 rpm for approximately 3 hours. The centrifugation was terminated when the consolidation process had reached steady state, determined by following the consolidation cake height. The tubes were removed from the centrifuge and the round end of the centrifuge tube was cut off and the cake was pushed out using a custom-made piston. The cake was cut into slices of a thickness of 2-3 mm

Table 2: Steric layer thickness as measured by Atomic Force Microscopy (AFM) (D8 2003)

	PCP1	PCP2	PCP3	PCP4
KCl	2	3	3-4	4-5
$CaSO_4$	1	4-5	3-4	4-5

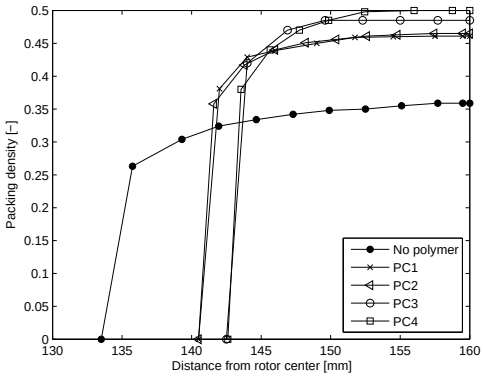

Figure 3: The packing density profiles of centrifuged MgO suspensions.

following a modification of the procedure described by (Meeten 1993). The water content, and thus the packing density of the slices, was determined by measuring the weight loss after drying at 105°C.

4 Results

The addition of superplasticizers to the MgO suspensions results in significant changes in the consolidation behaviour. Figure 3 shows the density of the centrifuged cakes at steady state. The transient consolidation process was followed, by measuring the cake height as a function of centrifugation time and it was found that a centrifugation time of 3 hours at 400 rpm was sufficient to reach steady state for this relatively coarse powder. Calculation of the area under each curve yielding the mass of the suspension shows similar masses for all suspensions indicating a good reliability of the measurements.
The density of all the centrifuged cakes increases towards the bottom of the centrifuge tube. This can be related to the stress gradient that develops in a particle network subjected to a centrifugal force field. In concentrated flocculated suspensions, a continuous particle network forms, which can support some stress up to a critical value. Once this critical stress, also called the compressive yield stress, P_y, is exceeded, the network consolidates to a higher packing density with a higher critical stress. The density profile of the centrifuged cakes thus gives information on the compressibility of the particle networks as the stress on the particle network increases towards the bottom of the cake. The compressible nature of all the particle networks suggests that all the suspensions are flocculated; a stable suspension is expected to display an essentially incompressible consolidation behavior ((Bergström et al. 1992), (Bergström 2001)). The maximum packing density, γ_m, varies with the addition of superplasticizer. The suspension where no poly-

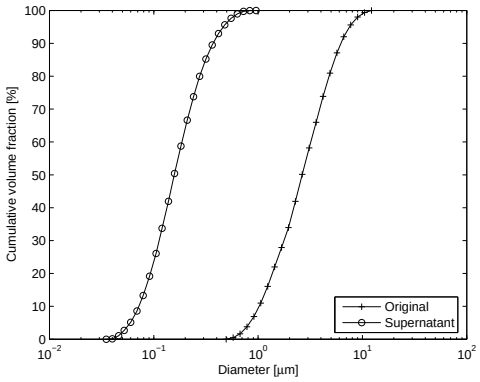

Figure 4: The particle size distribution of the original MgO powder and the fine fraction in the supernatant.

mer was added displays a relatively low maximum packing density, $\gamma_m \approx 0.36$. Adsorbing superplasticizers onto the MgO powder results in a significant increase in the maximum packing density, $\gamma_m \approx$ 0.44-0.50. The increase of the maximum packing density shows that adsorption of superplasticizers results in a significant reduction in the compressive yield stress of the particle network. It was also found that the addition of superplasticizers yields a "milky" supernatant that contains a small concentration of very fine particles. The MgO suspension without any addition of polymer results in the formation of a clear supernatant after centrifugal consolidation, which is typical for a strongly flocculated suspension. This suggests that at least a fraction of the MgO particles are stabilized by the addition of the superplasticizers. The particle size distribution was determined. It was found that it is a very fine submicron fraction that remains in the supernatants of the polymer-containing suspensions (Figure 4). Hence, addition of superplasticizers results in a segregation of the polydisperse MgO powder where the finest fraction is stabilized and not incorporated in the particle network.

5 Discussion

The consolidation behaviour of the flocculated MgO suspensions has been analysed as a function of the inter-particle forces. The inter-particle forces in the different systems have been estimated using Eqs. (1) - (8) and the input values given in table 3 and 4. Considering that the artificial electrolyte solution contains neither Cl^- or K^+-ions the AFM data for the adsorbed polymer layer obtained in the $CaSO_4$-solution are used (D8 2003). PCP2 is not included in this discussion as the effect of the sulphate ions on the conformations of the adsorbed molecules and possible desorption is unclear. The double

Table 3: Input values for the force calculations

n_1	n_2	ω_{UV}	ε_0	ε_1	γ_2	V_3	χ	I
-	-	rad/s	C^2/Nm^2	-	-	m^3	-	mol/m^3
1.735	1.325	$1.71 \cdot 10^{16}$	$8.854 \cdot 10^{-12}$	80	0.7	$2.6 \cdot 10^{-28}$	0.35	412

Table 4: Input values for the force calculations

Mix no.		1	3	4	5
ψ_0	10^{-3} V	-0.5	-0.2	0.5	0.2
δ	nm	1	3-4	4-5	-

layer force was assumed to commence outside the steric polymer layer instead of directly at the particle surface. In the calculations, a mean particle radius of 1325 nm has been used.

The calculated force curves are shown in figure 5. A positive value of the interaction force represents attraction. The figure shows how the inter-particle attraction increases as the separation distance decreases. Adsorption of the superplasticizers is assumed to infer a steep repulsive barrier that prevents the particles from coming into close contact. Hence, a polymer that yields a thick adsorbed layer, like PCP4, is expected to reduce the inter-particle bond strength more than a polymer that only results in a thin adsorbed layer, like PCP1. The values that are inserted in figure 5 represents the maximum bond strength at a separation distance that is twice the adsorbed layer thickness; hence, the point where the adsorbed polymer layers prevent the particles from coming into closer contact.

It is found that there is a good correlation between the estimated inter-particle bond strength (figure 5) and the experimentally obtained maximum packing density (figure 3). The results suggest that a thicker adsorbed polymer layer results in a particle network that is more easily consolidated to high packing fractions.

The addition of polymers to the MgO suspensions did not only facilitate consolidation of the particle network to a higher packing density, but it also stabilized a part of the particles. A suspension can be stabilized by the addition of polymers when the steric layer screens the van der Waals attraction to such a level that the particles do not stick when in contact. As a rule of thumb, a colloidally stable dispersion is obtained when the maximum inter-particle attraction is less than $2k_BT$ (where k_B is the Boltzmann constant and T is the temperature). While the range of the van der Waals attraction decreases with decreasing particle size (see Eqs. (1) and (4)), the range of the steric repulsion should be independent of particle size if the thickness of the adsorbed polymer layer is not affected by the surface curvature. Hence, a small particle may be stabilized by a specific polymer while a larger particle still will flocculate, see figure 6.

This effect can explain why a fine fraction of the MgO powder is stabilized by addition of the polymers (figure 4). The particles that remained in the supernatant have a mean

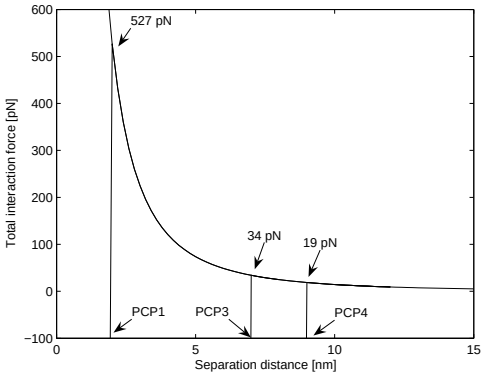

Figure 5: The calculated inter-particle force for MgO particles with PCP1, -3 and -4 adsorbed.

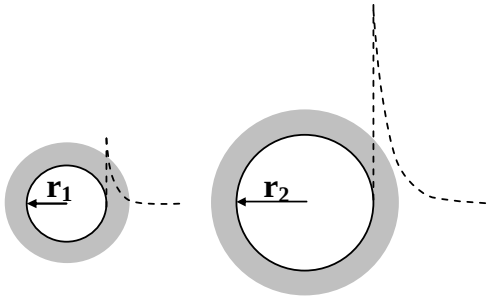

Figure 6: Schematic illustration of the increasing screening of the van der Waals attraction as a function of decreasing particle size ($r_1 < r_2$). The gray area is the steric layer and the dotted line represents the van der Waals attraction.

particle size radius of 70 nm. Estimates of the maximum attractive inter-particle energies for MgO particles of this size were performed using the procedure described previously. It was found that the estimated attractive energies are in the range of 1-2 $2k_BT$ for the PCP3 and PCP4 superplasticizers, while adsorption of PCP1 is estimated to result in a significantly higher attraction energy. It is also necessary to consider the effect that the removal of the fine fraction can have on the packing of the consolidated system. Considering only geometrical circumstances, the omission of the smallest part of the particles would decrease the maximum obtainable packing density. However, the fine fraction has a profound influence on the compressibility and consolidation resistance of aggregated particle networks. The compressive yield strength is expected to increase with a decrease in particle size, thus making it more difficult to attain a high packing density under relatively low compressive stresses. The fact that it was the same particle size fraction that stayed in suspension in all the polymer-modified experiments means that it is possible to compare the different systems.

6 Conclusion

MgO particles have been used as a model material for cement. The consolidation behaviour of the particle networks has been investigated with different polymeric additions yielding different steric layer thickness. It has been experimentally shown that the higher the maximum attractive inter-particle force is, the lower the consolidated packing density will be.

7 Acknowledgements

The participants in the EU-project Superplast are thanked for kindly providing the MgO powder and adsorption data (Laboratory of Powder Technology, EPFL, Switzerland) and superplasticizers (SIKA A.G., Switzerland). Annika Kauppi, Institute for Surface Chemistry, Stockholm is thanked for the electroacoustic data as well as helpful discussions during the experimental work. The Danish Concrete Society and "Saxhofs Gavebrev" are thanked for financial support.

References

Bergström, L. (1997), 'Hamaker constants in inorganic materials', *Advances in Colloid and Interface Science* **70**, 125–169.

Bergström, L. (2001), *Handbook of Applied Surface and Colloidal Chemistry*, John Wiley and Sons, Ltd., chapter Colloidal Processing of ceramics.

Bergström, L., Schilling, C. & Aksay, I. (1992), 'Consolidation behavior of flocculated alumina suspensions', *J.Am.Ceram.Soc.* **75**(12), 3305–3314.

Butt, H.-J. (1991), 'Measuring electrostatic, van der waals, and hydration forces in electrolyte solutions with an atomic force microscopy', *Biophys.* **60**, 1438–1444.

Chang, J., Velamakanni, B., Lange, F. & Pearson, D. (1991), 'Centrifugal consolidation of al2o3 and al2o3/zro2 composite slurries vs interparticle potentials: Particle packing and mass segregation', *Am. Ceram. Soc.* **74**(9), 2201–2204.

D8, S. (2003), Eu funded superplast project, d8 adsorption and layer thickness informations for superplastisizers. CONFIDENTIAL.

Flatt, R., Bowen, P., Siebold, A. & Houst, Y. (2003), Cement model powders for superplasticizer properties studies, *in* 'Proc. 11th ICCC', Vol. 2, Tech Book International, New Delhi, India, Durban, pp. 676–685.

Flatt, R. J. (1999), Interparticle Forces and Superplastisizers in Cement Suspensions, PhD thesis, Ecole Polytechnique Federale Lausanne.

Hunter, R. (1993), *Introduction to Modern Colloid Science*, Oxford University Press.

Meeten, G. (1993), 'A dissection method for analyzing filtercakes', *Chemical Engeneering Science* **48**(13), 2391–2398.

Pedersen, H. (1998), Particle Interactions: An AFM Study of Colloidal Systems, PhD thesis, The Technical University of Denmark.

Raviv, U. & Klein, J. (2002), 'Fluidity of bound hydration layers', *Science* (297), 1540–1543.

Vigil, G., Xu, Z., Steinberg, S. & Israelachvili, J. (1994), 'Interactions of silica surfaces', *Colloid and Interface Science* (165), 167–185.

Paper II

Relating the Molecular Structure of Comb-Type Superplasticizers to the Compression Rheology of MgO Suspensions

Kjeldsen, A.M., Flatt, R.J., and Bergström, L.
In: Cement and Concrete Research ***36****, pp.1231-1239 (2006)*

Relating the Molecular Structure of Comb-Type Superplasticizers to the Compression Rheology of MgO Suspensions

Ane M. Kjeldsen*, Robert J. Flatt**, and Lennart Bergström***

*Department of Civil Engineering, Technical University of Denmark DK-2800 Kgs. Lyngby, Denmark, e-mail: amk@byg.dtu.dk

**Sika Technology AG, Tüffenwies 16, Postfach, CH-8048 Zurich, Switzerland

***Materials Chemistry Research Group, Department of Physical, Inorganic and Structural Chemistry, Arrhenius Laboratory, Stockholm University, SE-106 91, Stockholm, Sweden

In: Cement and Concrete Research ***36****, pp.1231-1239 (2006)*

Abstract

We have investigated the effect of superplasticizers on the rheological properties of concentrated MgO suspensions. The comb-type anionic polymers with grafted polyethylene oxide chains adsorb onto the MgO surface and infer a steric repulsion where the range scale with the length of the PEO side chains. Consolidation experiments, where the packing density gradient of particle networks has been determined in response to a centrifugal force field, offer a simple, yet accurate, way of investigating flocculated, partly stabilized and stable suspensions under compression. The compression rheology behavior could be related to the estimated thickness of the adsorbed superplasticizers and a scaling analysis was used to quantitatively assess the importance of the length of the grafted PEO-chains on the magnitude of the inter-particle bond strength.

Keywords Rheology, superplasticizers, cement, suspensions, polymers

1 Introduction

Superplasticizers are able to reduce the porosity of the hardened concrete by allowing the fresh material to become workable with less water. This greatly enhances the durability and also makes it possible to substitute substantial volumes of cement with industrial waste materials, e.g. slag and fly ash (Ramachandran et al. 1998). The first generations of

superplasticizers, e.g. sulphonated naphthalene formaldehyde (SNF) and modified lignosulphonates (LS), resulted in significant improvements of the properties of fresh concrete and they are still widely used. Increasing demands on workability, high strength and enhanced durability spurred the development of new types of synthetic superplasticizers with improved performance ((Sakai & Daimon 1997), (Uchikawa et al. 1997)). These new generation superplasticizers are comb-type copolymers with an anionic backbone, commonly having carboxylic and/or sulphonate groups that can render the polymer a negative charge, and un-charged poly(ethylene oxide (PEO))- based chains of variable length grafted onto the anionic backbone at regular intervals. Numerous studies have investigated the mode of action of superplasticizers. Superplasticizers adsorb at the solid-liquid interface, and can impart a repulsive inter-particle force of electrostatic or steric origin that reduces or eliminates the adhesion between particles at close proximity. The relative importance of the double-layer and the polymer-induced contributions in reducing the degree of flocculation has been an issue of several studies. The high ionic strength and the relatively low surface charge densities in cementitious systems suggest that the steric repulsion should be dominating, in particular for the new comb-type copolymers ((Sakai & Daimon 1995), (Yoshioka et al. 1997), (Flatt 2001)). However, there are also studies suggesting that non-adsorbed polymers may play an important role, either through depletion interactions (Lewis et al. 2000) or nucleation inhibition (Kirby & Lewis 2004). There is a lack of quantitative experimental studies, relating the rheological properties to the polymer architecture, that corroborate the theoretical predictions based on calculations on inter-particle forces ((Yoshioka et al. 1997), (Flatt 2004*b*)) on cementitious systems. Systematic studies have been restricted by a limited access to a range of well-characterized polymers and also faced problems with quantification that are related to the very low yield stresses that the comb-type superplasticizers usually infer at full surface coverage. Hence, previous work has mainly reflected how the adsorbed amount at sub-monolayer coverage is related to the flow and rheology. Yamada and Hanehara (Yamada & Hanehara 2001) showed that competitive adsorption of sulfates decreases adsorption and thereby flow. Schober and Mäder (Schober & Maeder 2003) found that the spread of cement paste dispersed with various comb-type polymers varied linearly with the adsorbed amount regardless of the length of the grafted side chains. This study aims for a more fundamental understanding of the stabilization mechanism of comb-type superplasticizers. We have related the rheological behavior to the conformation of the adsorbed superplasticizers. Inert suspensions of MgO in an ionic solution, representing that of an ordinary Portland cement paste (OPC, measured on a paste with w/c=0.5 after 30 minutes), were used as a model system for cement. We have used a range of comb-type superplasticizers with a systematic variation in the length of the grafted polyethylene oxide side chains. The study was performed by centrifugal consolidation, also known as compressive rheology, which exploits rather than suffers from the tendency of a dispersed or weakly flocculated suspension to sediment. The conformations of the adsorbed polymers were estimated from scaling arguments ((Kauppi et al. 2005), (Hansen et al. 2003)) and the layer thickness and the associated interparticle bond strength could be related to the density of the consolidated particle networks.

Table 1: Properties of MgO powder after exposure to water at pH 12 (from (Perche 2004))
SSA: specific surface area

Powders	SSA* As-received powder m^2/g	SSA* after 30 min m^2/g	SSA* after 60 min m^2/g	Median Volume Diameter μm
MgO P98-C	2.51±0.01	7.53±0.03	7.55±0.08	2.90±0.5

2 Materials and Methods

2.1 Materials

2.1.1 MgO

Magnesium oxide (MgO) was used as a relatively inert model system for cement (Flatt et al. 2003). Model systems should have a pH sufficiently high to allow full ionisation of the superplasticizer (pH>12). Furthermore, the average zeta potential should be close to zero and the system should be chemically stable in the presence of divalent cations. Previous work has shown that MgO has a surface charge similar to that of cement, with a zeta potential close to zero at pH 12.5 (Flatt et al. 1997). However, recent work has shown that MgO is not completely inert at pH 12 ((Flatt et al. 2003), (Perche 2004)), and that an initial hydration to $Mg(OH)_2$ takes place. This hydration reaction essentially stops after 30 minutes and offers stable conditions for about 3.5 hours, before further conversion takes place, as determined by specific surface area measurements previously reported (Perche 2004) and given in table 1. The dead burned MgO powder used in the consolidation experiments had a density of 3.58 g/cm^3 and was from Martin Marietta Magnesia Specialties Inc. (Type MagChem P98, Baltimore, U.S.A.). This powder was air classified to obtain a powder with a particle size finer than 10 μm. All the experimental studies were performed within the 3 hour stable period after the powder has been mixed with water.

2.1.2 Electrolyte

We have chosen to work with an ionic solution that mimics the aqueous phase of the cement suspensions. Mixing cement suspensions with a water/cement ratio (w/c) of 0.5 during 30 minutes results in a supernatant that is supersaturated with respect to syngenite ($K_2Ca(SO_4)_2 \cdot H_2O$), which can result in precipitation. Dr. Yves Houst (EPFL) proposed to replace the potassium ions by sodium, which minimizes the risk of precipitation without affecting the ionic strength of the solution (unpublished work). In what follows we refer to this solution as YS (Yves' Solution). The YS is composed of 2.07 g/L of $CaSO_4 \cdot 2H_2O$, 12.5 g/L of Na_2SO_4 and 2.92 g/L of NaOH and has an ionic strength of 0.415 M, and a pH of 12.8.

Table 2: Information on the architecture of the comb-type polymers and maximum adsorbed amount at full surface coverage (from (Flatt et al. 1997), (Perche 2004))

Polymer	Average molar mass, M_w g/mole	PMA backbone length, M_w g/mole	PEO side chain length, M_w g/mole	Adsorption on MgO mg/g
PC1	23,000	6,200	1,000	1.29
PC2	113,000	30,000	1,000	1.32
PC3	25,000	6,100	2,000	1.1
PC4	61,000	7,100	5,000	1.08
PCA	35,000	9,000	550	n.a.
PCB	45,000	7,300	10,000	n.a.

2.1.3 Superplasticizers

We have used six different comb-type superplasticizers (noted PC 1-4 and A-B) in the study. All the polymers are composed of a polymethacrylic (PMA) backbone and grafted side chains of polyethylene glycol (PEG) and the length of the backbone and the grafted side chains have been systematically varied. The polymers PC1-4 were used in an EC-project called "Design and function of novel polymeric admixtures for more durable high performance concrete" and some details of these polymers have been published ((Schober & Maeder 2003), (Perche 2004), (Perche et al. 2003), (Kauppi et al. 2003)). The polymers A and B were synthesized specially for this study. Schematic drawings of the polymers are shown in figure 1. Mass average molecular weights determined by GPC are given in table 2 for the polymers. Side chain lengths are nominal values provided by the supplier. The backbone length is back-calculated from grafting degree and polymer molecular mass. Adsorption data obtained by Perche (Perche 2004) by solution depletion on suspensions of MgO is reported in the same table. The experimental procedure for those measurements is described in (Perche et al. 2003). All polymers were ultrafiltrated to eliminate unreacted components or oligomers.

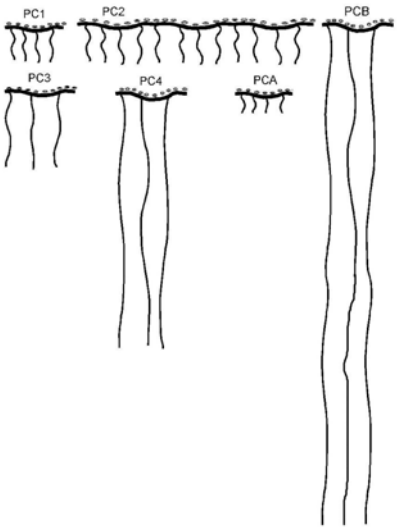

Figure 1: Schematic illustration of the molecular structure comb-type copolymers with a negatively charged polycarboxylate backbone with grafted polyethyleneoxide side chains of different length.

2.2 Experimental procedures

2.2.1 Suspension preparation and centrifugation

Concentrated MgO-suspensions at solids concentration of 20 vol% were prepared by mixing the MgO powder with the electrolyte solution YS. The MgO suspension was ultrasonicated in an ultrasonic bath for 5 minutes and then left with magnetic stirring for 30 minutes until the initial hydrolysis period had been completed. The polymers were added and the suspension was equilibrated for 30 minutes under magnetic stirring. We added an amount of polymer of 6 mg of polymer/g of the MgO powder, which ensures that the MgO surface is saturated by the polymer. One set of experiments was also performed at sub-monolayer coverage where the polymer PC 1 was added at a lower dosage; 0.41, 0.98, 2.00 and 4.00 mg polymer/g powder, respectively. The polymer-containing suspensions were transferred into a polyallomer tube with dimension ø25mm and length 89 mm. The bottom of the tubes had been made flat with an epoxy/lead ball mix, to minimise the radial stress gradient on the suspension and the resulting particle cake. The suspensions were centrifuged in a Mistral 2000 Small Capacity Bench centrifuge at 400 rpm for approximately 3 hours. The distance from the rotational centre to the bottom of the tube was 160 mm. The centrifugation was terminated when the consolidation process had reached steady state, as determined from the variation in the cake height during centrifugation. The consolidation cake was cut into slices of a thickness of 2-3 mm following

a modification of the procedure described by Meeten (Meeten 1993). The water content, and thus the packing density of the slices, was determined by measuring the weight loss after drying at 105°C. All experiments were repeated between 2 and 4 times and showed a variation in the packing density between 1 and 5% with a mean of 2%.

2.2.2 Particle size measurements

Particle size distributions of the remaining supernatant solutions were determined by light scattering using a Malvern Mastersizer 2000, Model APA2000 where particles between 20 nm to 2000 μm can be measured with an accuracy of $\pm 1\%$.

3 Results and Discussion

The rheological properties of a suspension are normally investigated by subjecting the system to a shear field. This can be done in several modes and give information about e.g. the steady shear viscosity as a function of shear rate or the shear yield stress. The yield stress is a very important parameter that is of profound importance for the flow properties of cementitious systems ((Banfill 1991), (Pashias et al. 1996)). Concentrated suspensions can develop a yield stress when the particles are flocculated resulting in the formation of a continuous particle network, which can support a stress up to a critical value, the yield stress. Weakly flocculated suspensions with relatively coarse particles, typical for cementitious systems with added comb-type superplasticizers, are very difficult to characterise using shear rheology as the particle gels are very fragile and unstable. Preliminary work on the MgO suspensions showed that it was not possible to obtain a reliable measure of the shear yield stress when the comb-type superplasticizers had been added. However, it is also possible to determine the yield stress of a particle network that is subjected to a compressive stress gradient ((Pashias et al. 1996), (Buscall et al. 1988)). The compressive yield stress is typically two orders of magnitude greater than the shear yield stress and thus more sensitive to small variations in the degree of flocculation also in weakly flocculated systems ((Buscall et al. 1988), (Channell & Zukoski 1997)).
Figure 2 illustrates how the compressive yield properties can be determined by a simple centrifugation experiment. The centrifugal acceleration infer a force to the particles that results in a settling or consolidation of the particle network. The consolidation proceeds until the stress gradient that is developed in the particle network is balanced by the strength of the particle network. When consolidation has reached steady state, the stress on the particle network must be balanced; hence we can assume that the compressive yield stress, P_y, equals the applied stress at all levels and positions in the particle network. Determining the packing density profile of the centrifuged cakes thus gives information on the compressibility and strength of the particle networks as the stress on the particle network increases towards the bottom of the cake. Sedimentation experiments, although under normal gravity, have in fact been used not only to study early hydration kinetics of cement but also to infer the dispersing character of lignosulfonate type superplasticizers in cement suspensions (Wheeler & Chatterji 1973).

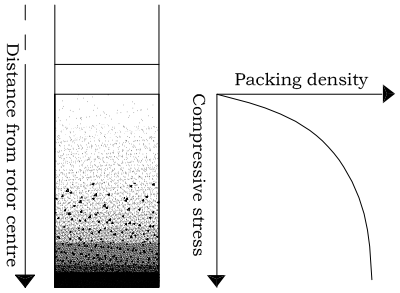

Figure 2: Schematic illustration of a consolidated particle network with the associated compressive stress curve. The packing density of the centrifuged cake increase towards the bottom of the tube as the compressive stress increases with distance from the rotor centre and with the accumulated weight of the particle network.

3.1 Compressive yield behaviour at full surface coverage

Figure 3 shows that the addition of comb-type superplasticizers to the MgO suspensions has a significant effect on the steady-state packing density profiles at a centrifugal speed of 400 rpm. All the suspensions displayed a compressible behavior with an increasing packing density towards the bottom of the centrifuge tube (increasing distance from the rotor centre).

This behavior is typical for flocculated particle networks since a fully stable suspension is expected to display an essentially incompressible consolidation behaviour ((Bergstrom 2001), (Bergström et al. 1992)). The MgO suspension without addition of any superplasticizer forms a particle network that attains a low packing density in the applied centrifugal force field (figure 3). This implies that the compressive yield stress is high and that the maximum stress that is applied at the bottom of the cake at a rotational speed of 400 rpm (approximately 6 kPa) only consolidates the MgO particle network to a packing density of $\gamma \approx 0.36$. Additions of superplasticizers result in an increase of the packing density at the bottom of the tubes, $\gamma \approx 0.43$-0.50, which shows that adsorption of the comb-type superplasticizers significantly reduces the compressive yield stress of these particle networks.

Centrifugation of the reference suspension without polymer addition resulted in the formation of a clear supernatant above the consolidated particle cake. This is a typical behaviour for a strongly flocculated suspension where all particles flocculate and are incorporated into the particle network. The addition of superplasticizers yielded a "milky" supernatant, containing small concentrations of very fine particles. Figure 4 shows one example of the particle size distribution in the "milky" supernatant with a mean diameter of 150 nm. Comparative measurements with other comb copolymers added yielded a similar behaviour and particle size in the "milky" phase. This suggests that at least a fraction of the MgO particles is colloidally stabilised by the addition of the superplasticizers and

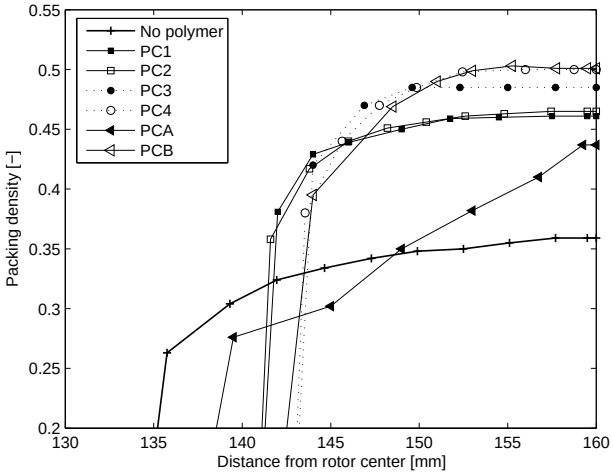

Figure 3: Packing density profiles at steady state for MgO suspensions with different comb-type superplasticizers added. The suspensions were centrifuged at 400 rpm for 3 hours.

thus not incorporated into the consolidated particle network.

The consolidation study at full surface coverage indicates that the packing density and thus also the compressive yield stress depends on the molecular structure of the comb-type superplasticizers. Figure 5 shows that the packing density obtained at the bottom of the tubes increases with the molecular weight of the grafted ethylene oxide side chains and approaches asymptotically a maximum value. This suggests that the length of the grafted side chains may control the consolidation behaviour of the particle network.

We have made an attempt to estimate the thickness of the adsorbed polymers at the surface of the MgO particles and rationalize how the polymers control the degree of flocculation. Recent direct force studies by Kauppi et al (Kauppi et al. 2005) on commercially available comb-type superplasticizers suggest that the grafted side chain are coiled rather than stretched. Scaling theory predicts that there is a transition between the two modes that depends on the distance between the chains (Flatt & Bowen 2006). The coiled chains in the so-called mushroom conformation are predicted to become stretched and transfer into the so-called brush conformation when the average spacing between chains is less than twice their hydrodynamic radius.

The adsorption data given by Perche et al (Perche et al. 2003) on PC 1, 2 and 4 can

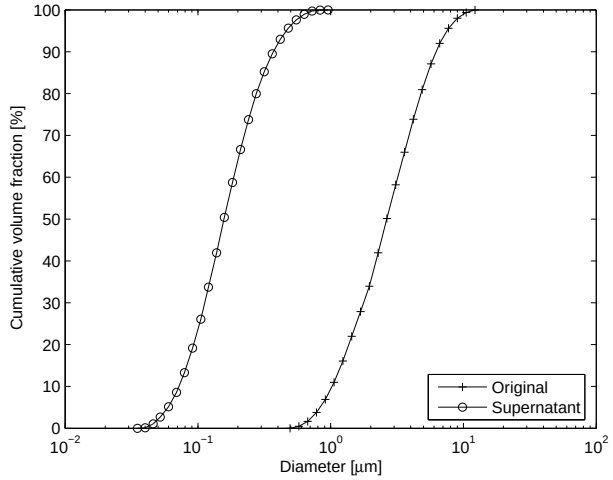

Figure 4: Particle size distribution of the MgO suspension (+) and the supernatant (o) that remains when a suspension containing the comb copolymer PC1 has been centrifuged at 400 rpm for 3 hours.

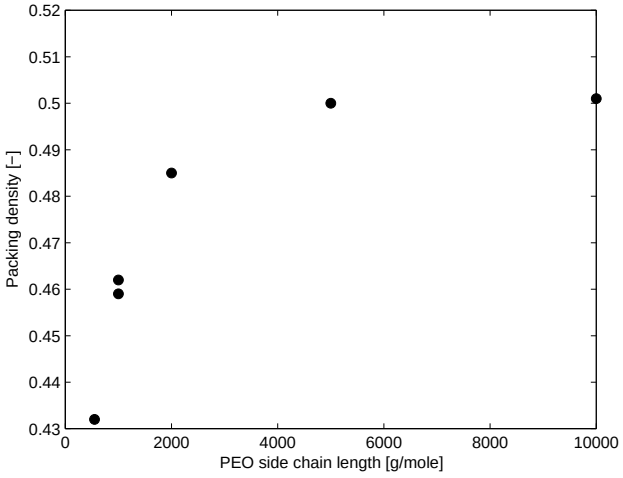

Figure 5: The highest attained packing density after centrifugation at 400 rpm, as a function of the molecular weight, of the polyethylene oxide side-chains on the superplasticizers.

be used to calculate the average area available on the surface of MgO for each PEO side chain at full surface coverage. The average separation distance D between the PEO side chains can be obtained with a simple calculation. Comparison with the estimated radius of gyration of PEO shows that the average separation distance is close to the radius of gyration but sufficiently large to support the use of the mushroom approximation in the estimation of the adsorbed layer thickness.
The layer thickness, δ, or the radius of gyration, R_F, of the adsorbed comb-type superplasticizers layer can thus be estimated from a simple expression for a mushroom conformation of the PEO side chains:

$$\delta = R_F = L_{PEO} P^{3/5} \tag{1}$$

Where L_{PEO} is the length of the ethylene oxide [-CH2-CH2-O-] segment (0.359 nm) and P is the number of segments in the chain.
Figure 6 shows that the maximum packing density of the consolidated particle networks scales with the inverse of the estimated layer thickness. The simple relation clearly corroborates the importance of the grafted PEO-side chains in imparting a steric repulsion that controls the consolidation of the particle network. The inverse scaling could also be used in future work and assist in the design of optimal architectures of new types of superplasticizers.

It should be noted that the maximum packing density that we report is attained at the applied rotational speed, 400 rpm. Experiments were also carried out at higher speeds (3000 rpm and 10000 rpm) but at these speeds, all cakes, irrespective of polymer addition, consolidated to identical heights. At 3000 rpm, the maximum obtained packing density was 0.51 while at 10000 rpm it was 0.54. Because of this, the maximum packing density obtained in the 400 rpm experiments is not the actual maximum obtainable packing density, γ_m, but the maximum obtainable packing density at these conditions.
The maximum packing density to which a particle network can pack is to a significant extent determined by geometrical factors, i.e. the shape and size distribution of the particles. The common packing density of 0.51 to which the particle networks consolidate to when the rotational speed is 3000 rpm is close to the maximum packing density that can be attained at 400 rpm when the layer thickness and thus the steric repulsion is large. This suggests that this packing density should be close to the maximum packing density. Hence, the MgO powder used in this study appears to have a relatively low maximum packing density of 0.51, which can probably mainly be related to the non-spherical shape. The slight increase in the measured packing density at even higher rotation rate (10000 rpm) may be related to compression and deformation of the hydrated surface layer of the powders and should thus not representative of the geometrical packing of the non-deformed powder.

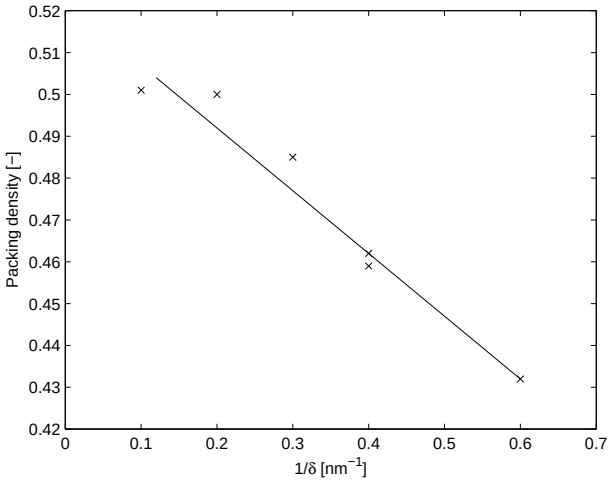

Figure 6: The highest attained packing density after centrifugation at 400 rpm, as a function of the inverse of the estimated adsorbed layer thickness, $1/\delta$.

3.2 Compressive yield behavior at sub-surface coverage

Superplasticizers are commonly added to cementitious systems at very low dosages, much below the amounts needed for full surface coverage. Figure 7 shows how the consolidation behavior varies with the amount of added PC 1 comb-type superplasticizer. We find that all the suspensions display a compressible behavior with an increasing packing density towards the bottom of the centrifuge tube (increasing distance from the rotor center). Increasing the addition of PC 1 results in an increase in the packing density at the bottom of the tubes. This suggests that an increase in the surface coverage reduces the compressive yield stress.

The relation between the maximum attained packing density at 400 rpm and the added amount of the superplasticizer PC 1 (figure 8) suggests a linear behavior between dosage and packing density at low dosage. It is interesting to relate this observation to the previous adsorption studies by Perche (Perche 2004) (reproduced in figure 9), where a linear relation between dosage and adsorbed amount in the low surface coverage region is clearly shown. This linear relation between dosage and surface coverage has also been confirmed by zeta-potential measurements (Perche et al. 2003). Hence, based on the assumption that there is a linear relation between dosage and adsorbed amount for PC1 on MgO in YS electrolyte, the data in figure 8 suggest that there should also be a linear relation between the attained packing density in centrifugal consolidation and the surface coverage at low surface coverage. At higher dosages, the situation is more delicate and a simple

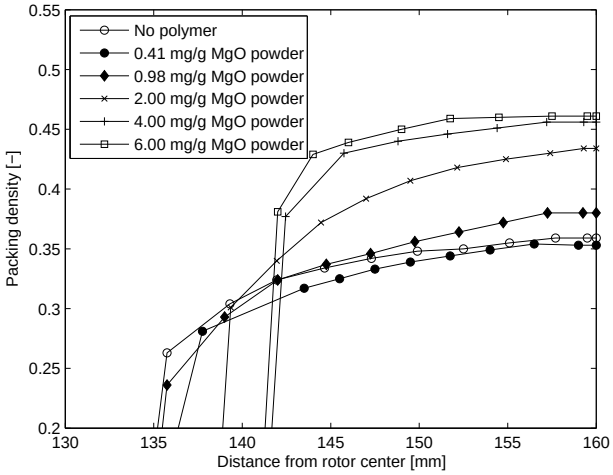

Figure 7: Packing density profiles at steady state for MgO suspensions that have been centrifuged at 400 rpm for 3 hours with various amounts of the superplasticizer PC 1 added.

linear relation is not expected to be valid.

The continuous increase of the maximum attained packing density with dosage (or surface coverage) of PC1 that asymptotically approach the packing density attained at full surface coverage also suggest that sub-monolayer coverage relates to a thinner "efficient" layer thickness compared to full surface coverage. As was shown in the previous section, it is clear that the layer thickness has a profound influence on the yield stress of the particle suspensions and from a technical perspective it is of interest in future studies to identify how the polymer structure can be optimized to yield a relatively large "efficient" layer thickness also at relatively low surface coverage.

3.3 Scaling relation between consolidation behaviour and the inter-particle bond strength

The centrifugal consolidation results show that it is the thickness of the adsorbed polymer layer that plays a decisive role in controlling the rheological properties. In this section we outline a scaling approach which links the consolidation behaviour of the polymer-coated MgO particle networks, to the magnitude of the inter-particle forces.
The compressive yield stress of a particle network, P_y can be written as a product of a packing density function $f(\gamma)$ and maximum attractive inter-particle force F_{max}:

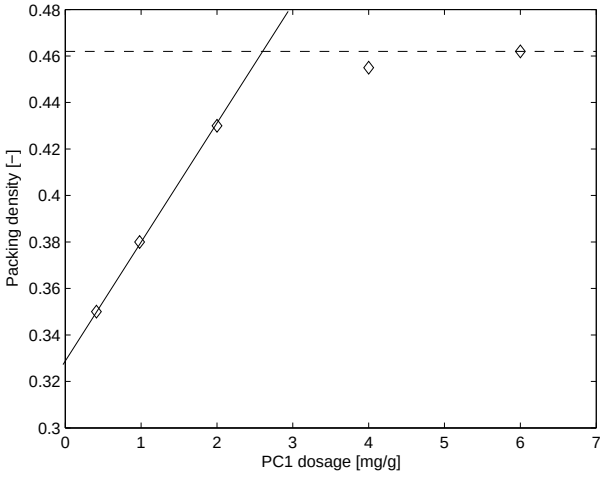

Figure 8: Packing density at the bottom of the particle networks centrifuged at 400 rpm as a function of the added amount of the PC 1 superplasticizer. The linear relation between addition of polymer and packing density at low dosage is indicated by the full line and the maximum packing density at full surface coverage is indicated by the broken line.

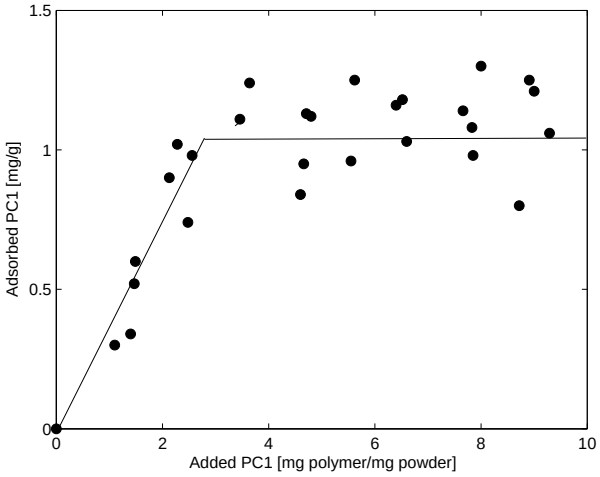

Figure 9: Adsorption isotherm of PC1 in aqueous media at pH 12. From (Perche 2004)

$$P_y \approx f(\gamma) F_{max} \tag{2}$$

In our experiments, we consolidate MgO suspensions containing various superplasticizers and measure the packing density profile. It is possible to estimate the applied stress by an integration procedure and thus obtain an estimate of how the packing density relate to P_y. Unfortunately, the small height of the consolidated cakes and the relatively small number of slices that the cake can be divided into means that we only obtain an accurate estimate of P_y at the bottom of the tube. Hence, it is difficult to determine the yield stress dependence on packing density with sufficient accuracy. However, the use of the same amount of MgO powder in all the experiments means that the values of P_y are essentially identical at the bottom of the centrifuged particle networks for all samples, within experimental error. Hence, under the condition of constant P_y, it is possible to obtain a scaling between F_{max} and $f(\gamma)$,

$$F_{max} \propto \frac{1}{f(\gamma)} \tag{3}$$

which allows us to investigate in a quantitative manner how the layer thickness of the adsorbed superplasticizers, controls the inter-particle forces and thus the consolidation behaviour.
The total inter-particle force between two particles consists of a summation of several contributions, e.g. the van der Waals force, the double layer force and the polymer induced steric force. The van der Waals force between two particles of equal radius a, and material (1) acting across a medium (2) can be approximated by ((Flatt 2004*a*), (Pedersen 1998)):

$$F_{vdW} \approx -A_{12} f_{retardation} \frac{dH}{dh} \tag{4}$$

where A_{12} is the Hamaker constant (see (Bergström 1997)), $f_{retardation}$ is a retardation factor that incorporates the retardation of the dipole interaction over large distances (Russel et al. 2001), H is a geometrical factor dependant on the shape of the interacting particles (see (Bergström et al. 1992)) and h is the separation distance. This relation simplifies to

$$F_{vdW} \approx -A_{12} \frac{a}{12h^2} \tag{5}$$

at close separation distances where the retardation is negligible.

Considering the very low surface charge and the high ionic strength that characterize these systems, it is possible to ignore the double layer contribution and simply estimate the maximum inter-particle bonding force, F_{max}, from the van der Waals interaction at a separation distance twice the layer thickness, δ, of the adsorbed polymer (Flatt 2004*b*). Since we are only doing a scaling approach, it is sufficient to write:

$$F^*_{max} \propto \delta^{-2} \tag{6}$$

The packing density dependence, $f(\gamma)$, in equation (2) has received much attention and several models have been proposed ((Buscall et al. 1988), (Channell & Zukoski 1997), (Bergström et al. 1992)). The proposed models generally account for a divergence in P_y as the maximum packing density γ_{max} is approached, e.g. by a term in the form of $(\gamma_{max} - \gamma)^{-1}$. The inhomogeneous nature of the particle network and the associated density and fraction of the network through which the stress is transmitted, is usually included in the form of a power law dependence of P_y on the packing density, e.g. as γ^n (with $n \geq 2$). We have somewhat arbitrarily chosen a simple form of the packing density dependence (Flatt & Bowen 2006):

$$f(\gamma) \approx \frac{\gamma^3}{\gamma_{max} - \gamma} \tag{7}$$

The inverse of this form of $f(\gamma)$ with a maximum packing density γ_{max}, of 0.51 has been used to evaluate the scaling behaviour between the packing density that is attained at the bottom of the tubes centrifuged at 400 rpm against the inter-particle bond strength in figure 10. We find that figure 10(a) clearly establishes a linear scaling relation for the systems at full surface coverage that corroborates the importance of the range of the steric repulsion on the consolidation behaviour. We infer that similar relations, if not the same, must exist for shear rheology, although experimental issues discussed earlier may render their determination difficult. To our knowledge it is the first time that such a quantitative relation between superplasticizer structure and rheological properties of cement-like suspensions has been established.

It is tempting to extend the scaling approach to systems with incomplete surface coverage. The main problem in doing this consists in determining a relevant average maximum attractive inter-particle force. We propose a simple *ad-hoc* approach which consists in determining the average inter-particle force by a weighted average of the layer thickness of the polymer covered surfaces:

$$F_{max} = \left(\frac{\theta^2}{\delta^2} + \frac{8\theta(1-\theta)}{(\delta + \delta_0)^2} + \frac{(1-\theta)^2}{\delta_0^2} \right) \tag{8}$$

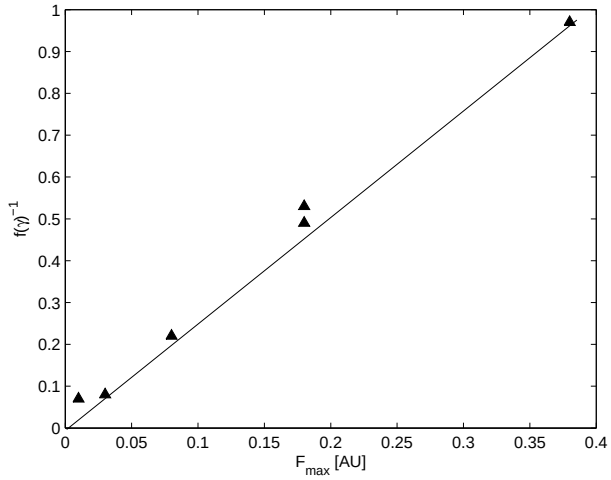

(a)

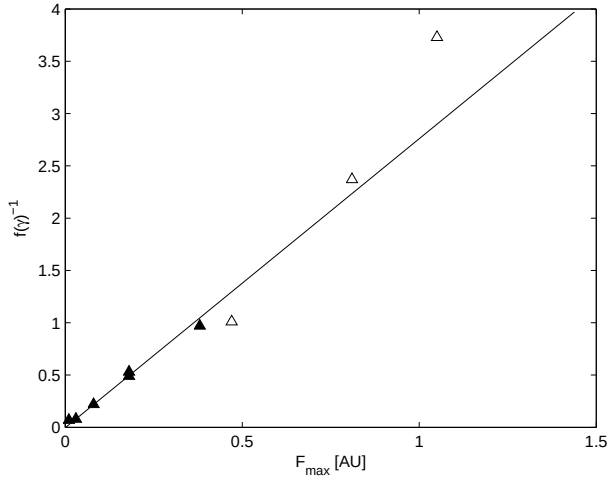

(b)

Figure 10: The inverse of the assumed packing density function $f(\gamma) \approx \frac{\gamma^3}{\gamma_{max}-\gamma}$ versus the estimated maximum attractive interparticle force, F_{max}. The points relate to the values for highest attained packing density after centrifugation at 400 rpm, and the F_{max} in arbitrary units calculated from the estimated layer thickness of the specific superplasticizer. Filled points relate to the systems at full surface coverage and the open triangles in fig b) to the systems at sub-monolayer coverage of the superplasticizer PC 1

where θ is the surface coverage and δ_0 can be viewed as a solvation layer of half the minimum distance of approach for particles that are not coated by polymers.
To use equation (8), we need an estimation of the surface coverage. In the low dosage range, we can assume a linear relation between dosage and surface coverage (Perche 2004). However, the slope of the relation is not unity, indicating a constant partition between solution and surface. We therefore need to determine a "pseudo-saturation dosage", $m*$, by which low dosages, m, can be normalized to obtain surface coverage $m/m*$. Equations (3) and (6) combine to give the scaling relation

$$\delta_\theta^* \approx \sqrt{f(\gamma)} \tag{9}$$

where δ_θ^* denotes an average layer distance that would give a force equivalent to that in equation (8). This average layer thickness is a function of surface coverage θ and increases from δ_0 to δ as θ goes from zero to one.
As stated above, for low values of surface coverage, we expect θ to be proportional to dosage m. Therefore and according to equation (9), a plot of $\sqrt{f(\gamma)}$ versus dosage is of the same nature as an equivalent plot versus surface coverage. In figure 11 we see that this relation is linear in the low surface coverage range. Extrapolating this linear trend to the point where $\sqrt{f(\gamma)}$ corresponds to full surface saturation by PC1 is can estimate of the "pseudo-saturation dosage" as about 3.5 mg/g (arrow in figure 11). We now have the value m_0 which we can use to calculate surface coverage in the low dosage range by $m/m*$.

The next step in our analysis of incomplete surface coverage is to estimate δ_0. We obtain this from the point where the force F_{max} at which $1/f(\gamma = 0.36)$ lie on the linear regression in figure 10(a) (0.36 is the packing density of the centrifuged MgO particle network that is obtained in the absence of polymer).
With the above, we get reasonable estimate of F_{max} also for sub-monolayer coverage, plotted in figure 10(b). We find that the sub-monolayer data line up quite well with the extrapolation from data of complete surface coverage (filled symbols). However, it must be emphasized that further work is needed to determine the most appropriate way of determining the average inter-particle force. Furthermore, as surface coverage and thus also the attained packing density of the consolidated particle network decreases, the estimates of $1/f(\gamma)$ will become increasingly sensitive to the exact form of $f(\gamma)$ (equation (7)). Thus, these results at incomplete surface coverage must be viewed as demonstrating the potential extension of our scaling approach rather than a definitive word on the subject.

4 Summary and conclusions

The use of a compression rheology approach based on the analysis of centrifugally consolidated suspensions of MgO particles offers a novel tool to study and quantify the effect

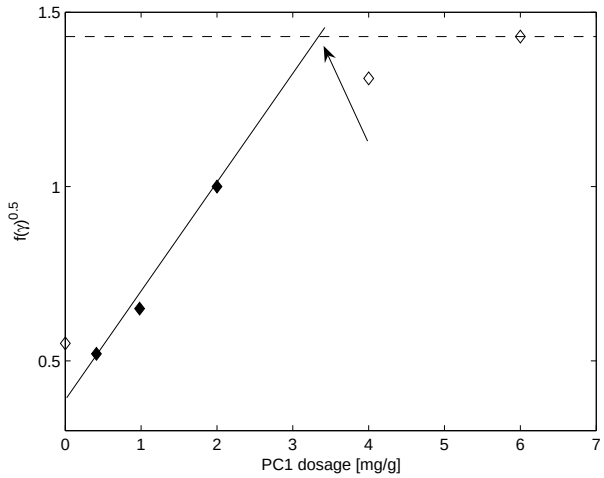

Figure 11: Plot of $\sqrt{f(\gamma)}$ versus dosage, m. The continuous line is the linear regression on the low dosage data argued for in the text. The discontinuous line is the value of $\sqrt{f(\gamma)}$ for full surface coverage by PC 1. The interception of both lines indicated by the arrow indicates the point used to determine the "pseudo-saturation dosage" $m*$ that is used to estimated surface coverage in the low dosage range by $m/m*$ (see text).

of the molecular structure of comb-type superplasticizers on the rheological properties. This simple experimental approach by-passes the issue of sedimentation and poor sensitivity that has been a common problem in steady-shear investigations. We found that an increased length of the grafted ethylene-oxide side chains of the adsorbed comb-type superplasticizers reduces the strength of the flocculated particle network and results in an increased packing density when the suspensions are consolidated at moderate rotational speeds. This is consistent with an increase in the range of the polymer-induced steric repulsion which reduces the degree of flocculation and thus also the compressive yield stress. Compression rheology studies at different dosage of a superplasticizer suggest that a reduction in the surface coverage increase the compressive yield stress. We showed that there is a linear relation between the attained packing density of the centrifuged suspensions and the surface coverage at low dosage. We have also presented scaling relations for the influence of the length of the grafted ethylene-oxide chains on the adsorbed layer thickness and the inter-particle forces. It was possible to establish a quantitative link between the molecular structure of the comb-type superplasticizers and the compression rheology behavior of cement-like suspensions, based on established models for how the compressive yield stress should vary with packing density and the inter-particle forces. Suggestions for how the quantitative approach could be developed further were illustrated by an attempt to also treat systems at sub-monolayer coverage.

5 Acknowledgements

Dr. Irene Schober (Sika Technology AG) is specially thanked for providing the purified polycarboxylate polymers for this study. The authors also acknowledge useful discussions with members of the EU project Superplast as well as financial support by the European commission for this project. Ane Kjeldsen was supported by The Danish Concrete Society, "Saxhofs Gavebrev" and SIKA Technology AG. Annika Kauppi, Institute for Surface Chemistry (now at Sandvik Tooling, Sweden) is thanked for her help in providing materials and materials data.

References

Banfill, P., ed. (1991), *Rheology of fresh cement and concrete: Proceedings of an international conference*, Spon, Liverpool 1990.

Bergström, L. (1997), 'Hamaker constants in inorganic materials', *Advances in Colloid and Interface Science* **70**, 125–169.

Bergstrom, L. (2001), *Handbook of Applied Surface and Colloidal Chemistry*, John Wiley and Sons, Ltd., chapter Colloidal Processing of ceramics.

Bergström, L., Schilling, C. & Aksay, I. (1992), 'Consolidation behavior of flocculated alumina suspensions', *J.Am.Ceram.Soc.* **75**(12), 3305–3314.

Buscall, R., Mills, P., Goodwin, J. & Lawson, D. (1988), 'Scaling behaviour of the rheology of aggregate networks formed from colloidal particles', *J. Chem. Soc., Faraday Trans.* **84**(1), 4249–4260.

Channell, G. & Zukoski, C. F. (1997), 'Shear and compressive rheology of aggregated alumina suspensions', *AIChE J.* **43**, 1700–1708.

Flatt, R. & Bowen, P. (2006), 'Yodel: A yield stress model for suspensions', *J. Am Ceram Soc.* **89**(4), 1244–1256.

Flatt, R., Bowen, P., Siebold, A. & Houst, Y. (2003), Cement model powders for superplasticizer properties studies, *in* 'Proc. 11th ICCC', Vol. 2, Tech Book International, New Delhi, India, Durban, pp. 676–685.

Flatt, R., Houst, Y., Bowen, P., Hofmann, H., Widmer, J., Sulser, U., Maeder, U. & Bürge, T. (1997), Interaction of superplasticizers with model powders in a highly alkaline medium, *in* V. Malhotra, ed., 'Fifth CANMET/ACI international conference on Superplasticizers and other chemical admixtures in concrete', number SP-173, American Concrete Institute, Farmington Hill, Mi, USA, pp. 743–762.

Flatt, R. J. (2001), *Polymers in Particulate Systems - Properties and Applications*, Marcel Dekker, Inc., chapter Polymeric Dispersions in Concrete, pp. 247–294.

Flatt, R. J. (2004*a*), 'Dispersion forces in cement suspensions', *Cem Concr Research* **34**, 399–408.

Flatt, R. J. (2004*b*), 'Towards a prediction of superplasticized concrete rheology', *Materials and Structures* **37**, 289–300.

Hansen, P., Cohen, J., Podgornik, R. & Paresgian, V. (2003), 'Osmotic properties of poly(ethylene glycols): quantitative features of brush and bulk scaling laws', *Biophysical* **84**, 350–355.

Kauppi, A., Andersson, K. M. & Bergström, L. (2005), 'Probing the effect of superplasticizer adsorption on the surface forces using the colloidal probe afm technique', *Cem Concr Res* **35**, 133–140.

Kauppi, A., Banfill, P., Bowen, P., Galmiche, L., Houst, Y., Lafuma, F., Mäder, U., Perche, F., Petersen, B., Reknes, K., Schober, I., Siebold, A. & Swift, D. (2003), Improved superplasticizers for high performance concrete, *in* 'Proc. 11th ICCC', Tech book International, New Delhi, India, Durban, pp. 528–537.

Kirby, G. & Lewis, J. (2004), 'Comb polymer architecture effects on the rheological property evolution of concentrated cement suspensions', *Am Ceram Soc* **87**(9), 1643–1652.

Lewis, J., Matsuyama, H., Kirby, G., Morissette, S. & Young, J. (2000), 'Polyelectrolyte effects on the rheological properties of concentrated cement suspensions', *Am Ceram Soc* **83**(8), 1905–1913.

Meeten, G. (1993), 'A dissection method for analyzing filtercakes', *Chemical Engeneering Science* **48**(13), 2391–2398.

Pashias, N., Boger, D., Summers, J. & Glenister, D. (1996), 'A fifty cent rheometer for yield stress measurement', *J. of Rheology* **40**(6), 1179–1189.

Pedersen, H. (1998), Particle Interactions: An AFM Study of Colloidal Systems, PhD thesis, The Technical University of Denmark.

Perche, F. (2004), Adsorption de polycarboxylates et de lignosulfonates sur poudre modèle et ciments, no 3041, EPFL, Lausanne, Switzerland.

Perche, F., Houst, Y., Bowen, P. & Hofmann, H. (2003), Adsorption of lignosulfonates and polycarboxylates - depletion and electroacoustic methods, *in* V. Malhotra, ed., 'Proc. 7th CANMET/ACI International Conference on Superplasticizers and Other Chemical Admixtures in Concrete', Vol. Supplementary papers, Berlin, Germany, pp. 1–15.

Ramachandran, V. S., Malhotra, V. M., Jolicoeur, C. & Spiratos, N. (1998), Superplasticizers: Properties and applications in concrete, Technical report, Ministry of public works and government services, Ottawa, Ontario, Canada.

Russel, W., Saville, D. & Schowalter, W. (2001), *Colloidal Dispersions*, Cambridge University Press.

Sakai, E. & Daimon, M. (1995), *Materials science of concrete*, Vol. IV, The American Ceramic Society, Westerville, OH, USA, chapter Mechanisms of superplastification, pp. 91–111.

Sakai, E. & Daimon, M. (1997), Dispersion mechanisms of alite stabilized by superplasticizers containing polyethylene oxide graft chains, *in* V. Malhotra, ed., 'Proceedings of the 5th Canmet/ACI International Conference on Superplasticizers and Other Chemical Admixtures in Concrete', number SP-173, American Concrete Institute, Detroit, pp. 187–202.

Schober, I. & Maeder, U. (2003), Compatibility of polycarboxylate superplasticizers with cement and cementitious blends, *in* V. Malhotra, ed., 'Proc. 7th Canmet/ACI Int. Conf. on Superplasticizers and Other Chemical Admixtures in Concrete', number SP-217, American Concrete Institute, Farmington Hills, pp. 453–448.

Uchikawa, H., Hanehara, S. & Sawaki, D. (1997), 'The role of steric repulsive force in the dispersion of cement particles in fresh paste prepared with organic admixtures', *Cem and Concr Res* **27**(1), 37–50.

Wheeler, J. & Chatterji, S. (1973), 'The hindered setting of cement particles in freshly prepared portland cement pastes: literature review-3', *Indian Concrete Journal* pp. 227–229.

Yamada, K. & Hanehara, S. (2001), 'Interaction mechanism of cement and superplasticizers - the roles of polymer adsorption and ionic conditions of aqueous phase', *Concrete Science and Engineering* **3**, 135–145.

Yoshioka, K., Sakai, E. & Daimon, M. (1997), 'Role of steric hindrance in the performance of superplasticizers in concrete', *Am. Ceram. Soc.* pp. 2667–2671.

Paper III

Modelling Inter-Particle Forces and Resulting Agglomerate Sizes in Cement-Based Materials

Kjeldsen, A.M. and Geiker, M.

Paper in the proceedings of: *SCC2005 - Combining the Second North American Conference on the Design and Use of Self-Consolidating Concrete and the Fourth International RILEM Symposium on Self-Compacting Concrete, Chicago, Illinois, USA, pp. 105-113, 2005*

Modelling Inter-Particle Forces and Resulting Agglomerate Sizes in Cement-Based Materials

Ane M. Kjeldsen* and Mette Geiker

Department of Civil Engineering, Technical University of Denmark DK-2800 Kgs. Lyngby, Denmark, e-mail: amk@byg.dtu.dk

Paper in the proceedings of: SCC2005 - Combining the Second North American Conference on the Design and Use of Self-Consolidating Concrete and the Fourth International RILEM Symposium on Self-Compacting Concrete, Chicago, Illinois, USA, pp.105-113, 2005

Abstract

The theory of inter-particle forces versus external shear in cement-based materials is reviewed. On this basis, calculations on maximum agglomerate size present after the combined action of superplasticizers and shear are carried out. Qualitative experimental results indicate that external shear affects the particle size distribution of $Mg(OH)_2$ (used as model material) as well as silica, whereas the addition of superplasticizers affects only the smallest particles in cement and thus primarily acts as water reducers and not dispersers.

1 Introduction

For decades now, silica fume has been used as a pozzolanic binder in concrete. It is used for its ability to improve selected engineering properties in a number of ways. It is widely recognized that silica fume increases durability by reducing the porosity of the material. Geometrically, this can be explained by the size of the silica fume particles, being about 1/100 of that of cement, and thus filling out the porosity between the cement grains. Chemically, the effect can be explained by a pronounced pozzolanic reaction (Neville 1995). However, while the size of the silica fume particles in theory is geometrically beneficial, it is also prone to agglomerate (Diamond 2003). Agglomeration is caused by the attractive van der Waals force, the effect of which increases with decreasing particle size. The addition of silica fume results in less workable mixes, requiring more water to become workable. As the addition of more water would counteract the reduction of porosity, the use of silica fume also created a need for a dispersant, i.e. superplasticizers. Another aspect of the interaction between these particles is the dispersion caused by the action of an external force, e.g. shear during mixing, and a subsequent possible reagglomeration. Assuming that a given applied shear breaks up a number of particle agglomerates (see e.g. (Sonntag & Russel 1986)), the removal of shear can result in reagglomeration of some of these particles ((Lootens 2004), (Wallevik 2003), (Hattori & Izumi 1990)). Again, it

is the action of the attractive van der Waals force causing this. The full understanding of the combined action of superplasticizers and shear on cement-based materials calls for an understanding of the adsorption of the superplasticizers as well as the effect of the inter-particle forces acting between the particles.

2 Theory

2.1 Inter-particle forces

The total inter-particle force between two particles consists of a summation of all the relevant inter-particle forces affecting the particles. In the case of cement-based materials, these are the attractive van der Waals force, the repulsive electrostatic double layer force and the repulsive polymer induced steric force. The latter can be calculated when the adsorbed steric layer thickness is known. When no polymers are adsorbed to the particles, experiments indicate (see e.g. (Zhou et al. 2001)) that a so-called solvation layer, $\delta_{solvation}$ solvation exist around each particle in an aqueous solution. The layer comes from polarisation of the water molecules and has an approximate thickness of 1 nm. By the addition of polymers, they will absorb to the surface of the particles and the solvation layer will disappear.
The van der Waals force between two particles of equal radius a and material ($_1$) acting across a medium ($_2$) can be approximated by ((Flatt 1999), (Pedersen 1998)):

$$F_{vdW} \approx -A_{12} f_{retardation} \frac{dH}{dh} \tag{1}$$

where A_{12} is the Hamaker constant (see e.g. (Bergström 1997)), $f_{retardation}$ is a retardation factor that incorporates the retardation of the dipole interaction over large distances (Russel et al. 2001), H is a geometrical factor dependant on the shape of the interacting particles (Bergström et al. 1992) and h is the separation distance. The double layer force can be described by (Flatt et al. 2003):

$$F_{Electrostatic} = -2\varepsilon_0 \varepsilon_r a \pi \psi_0^2 \cdot \frac{\kappa e^{-\kappa h}}{1 + e^{-\kappa h}} \tag{2}$$

where ε_0 is the permittivity of vacuum, ε_r is the relative permittivity of the medium, ψ_0 is the surface potential of the particle and κ is the inverse of the Debye-length. With the surface potentials usually found in cement-based suspensions of high ionic strengths, the electrostatic force becomes negligible, compared to the van der Waals force and the polymer induced steric force.

The interaction between two spheres having adsorbed polymers on the surface can be described by various simplified expressions. One expression reported by Bergström et al, (Bergström et al. 1992) for small organic acids is written:

$$F_{Steric} = 2\pi a \cdot \frac{\gamma_2^2}{\overline{V}_3} k_B T (\frac{1}{2} - \chi)(h - 2\delta) \tag{3}$$

where γ_2 is the solids volume fraction of chains in the adsorbed layer, V_3 is the partial molecular volume of the medium, χ is the polymer segment-solvent interaction parameter and δ is the thickness of the steric layer. The choice of V_3, γ_2, and χ becomes unimportant, as the steric layer thickness will dominate the expression. In reality, the adsorption of polymers will act as a wall, screening the van der Waals force at distances below the steric layer thickness.

2.2 Shear stress

Application of a constant shear stress on a cement-based suspension will disperse a number of the agglomerated particles. The more exact theory for porous clusters of many particles, subjected to fluid stresses is elaborate and complicated and an in-depth description is given in ((Sonntag & Russel 1986),(Sonntag & Russel 1987)). In the present paper, the simplified theory described in (Yang & Jennings 1995) will be used. By assuming two beads of radius r_1 and r_2, interacting in a Bingham fluid, the force acting on the particles by application of a constant shear stress (τ), is given by:

$$F_{Shear} = 3\pi r_1 r_2 \tau \tag{4}$$

It is assumed here that one large agglomerate consisting of a given number of particles can be equilibrated to one large particle, and that subjection to shear stress will break up the agglomerate into two smaller agglomerates with identical radius. The principle is shown in figure 1. Correlation between the maximum attractive inter-particle forces acting between two particles of similar size and the applied external shear stress can then be used to predict the maximum agglomerate size in a cement-based suspension after shear. However, this prediction does not take into account the reagglomeration when the shear stress is removed.

3 Experimental

A number of qualitative results, demonstrating the combined action of superplasticizers and external force on aqueous suspensions of silica fume and magnesium oxide (MgO)

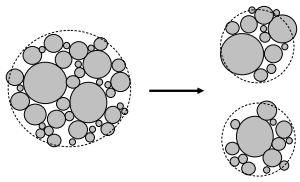

Figure 1: Principle of agglomerate break-up

Table 1: Parameters used for calculation of total inter-particle force

A_{12} J	V_3 m^3	ε_0 C^2/Nm^2	ε_r	κ nm^{-1}	γ_2	$\delta_{Solvation}$ nm	δ nm	χ
$2.37{\cdot}10^{-20}$	$2.6{\cdot}10^{-28}$	$8.84{\cdot}10^{-12}$	80	2.09	0.7	1	4	0.35

were carried out using 65 kHz ultrasound as external force source. The suspensions were made with an artificial pore solution consisting of 2.07 g/L $CaSO_4{\cdot}2H_2O$, 12.5 g/L $NaSO_4$ and 2.92 g/L NaOH and having an ionic strength of 0.415 M and a pH of 12.5. Particle size measurements were carried out using a Malvern Mastersizer 2000 and all suspensions were mixed gently by hand for 3 minutes prior to any treatment. The results are shown in figure 3(a) and 3(b) (note the different axes).

4 Results

Using equations (1) and (3), the total inter-particle force, with no stabilizing polymer addition as well as at various separation distances equal to twice the adsorption layer thickness, can be calculated. Parameters used in the calculations are shown in table 1. Shear stress has been converted into applied shear force by means of equation (4). It is now possible to determine the force necessary to break up agglomerates corresponding to any given size, given the assumptions described in the theoretical section. An example of this is shown in figure 2 (note abscissa showing radius of particle, rather than size).
In the example, it is seen that when a polymer is added and the applied shear stress has a magnitude of 5 Pa, the external forces should be able to break up agglomerates with diameters larger than approximately 1 μm (radius 500 nm). The calculations have been carried out for two suspensions, one with and one without polymer addition. Different shear stresses have been applied and the result is shown in table 2.

5 Discussion

As seen in table 2, the size of the applied shear stress necessary to obtain a given agglomerate size is reduced remarkably by the addition of the adsorbing polymer. Without

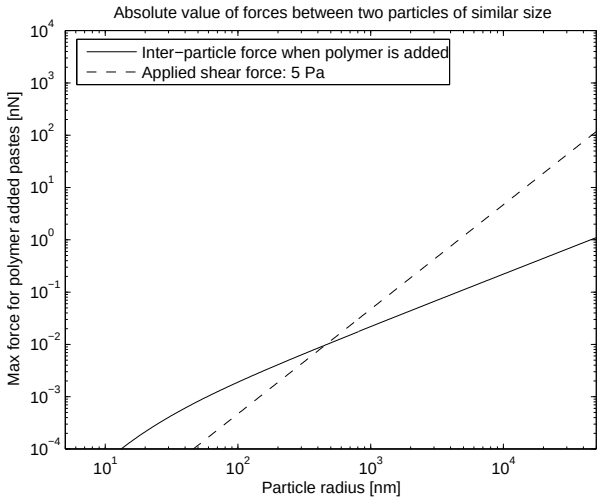

Figure 2: Comparison between inter-particle forces and external forces

Table 2: Max agglomeration size after applied shear force. Shear stresses are chosen from common stress values (Thrane 2005)

	1 Pa	5 Pa	50 Pa	100 Pa
Polymer addition	22 μm	1 μm	-	-
No polymer addition	100 μm	20 μm	2 μm	1 μm

polymer addition, achieving a max agglomerate size of 1 μm requires a shear stress of 100 Pa, while addition of polymer reduces the necessary stress to 5 Pa. As the ultimate agglomerate size of the material has a large influence on the particles packing ability, the addition of superplasticizer will obviously also have a great effect on the obtained durability of the material. In the calculations, a polymer adsorption thickness of 4 nm has been assumed. However, this thickness can vary from polymer to polymer and is for industrial superplasticizers not known.

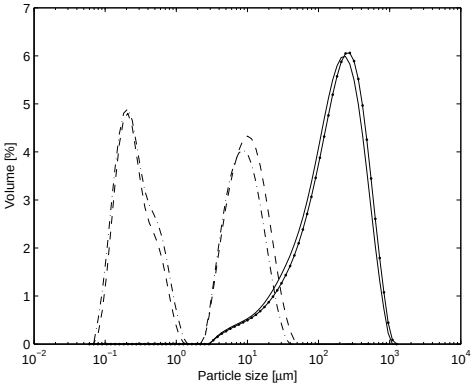

(a) Silica fume

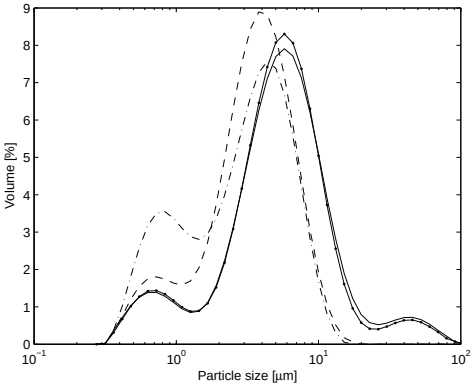

(b) $Mg(OH)_2$

Figure 3: – No treatment, —●— addition of superplasticizer, –– ultrasonic treatment, –- addition of superplasticizer and ultrasound treatment

Figure 3(a) shows that addition of superplasticizers to an aqueous silica fume suspension has no effect on the resulting particle size distribution. Contrary, ultrasound treatment

changes the resulting particle size distribution pronounced while a combination with superplasticizer shows no additional effect. The mean particle size is given by the supplier as being well below 0.5 μm (webpage Elkem 2005), but it seems that the mean particle size as supplied is quite a bit larger than that. This feature is probably caused by a number of the particles being sintered together during the production process (Diamond 2003). Thus, to obtain the beneficial geometrical effect of the single particles, mechanical impact alone is necessary. For $Mg(OH)_2$, like for silica fume, the addition of superplasticizer alone does not alter the particle size distribution. Ultrasonic treatment clearly disperses some of the larger particle agglomerates, reducing the maximum particle size from 100 μm to about 20 μm, followed by an increase in the smaller particles. The combination of ultrasonic treatment with superplasticizer addition does not affect the largest particles, but causes a decrease in particles with sizes between 2 μm and 7 μm, combined with an increase in particles with sizes below 2 μm. This can be explained by the fact that the attractive inter-particle force increases with decreasing particle/agglomerate size. This in turn means that the largest agglomerates can be broken by mechanical alone, but to be able to break up the smallest agglomerates in $Mg(OH)_2$, shear must be combined with addition of superplasticizer, decreasing the attractive forces between the particles.

6 Conclusion

According to theory, the necessary shear to break up agglomerates of a given size is reduced markedly by the addition of superplasticizers. The action of superplasticizers is to absorb to the surface of cement grains. This has two effects: 1) reduction of the water demand of cement and 2) partly screening the attractive van der Waals force. This liberates water and facilitates a more homogeneous mixing of concretes with silica fume addition. The smallest agglomerates in $Mg(OH)_2$ were dispersed partly by ultrasound, partly by superplasticizer addition, while the largest part was affected only by the ultrasound treatment. Silica fume is purely dispersed by physical agitation and seems unaffected by the addition of superplasticizer.

References

Bergström, L. (1997), 'Hamaker constants in inorganic materials', *Advances in Colloid and Interface Science* **70**, 125–169.

Bergström, L., Schilling, C. & Aksay, I. (1992), 'Consolidation behavior of flocculated alumina suspensions', *J.Am.Ceram.Soc.* **75**(12), 3305–3314.

Diamond, S. (2003), Densified silica fume - it is what you think it is?, *in* 'Proceedings of Advances in Cement and Concrete', Copper Mountain, Colerado, USA, pp. 233–248.

Flatt, R., Bowen, P., Siebold, A. & Houst, Y. (2003), Cement model powders for superplasticizer properties studies, *in* 'Proc. 11th ICCC', Vol. 2, Tech Book International, New Delhi, India, Durban, pp. 676–685.

Flatt, R. J. (1999), Interparticle Forces and Superplastisizers in Cement Suspensions, PhD thesis, Ecole Polytechnique Federale Lausanne.

Hattori, K. & Izumi, K. (1990), *Rheology of fresh cement and concrete*, E&F Spon, chapter A new viscosity equation for non-Newtonian suspensions and its application, pp. 83–92.

Lootens, D. (2004), Cements and concentrated model suspensions. Flow, jamming and flocculation, PhD thesis, Université Pierre at Marie Curie.

Neville, A. (1995), *Properties of Concrete*, Longman.

Pedersen, H. (1998), Particle Interactions: An AFM Study of Colloidal Systems, PhD thesis, The Technical University of Denmark.

Russel, W., Saville, D. & Schowalter, W. (2001), *Colloidal Dispersions*, Cambridge University Press.

Sonntag, R. & Russel, W. (1986), 'Structure and breakup of flocs subjected to fluid stresses - i. shear experiments', *Journal of Colloid and Interface Science* **113**(2), 399–413.

Sonntag, R. & Russel, W. (1987), 'Structure and breakup of flocs subjected to fluid stresses - ii. theory', *Journal of Colloid and Interface Science* **115**(2), 378–389.

Wallevik, J. (2003), Rheology of particle suspensions. Fresh concretes, mortar and cement paste with various types of lignosulfonates, PhD thesis, Norwegian University of Science and Technology.

webpage Elkem (2005), www.materials.elkem.com.

Yang, M. & Jennings, H. (1995), 'Influences of mixing methods on the microstructure and rheological behavior of cement paste', *Advances in Cement Based Materials* **2**, 70–78.

Zhou, Z., Boger, D., Scales, P. & Healey, T. (2001), *Polymers in Particulate Systems: Properties and Applications*, Marcel Dekker, New York, chapter Shear and compressional rheology principles in ceramic processing, pp. 157–195.

Paper IV

Relating initial particle packing and characteristic pore size to inter-particle forces

Submitted to Cement and Concrete Research
Kjeldsen, A.M., Stang, H., and Geiker, M.

Relating inter-particle forces in fresh cement-based materials to packing and mean pore size

Ane M. Kjeldsen*, Henrik Stang, and Mette Geiker

Dept. of Civil Engineering, Technical University of Denmark DK-2800 Kgs. Lyngby, Denmark, e-mail: amk@byg.dtu.dk

Submitted for publication in Cement and Concrete Research

Abstract

Calculations of inter-particle forces in fresh cement-silica fume suspensions were carried out and in combination with considerations on geometrical packing, a conceptual model for packing and pore size was proposed. To determine the validity of the model, cement-based suspensions with varying additions of silica fume, and with and without superplasticizer were studied experimentally by compressive consolidation. The employed consolidation equipment enabled the simultaneous determination of flow through the material and obtained packing density. Modelling the consolidation process made it possible to determine a characteristic mean pore diameter in the studied systems and showed, as expected, a significant effect of addition of silica fume as well as superplasticizer. The addition of the superplasticizer or application of high enough consolidation pressure caused the packing characteristics of the cement-silica fume mix to resemble that of larger grain size populations, where inter-particle forces are negligible. Experimental results were found to correlate well to the proposed model.

Keywords Consolidation, particle packing, mean pore size, inter-particle forces, Portland cement, silica fume

1 Introduction

The durability of concrete structures is dependant on a variety of factors, like pore structure, crack formation, and environmental exposure. The ability of the concrete matrix to resist transportation of harmful substances like chloride and sulphate ions is a determining factor in the durability of the concrete and reinforcement. In terms of water transport ability, the minimum permeable pore diameter of a porous network is of major importance. In non-saturated systems, capillary forces and surface tension of the pore liquid cause the size of the involved pores to be of major relevance. The larger the connected pores are, the greater the permeability will be.

Addition of a colloidal (i.e. sub-micron) sized material, e.g. silica fume, may help decrease

larger pores in cement-based materials by filling out the cavities between the cement particles. In a hydrated cement-based material, a combination of sub-micron particles, e.g. silica fume, and cement may be optimal for several reasons. Besides the initial reduction of the porosity, it may act as nucleation agent, facilitating a more homogeneous material. Since it is pozzolanic, it will also cause the formation of more C-S-H gel (cf. (D.P.Bentz et al. 2000)), which has very poor transport abilities (Garboczi & Bentz 1996). Disadvantages to silica fume addition may be an increased early age cracking and a reduced critical chloride content limit. Also, adding silica fume to cement results in much less workable mixes. Increasing workability by addition of more water will also increase the porosity. Thus, the addition of silica fume has created a need for a dispersant, i.e. superplasticizers. Superplasticizers can act on cement-based systems by different mechanisms, depending on the type of superplasticizer used. In the current study, a polycarboxylate polymer is used. This superplasticizer acts by adsorbing onto the particle, imparting a repulsive steric force, thus reducing or eliminating the attractive forces that causes small particles to agglomerate. The adsorption of the superplasticizer at the same time reduces the need for water, by dispersing the agglomerated particles, and thus releasing the water trapped in the agglomerates (Ramachandran et al. 1998).

Colloidal stability of the system has a profound influence on the packing of the system. Instable particles in suspension are affected by attractive forces, causing them to stick to each other upon contact. If the particles have been stabilized, e.g. via the adsorption of superplasticizers, they will be dispersed and able to re-arrange. Consolidation of flocculated and stable suspensions, using a model cement material have been investigated in (Kjeldsen et al. 2004) and (Kjeldsen et al. 2006). These investigations benefitted from the fact that suspension instability renders it difficult for the particles to rearrange during consolidation and the resulting particle network may be very porous. Oppositely, stabilized particles will be able to rearrange during consolidation thus creating a more dense particle network. The principle is shown in figure 1.

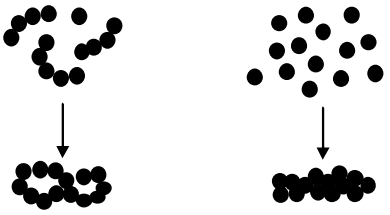

Figure 1: Consolidation behavior of flocculated (instable, left) and dispersed (stable, right) colloidal suspensions.

The studies on the model material showed a profound influence of the adsorbed superplasticizer on resulting packing density and a correlation between the superplasticizer adsorption thickness and subsequent calculated inter-particle forces was found.

The aim of this study is, by means of consolidation experiments, to examine the effect of inter-particle forces on the packing and pore structure of suspensions of cement and silica fume in combination. The employed consolidation equipment enabled rapid determination of flow through the material and obtained packing density. Combining flow measurements with knowledge on flow through a pipe, characteristic mean pore diameters were calculated.

2 Theory

2.1 Geometry

The packing behavior of aggregate (sand and stones) in concrete is well understood and a number of models have been developed to predict packing density of granular mixes of sand and stones. The linear packing model, developed by Stovall and co-workers (Stovall et al. 1986) and expanded by de Larrard (de Larrard 1999) is an example of such a model. The linear packing model deals with the concept of residual packing density, β_i, being the packing density of each grain class, i, on its own, and the mutual quantities of each grain class, y_i.

In the development of the linear packing model, two extreme situations are considered. The first situation is a binary mix (mix of two grain classes) with no interaction, meaning that the diameter, d, of one is much larger than the other. The other extreme is a binary mix with total interaction meaning that the two classes of grains have the same diameter but different residual packing densities. The two extremes are then combined in a general expression using a so-called packing restriction and subsequently expanded to multi-component mixtures. The expression for the packing in the general case, with n classes, is shown in equation (1) (de Larrard 1999).

$$\Gamma_i = \frac{\beta_i}{1 - \sum_{j=1}^{i-1}[1 - \beta_i + b_{ij}\beta_i(1 - 1/\beta_j)]y_j - \sum_{j=i+1}^{n}[1 - a_{ij}\beta_i/\beta_j]y_j} \tag{1}$$

a_{ij} and b_{ij} are parameters taking into account the interaction between the different grain classes, $d_1 \geq d_i \geq d_n$. In (de Larrard 1999) the interaction parameters are found, by calibration with experimental results, to be:

$$\begin{aligned} a_{ij} &= \sqrt{1 - (1 - d_j/d_i)^{1.02}} \\ b_{ij} &= 1 - (1 - d_i/d_j)^{1.50} \end{aligned} \tag{2}$$

For each grain class, a packing density, Γ_i is calculated and it can be shown, that:

$$\Gamma = \min_{1 \leq i \leq n} (\Gamma_i) \tag{3}$$

The result of a such calculation yields the so-called *virtual* packing density which is not achievable in practice and in order to obtain realistic results, de Larrard introduced the compressible packing model. The compressible packing model includes a compaction factor, K, given by:

$$K = \sum_{i=1}^{n} \frac{y_i/\beta_i}{1/\gamma - 1/\Gamma_i} \tag{4}$$

The actual packing of the granular mix, γ is then determined by choosing a given compaction, K, that depends on the packing process (e.g. pouring, vibrating).

An example of the packing of a binary mix with d_1=10 μm and d_2=100 nm is shown in figure 2. A compaction index $K = 5$ is chosen.

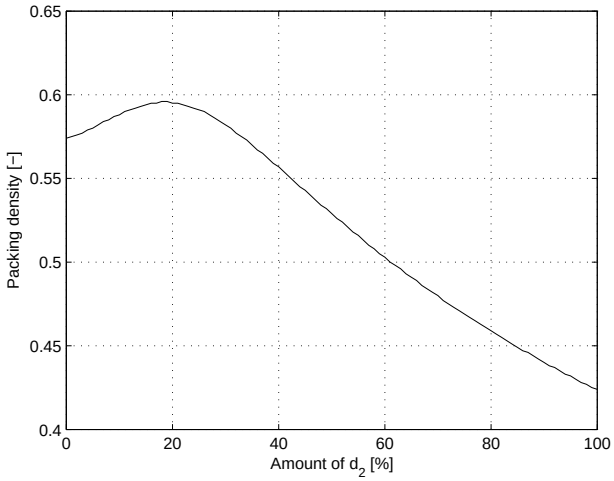

Figure 2: Example of the calculated packing of a binary mix

2.2 Particle forces

For powdered materials, like silica fume and cement, inter-particle forces may in reality play a crucial role in the resulting packing characteristics. It is therefore necessary to

take inter-particle force interactions into consideration, when interpreting experimental packing results. In the following, the dominating inter-particle forces in cement-based suspensions are reviewed. In appendix 1, the equations necessary to perform the calculation of inter-particle forces, are given.

The dominating inter-particle forces in cement and concrete are the van der Waals force, the electrostatic double-layer force, and the steric (polymer induced) force.

The van der Waals force arises from the interaction of atomic and molecular electric dipoles whose orientations are correlated so they attract each other. The van der Waals force is always attractive between like materials.

Immersing an inorganic particle in an aqueous solution usually results in the build-up of a charge at the solid-liquid interface. Ions of opposite charge (counterions) are attracted to the charged interface and form a diffuse ion "cloud" adjacent to the charged particle surface, called the electrostatic double-layer force. The magnitude of the electrostatic double-layer force is closely related to the so-called zeta-potential. The zeta-potential of cement in a high pH solution is very small. Both negative and positive values have been reported in literature (see e.g. (Nägele 1985), (Uchikawa et al. 1997)), all of them around plus/minus a couple of mV. This zeta-potential does not give rise to a very pronounced electrostatic force, and for cement suspensions, the electrostatic force between particles can thus usually be ignored. Oppositely, the zeta-potential of silica fume particles, suspended in a high pH media is very high. Flatt et al (Flatt et al. 1998) reported zeta-potential values around -50 mV in a 0.01 M NaOH-solution. This zeta-potential gives rise to a repulsive force between silica fume particles and thus counteracts the van der Waals force effect. Electrostatic interactions between particles with different or oppositely signed zeta-potentials at close separation distance, are attractive.

The action of the superplasticizer used in the current study is mainly to absorb onto the cement particles in a specific layer thickness and thus create a steric barrier, preventing the particles to come into close contact (see e.g. (Kjeldsen et al. 2004), (Kjeldsen et al. 2006)). In (Flatt et al. 1998), the zeta-potential of silica fume in a suspension of 0.01 M NaOH was measured with and without the addition of polycarboxylate, polysulphonate superplasticizers. The similar zeta-potentials obtained with and without superplasticizer addition indicate that the superplasticizer does not adsorb onto silica fume particles. This is supported by the fact that an anionic superplasticizer should not be able to adsorb onto the highly negatively charged silica fume particles.

The presence of the so-called solvation force, stemming from the orientation of the polar water molecules near a surface, will prevent all particles immersed in water, from physical contact. The solvation force is active for approximately one layer of water molecules, i.e. about 0.3 nm (see e.g. (Butt 1991), (Raviv & Klein 2002)).

A number of effects can assist in keeping the particles dispersed. For instance, agglomeration of silica fume particles may, to some extend, be resisted by Brownian motion. Colloids undergo Brownian motion because they are bombarded by solvent molecules. It is the kinetic energy of the solvent molecule that causes them to move. Because the energy, with which the colloids are being bombarded, is the same for all particles, the smaller particles will exhibit the effect more pronounced than the larger ones. This small size of silica fume particles at the same time leaves them more or less unaffected by application of a shear force. Cement particles are large enough to be unaffected by Brownian motion, but are instead sensitive to shear and gravity. Gravity is a continuously acting force, but while the application of shear may be able to break up some agglomerates, the subsequent removal of shear, may also make re-agglomeration possible. In the current experiments, shear is induced by the consolidation force and will therefore henceforth be referred to as the consolidation force.

Based on the above, determining the resulting force between cement (C) and silica fume (SF) particles may be able to determine with which particle interactions agglomeration is more likely to occur. In equations (5)-(7) the inter-particle forces that are deemed relevant in each case are listed. It is assumed that the principle of superposition can be applied:

$$F_{i(C-C)} \approx F_{vdW} + F_{Solvation} + F_{Steric} \quad (5)$$
$$F_{i(SF-SF)} \approx F_{vdW} + F_{Electrostatic} + F_{Solvation} \quad (6)$$
$$F_{i(C-SF)} \approx F_{vdW} + F_{Electrostatic} + F_{Solvation}(on\ SF) + F_{Steric}(on\ C) \quad (7)$$

Also the relevance of external forces acting, is determined by the particle size:

$$F_{ex(C-C)} \approx F_{Consolidation} + F_{Gravity} \quad (8)$$
$$F_{ex(SF-SF)} \approx F_{Brownian} \quad (9)$$
$$F_{ex(C-SF)} \approx F_{Consolidation}(on\ C) + F_{Gravity}(on\ C) + F_{Brownian}(on\ SF) \quad (10)$$

Using the equations described in appendix 1, in the combinations described above, enables the determination of inter-particle forces as a function of distance between the particles.

It is assumed that the mean particle size of silica fume is 100 nm and that of cement is 10 μm. Furthermore, the solvation layer thickness is assumed to be 0.3 nm while the steric layer thickness is assumed to be 6.0 nm. The result is shown in figure 3. In figure 3(a) the different attractive particle interactions without superplasticizer addition has been plotted as a function of separation distance. The pure cement interaction calculated by equation (5) constitutes the largest attractive force, followed by the cement-silica fume

interaction. Both interactions have their maximum value at twice the solvation layer thickness. The pure silica fume interaction has its maximum around 8 nm. After this point, it is dominated by a strongly repulsive electrostatic force (as previously described). Figure 3(b) shows the same particle interactions, but now with superplasticizer addition. The pure cement interaction now has its maximum attraction at 12 nm separation distance, due to the adsorbed superplasticizer. For the silica fume-cement interaction, the maximum force is at 6.3 nm separation distance, due to the absorbed superplasticizer on the cement grain, and the solvation layer at the silica fume grain. The pure silica fume interaction has not been changed by the addition of superplasticizer. The estimated maximum gravitational force (calculated from appendix 1) has a magnitude of ~ 10 pN for cement sized particles, while the Brownian force has a magnitude of about $\sim 10^{-1}$ pN for silica fume sized particles. These are indicated by the horizontal dotted lines.

From this comparison between the inter-particle forces, and the external forces, it is seen that Brownian force will be able to keep interacting silica fume particles dispersed at all times. This may go against the common perception of silica fume being highly agglomerated. But while silica fume actually *is* a highly agglomerated material, this is not due to attractive inter-particle forces. Instead, the nature of the production process tends to fuse a large number of silica fume particle together, creating larger clusters (Diamond 2003), many of which are able to break apart by ultrasonic treatment. Gravity may be able to keep the silica fume and cement from agglomerating, provided superplasticizer has been added. Without this, they will tend to agglomerate. The maximum attraction between pure cement particles is larger than the gravitational force, irrespective of superplasticizer addition. As previously mentioned, a shear force may be able to break up a number of the agglomerated particles but upon removal of this force, these particles may be free to re-agglomerate. In consolidation experiments, close packing is obtained and re-agglomeration may therefore be resisted. Due to the size effect of the interacting particles, the pure cement interaction will be most affected by the application of the consolidation force.

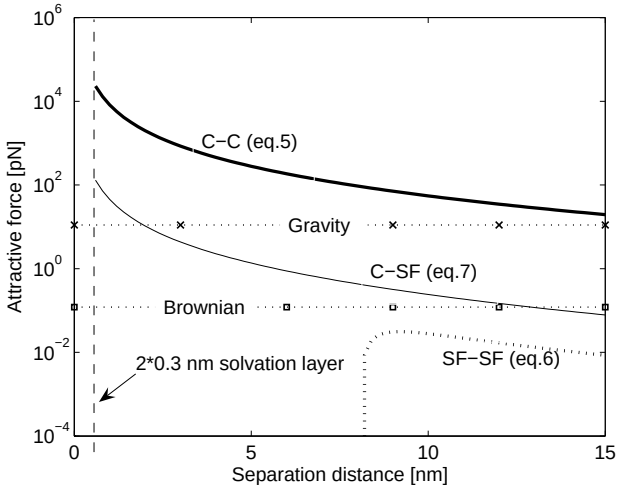

(a) Inter-particle force interaction without superplasticizer addition.

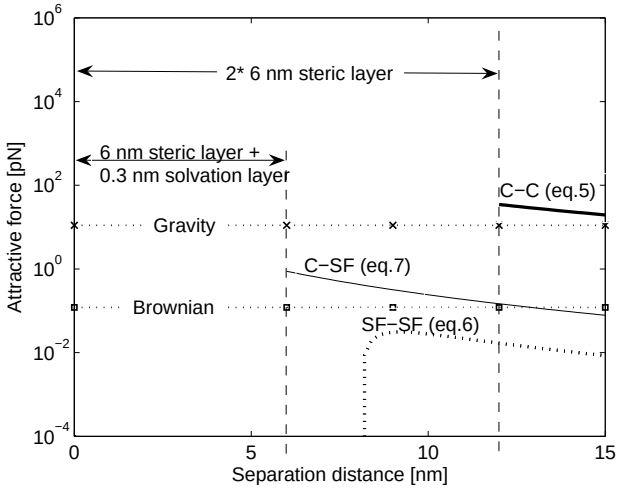

(b) Inter-particle force interaction with superplasticizer addition.

Figure 3: Inter-particle force interaction with and without superplasticizer addition between two cement grains (C-C) each with a diameter of 10 μm, two silica fume grains (SF-SF) each with a diameter of 100 nm, and a cement and a silica fume grain (C-SF).

2.3 Conceptual packing and pore size model

The above considerations on geometry and inter-particle forces can now be combined in a conceptual model. In figure 4, a model where no consolidation force is applied is shown.

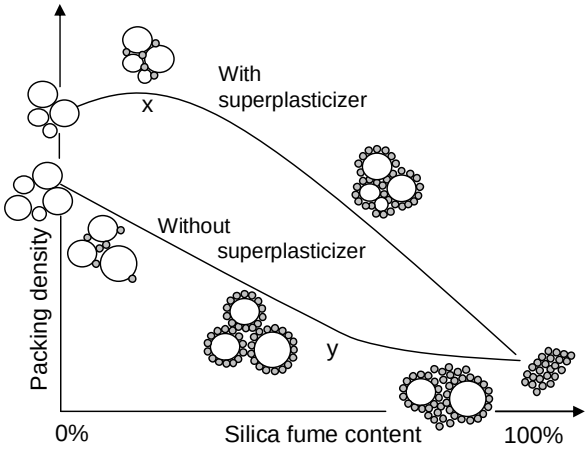

Figure 4: Conceptual packing model where inter-particle forces have been included.

In the top curve, superplasticizer has been added, screening the attractive forces between cement and silica fume. The top curve will therefore resemble that of a geometrical packing model. The packing density will increase when silica fume is added, until the point, x, where it just fills the cement porosity. After this, the packing density will be reduced linearly until it reaches the packing density of 100% silica fume. Changes from linearity are due to wall effects (a large grain in a sea of small grains) and loosening effects (a small grain between a number of large grains). In the bottom curve, it is assumed that silica fume and cement will agglomerate with each other when silica fume is added. This will cause the immediate decrease of packing density. The subsequent linear section represents the situations where all silica fume is agglomerated in some way to the cement particles. The last section succeeding the point, y, represents the situation where there is an excess of silica fume. The excess silica fume is prohibited from agglomerating to any cement-particles, because the existing agglomerates are now so large, that they are influenced by external dispersive forces.

Applying consolidation force to the mix will result in increased packing densities, because more attractive inter-particle forces may be overcome. Each cement-silica fume mix will have a characteristic packing density, achievable by application of a given minimum consolidation force. Ultimately, this packing density is the same with or without the addition of superplasticizers. The principle is sketched in figure 5 for increasing consolidation force $F_0 < F_1 < F_2$.

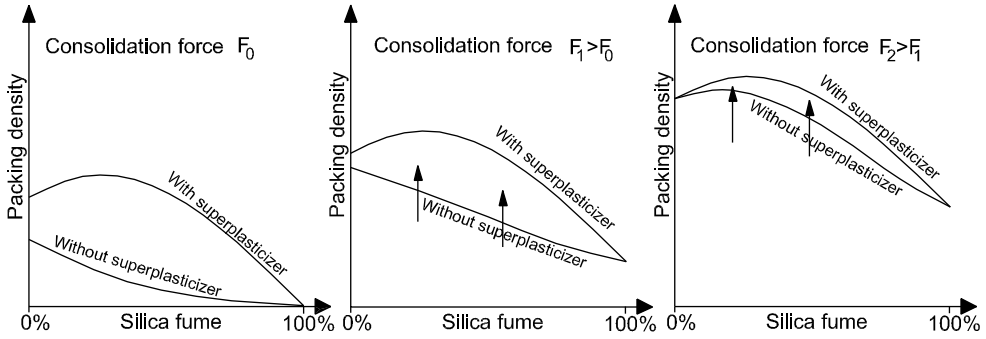

Figure 5: Conceptual cement-silica fume packing model where inter-particle forces have been included. The increasing application of consolidation force causes the packing density of each mix to increase towards its characteristic maximum.

As the consolidation force has more pronounced influence on larger particles, the cement alone will rapidly reach its ultimate packing density, irrespective of polymer addition.

From the conceptual packing model, it is now possible to specify an expected pore size model. First, the situation without consolidation is considered. When superplasticizer has been added, purely geometrical packing rules apply: Prior to the point, x, where silica fume just fills the porosity between the cement grains, the characteristic pore size may be linearly decreasing from the characteristic pore size of cement to the characteristic pore size of silica fume. After this point, the characteristic pore size of silica fume should be governing.

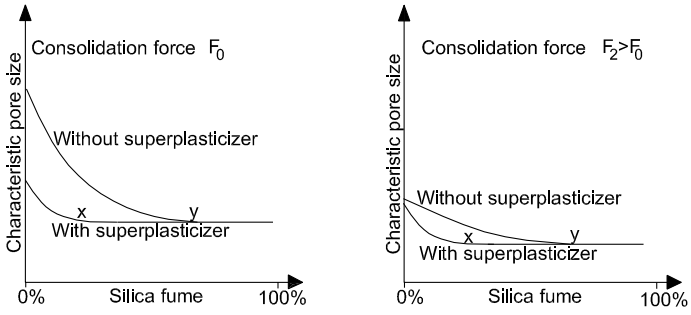

Figure 6: The conceptual characteristic pore size model.

When no superplasticizer has been added, and the attractive inter-particle forces play a role in the resulting packing, the characteristic pore size will be continuously decreasing

from that of the cement to that of the silica fume, until the point, y, where the silica fume does not agglomerate further to cement. The principle is shown in figure 6, left. The application of consolidation force will result in some changes, in principle similar to the changes in packing density, as seen in figure 6, right.

3 Experimental

3.1 Materials

The cement used was a Portland BASIS® cement delivered in 25 kg bags, from Aalborg Portland A/S with a density of 3.10 g/cm^3. This type of cement contains 14% limestone filler. The silica fume (SF) was an Elkem Microsilica® with a density of 2.45 g/cm^3. Particle size distributions were measured according to the description given in section 3.2 and are given in figure 7.

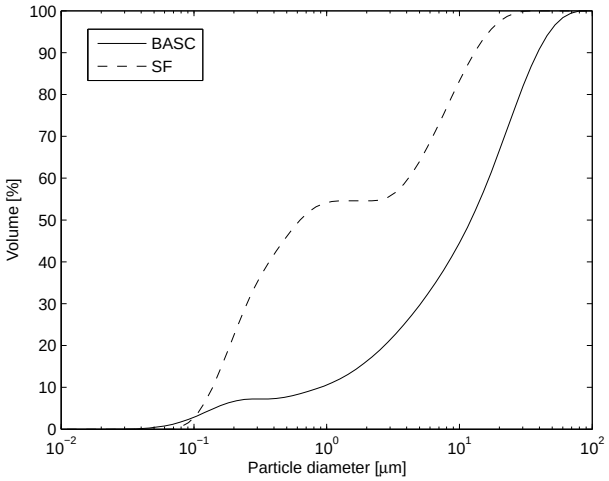

Figure 7: Particle size distribution of the cement (BASF) and silica fume (SF) used

The superplasticizer used was a non-commercial polycarboxylate polymer (PC4) produced in connection with the EC-project called "Design and function of novel polymeric admixtures for more durable high performance concrete". Some details of the polymer has been published, e.g. in (Schober & Mäder 2003), (Perche 2004), (Perche et al. 2003), (Kauppi et al. 2003), and (Kjeldsen et al. 2006).

An artificial pore solution with an ionic strength of 0.415 M was used as the suspending medium. The solution consisted of 2.0658 g/L $CaSO_4{\cdot}2H_2O$, 12.4960 g/L Na_2SO_4, and

2.9167 g/L NaOH. The solution mimics the aqueous phase of a cement suspension with water/cement ratio of 0.5, as measured 30 minutes.

3.2 Methods

3.2.1 Sample preparation

Powders were initially mixed together with a spatular. The pore solution was added to the mix and stirred by hand for 1 minute. The suspension was subsequently placed in an ultrasonic bath and ultrasonicated for 3 minutes. At this time, superplasticizer was added and the mix was subjected to 1 minute of ultrasonic treatment. When superplasticizer was added, an amount of polymer of 6 mg of polymer/g of the cement was used. Based on adsorption isotherms of the polymer onto a model material (see e.g. (Perche 2004)) this amount was deemed satisfactory in order to achieve full surface coverage of the cement particles.

The water/powder ratio was varied to obtain a workable paste in each experiment.

3.2.2 Particle size measurements

Particle size distributions were determined by light scattering using a Malvern Mastersizer 2000, Model APA2000 where particles between 20 nm to 2000 μm can be measured with an accuracy of 1%. The method requires knowledge of the dielectric properties of the material investigated. For the cement, the mean properties of the klinker phase were used, neglecting the effect of the lime filler particles. All materials were suspended in pore solution and ultrasonicated for 5 minutes prior to testing.

3.2.3 Consolidation experiments

The test equipment comprises a steel tube, a steel piston, a filter, and a steel base. A schematic drawing is shown in figure 8. The equipment was developed by (Olesen & Stang 1997). The steel tube is 200 mm long with an inner diameter, D, of 25 mm, and it is based on top of the base. The tube has small holes penetrating the tube wall at the level of the filter, thus permitting water to drain from the filter. The piston is a cylindrical bar which fits into the tube. A rubber ring at the bottom of the piston ensures a close packing between the piston and the tube wall. The filter is composed of five filters with increasing coarseness from the top down. The top filter is a sheet of blotting paper, while the bottom filter is a steel mesh.
The piston is placed in the tube and the setup is turned upside down. The suspension is transferred from the beaker to the tube. The piston is moved upwards until the suspension top reaches just below the level of the filter holes. The base, with filters, is placed on top, and the entire arrangement is turned around again. This procedure ensures the use of all of the suspension, and that no air is trapped within the system. The arrangement was placed in a universal testing machine and the piston was exposed to a constant

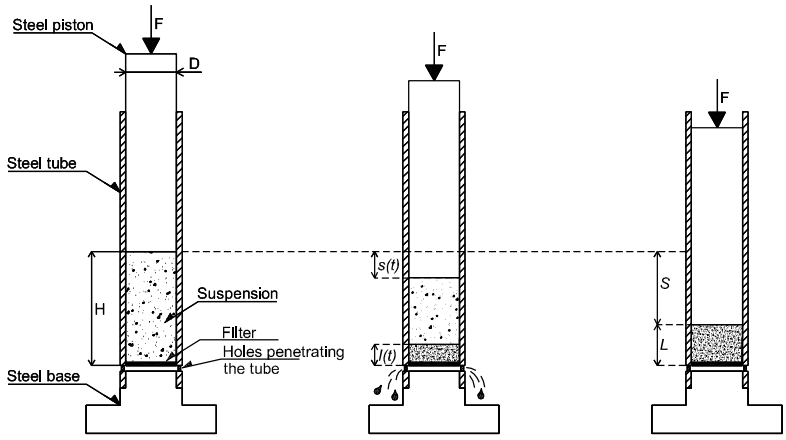

Figure 8: Schematic representation of the equipment for consolidation tests

load, F corresponding to a uniformly distributed pressure of 2 and 4 MPa, respectively. Corresponding values of load, deformation and time were recorded.

When the piston is loaded, water flows from the suspension through the filter (at the bottom) and a consolidation process develops. The consolidation will start at the level of the filter (at the bottom of the tube) and advance to the top. The height of the consolidated material is termed *l(t)*, while the deformation is termed *s(t)*. The initial suspension height prior to loading is *H*. When full consolidation is achieved, deformation will come to a rest, and the test is terminated. The principle is shown in figure 8.

After termination, the consolidated material was removed from the tube, weighed, dried at $105°C$, and weighed again, thereby determining the porosity, ϕ, and resulting packing, $\gamma = 1 - \phi$, of the material.

Selected mixes were tested three times in order to determine variability of the results. Packing results varied less than 1%. Characteristic mean pore diameter varied with about $\pm$ 0.03 μm.

3.2.4 Flow modelling

During consolidation, the pore solution flows through the consolidating material. The amount of solution flowing through the material is a function of the permeability of the material. It is assumed that this permeability is constant during consolidation. Furthermore, it is assumed that Darcy's law for laminar flow in a tube can be applied. It states that the volume of flow per time unit, Q, is proportional to the cross-sectional area of the

flowing water, A, the pressure drop in the tube, p, and the length of the tube, l:

$$Q = \alpha \cdot A\frac{p}{l} \tag{11}$$

The proportionality factor, α, is then the permeability. Furthermore, it is assumed that the volume of flow at time t is proportional to the increase in the amount of solidified material:

$$Qdt = \beta dlA \tag{12}$$

where β is the water expelled per length of consolidated material. Combining equation (11) and (12) yields a differential equation that can be solved with regards to the length of the consolidated material:

$$l^2 = 2\frac{\alpha}{\beta}pt \tag{13}$$

At the end of the consolidation, $l = L$ and $t = t_{end}$. Furthermore, by definition βL must be equal to the total deformation of the suspension, S. This gives:

$$\alpha p = \frac{SL}{2t_{end}} \tag{14}$$

Combining equation (11) and (14) yields an expression for the flow through the material as a function of length of the consolidated material (Olesen & Stang 1997):

$$Q(l) = \frac{SLA}{2t_{end}l} \tag{15}$$

To model the flow through a single pore with diameter, x, the Hagen-Poiseuille equation for a Newtonian liquid in a cylindrical pore is used (Geankoplis 2003):

$$p = \frac{32\mu v\tau l}{x^2} \tag{16}$$

where,

μ is the viscosity of the liquid
v is the average velocity of the liquid
τ is a factor accounting for the tortuosity of the system, $\tau > 1$

If the system consists of varying amounts (n), and sizes of pores with the same tortuosity, the contribution from each of these must be summed up:

$$p = \frac{32\mu v\tau l}{\sum n_i x_i^2} \tag{17}$$

For a continuous pore size distribution, the summation is replaced by an integral over the pore size multiplied by a distribution function, *f(x)*:

$$p = \frac{32\mu v\tau l}{\int_0^\infty x^2 \cdot f(x)\, dx} \tag{18}$$

Since $\int_0^\infty x^2 f(x) dx$ is equal to the mean of the diameter squared, $\overline{x^2}$, equation (18) reduces to:

$$p = \frac{32\mu v\tau l}{\overline{x^2}} \tag{19}$$

The volumetric flow rate in a pore can be described by:

$$Q_x = v\pi\frac{x^2}{4} \tag{20}$$

It is now assumed that all porosity is accessible for the flow, i.e. that no closed porosity is present. This seems a valid assumption, as no hydration has yet taken place. The measured porosity, ϕ, can then be calculated by knowledge of the pore volume, V_{pores}, and the total volume, V_{total}:

$$\phi = \frac{V_{pores}}{V_{total}} \tag{21}$$

From considerations similar to the ones used in equations (16) - (19), the volume of pores can be calculated by:

$$\begin{aligned} V_{pores} &= \sum n_i\pi\left(\frac{x_i}{2}\right)^2\tau l \\ &= \frac{\pi}{4}\tau l\int_0^\infty x^2 f(x)\, dx \\ &= \frac{\pi}{4}\tau l\cdot\overline{x^2} \end{aligned} \tag{22}$$

The porosity is then given by:

$$\phi = \tau\frac{\overline{x^2}}{D^2} \tag{23}$$

where,

D is the diameter of the entire tube

The flow in the entire tube can similarly be described by an integral of the flow in one pore, over all the pore sizes:

$$\begin{aligned} Q &= \sum n_i v\pi\frac{x_i^2}{4} \\ &= \frac{\pi}{4}v\int_0^\infty x^2 f(x)\, dx \\ &= \frac{\pi}{4}v\overline{x^2} \end{aligned} \tag{24}$$

With $A = \pi \left(\frac{D}{2}\right)^2$, combining equations (15), (19), (23), (24), and rearranging gives:

$$\sqrt{\overline{x^2}} = 4\tau\sqrt{\frac{\mu SL}{p\phi t_{end}}} \tag{25}$$

Since $\sqrt{\overline{x^2}} \neq \overline{x}$, the result may be considered a characteristic mean diameter, $\overline{x_c}$, different from the real mean diameter, $\overline{x}$. The error induced differs depending on the pore size distribution considered. Assuming that the pore size distribution may resemble the particle size distribution, a so-called Rosin-Rammler distribution of the form

$$F(x) = 1 - e^{-ax^b} \tag{26}$$

may be considered. a and b are constants. Assuming simple cubic lattice packing of the largest and smallest cement and silica fume particles (from figure 7), upper and lower pore size values can be roughly estimated. Subsequently, a and b can be fitted to obtain the distribution function. Integrating over $x^2 \cdot f(x)$ to obtain $\overline{x^2}$ shows that $\overline{x_c}$ may be as high as double $\overline{x}$.

To estimate t_{end} in equation (25)the curve of the suspension deformation as a function of time, obtained from the consolidation experiments, is used. An example of this curve is shown in figure 9. The first inclined part of the curve represents the solidification phase while the second part is the phase following the completion of the solidification. t_{end} may be estimated as the intersection of a linear line fitted to the inclined part of the curve with a linear line fitted to the constant part of the curve. However, the accurate determination of t_{end} can be a difficult matter and instead an approach described in (Stang et al. 2006) is used.

According to equation (13) plotting the square of the cake height against time will yield a straight line. An example is shown in figure 10. The slope, C of the line is then given by $2\frac{\alpha}{\beta}p$. At the end of consolidation, equation (13) is then:

$$L^2 = Ct_{end} \Rightarrow t_{end} = \frac{L^2}{C} \tag{27}$$

Equation (25) now has the form:

$$\overline{x_c} = 4\tau\sqrt{\frac{\mu SC}{p\phi L}} \tag{28}$$

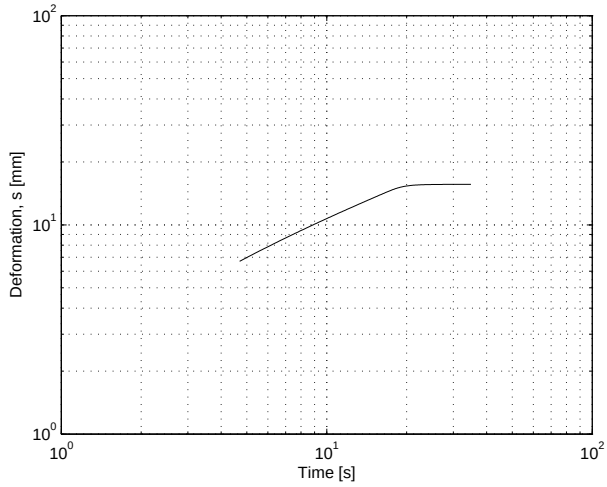

Figure 9: Example of curve obtained during a consolidation-experiment with a 2 MPa load. The suspension consisted of 90% cement and 10% silica fume.

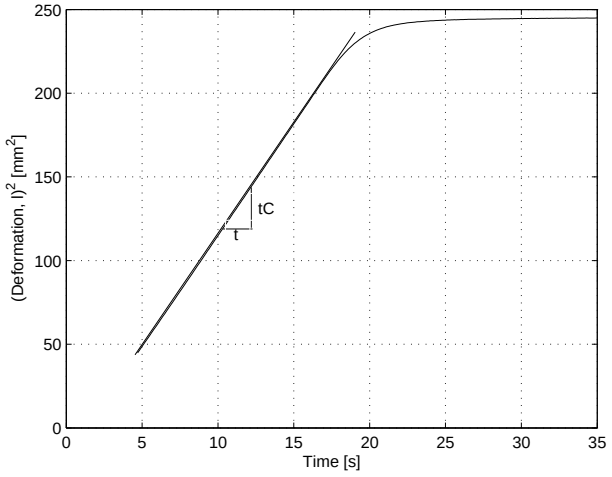

Figure 10: Example of curve for determination of C. Same experimental conditions as in figure 9 apply.

4 Results and discussion

In table 1 and 2, experimental results on deformation, S, cake height, L, and time of consolidation termination at 2 MPa and 4 MPa, respectively, are given.

Table 1: Material combinations and experimental consolidation results at 4 MPa pressure. SP is superplasticizer

Cement %	Silica fume %	SP	Deformation, S mm	Cake height, L mm	Packing, γ -	C mm^2/s	t_{end} s
100	0	-	11.94	14.5	0.60	65.4	3
90	10	-	14.33	14.0	0.60	26.5	7
80	20	-	20.31	14.0	0.59	8.2	24
60	40	-	31.84	15.2	0.55	1.9	119
40	60	-	32.37	18.0	0.49	2.0	160
0	100	-	23.32	13.5	0.46	2.6	70
100	0	+	15.76	11.8	0.60	11.7	12
90	10	+	19.72	15.6	0.60	0.9	271
80	20	+	14.19	15.5	0.61	1.0	239
50	50	+	28.57	17.7	0.54	0.9	345

Table 2: Material combinations and experimental consolidation results at 2 MPa pressure. SP is superplasticizer

Cement %	Silica fume %	SP	Deformation, S mm	Cake height, L mm	Packing, γ -	C mm^2/s	t_{end} s
100	0	-	15.9	31.5	0.58	101.0	10
90	10	-	15.7	15.3	0.58	12.5	19
80	20	-	15.9	16.0	0.57	4.2	60
70	30	-	23.6	18.0	0.54	2.2	147
60	40	-	22.8	18.0	0.51	1.9	175
40	60	-	27.5	22.0	0.46	1.8	266
20	80	-	20.0	12.0	0.43	1.3	114
0	100	-	23.8	12.0	0.42	0.7	168
100	0	+	10.2	32.5	0.57	3.1	345
90	10	+	11.4	15.5	0.58	1.7	144
81	19	+	10.5	16.0	0.59	0.3	808
50	50	+	19.8	17.0	0.51	0.3	923
30	70	+	12.3	10.6	0.47	0.2	551
20	80	+	13.9	12.5	0.46	0.2	659
0	100	+	21.4	10.2	0.43	0.5	230

4.1 Packing characteristics

In figure 11 the packing results are shown. As seen, the packing characteristics resemble the conceptual model shown in figure 5. The packing obtained when superplasticizer has been added, seems to be similar to what is obtained in larger grain size populations, i.e. when only geometrical effects influence the packing. Without superplasticizer addition, the addition of silica fume decreases the packing of the resulting mix throughout all combinations. As expected, an increased consolidation pressure (and thus an increased consolidation force), in general moves the curves upwards and moves the no-superplasticizer curve towards the superplasticized curve.

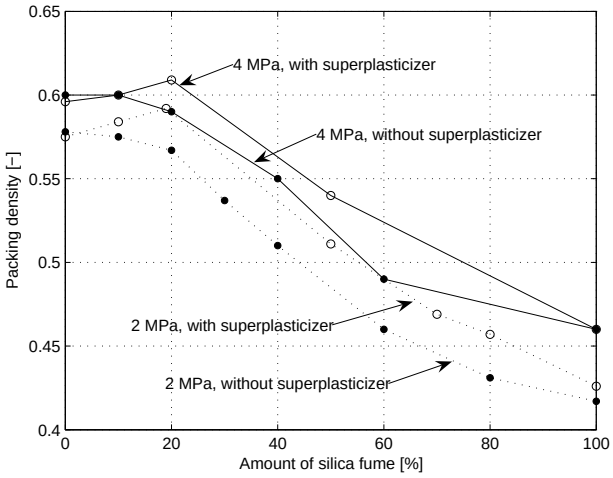

Figure 11: Experimental packing results obtained from the consolidation experiments.

The addition of superplasticizer to pure silica fume suspensions does not give rise to any distinct differences in packing, indicating, as assumed, that the superplasticizers do not absorb onto the silica fume particles. The addition of superplasticizer to cement alone does not seem to yield any difference in packing results. This is most likely due to the consolidation pressure exceeding the inter-particle forces between the cement grains. To confirm this assumption, an estimate of the load needed to overrule cement inter-particle forces, is made: At full consolidation, the consolidation force, F, acting on the system is equal to the sum of the attractive inter-particle forces, ΣF_i. The sum of the inter-particle forces must be proportional to the number of particle contacts, n, which in turn must be proportional to the number of particles, N:

$$\begin{aligned} F &= \sum F_i \\ &\propto nF_i \\ &\propto NF_i \end{aligned} \tag{29}$$

The pressure, P, on the particle network must then be the force divided by the area of the particles, A:

$$P \propto \frac{NF_i}{A} \tag{30}$$

Assuming the particles are ordered in a simple cubic lattice, there will be one particle, per squared particle diameter, d^2, so that:

$$\frac{N}{A} \propto \frac{1}{d^2} \tag{31}$$

With a cement particle diameter of 10 μm and a maximum attractive inter-particle force of 10^4 pN (from figure 3) the pressure becomes:

$$P \cong \frac{10^4 pN}{(10\mu m)^2} = 0.0001\ MPa \tag{32}$$

For comparison, a cement particle diameter of 1 μm would need 10 times this pressure to overcome the inter-particle forces. The result in equation (32) show that a pressure of 2 and 4 MPa will cause similar consolidation with or without superplasticizer addition. In (Olesen & Stang 1997), similar experiments (without superplasticizer addition) were carried out on Rapid cement and Elkem silica fume using the same equipment and a 10 MPa pressure. Packing results from these experiments, together with the current results (with superplasticizer) are shown in figure 12.
As seen, similar packing characteristics are obtained between two suspensions with superplasticizer and one without, because the pressure of 10 MPa is high enough to overrule all effects of attractive inter-particle forces, and compress the mixes to a characteristic packing density. A similar result was obtained in (Kjeldsen et al. 2006) on a model powder, using centrifugation as consolidator.

Sub conclusions
Calculations and experimental results indicate that:

- The suggested conceptual packing model correlates well to experimental results
- The selected anionic superplasticizer does not absorb onto the silica fume particles, but Brownian motion and electrostatic repulsion is enough to keep the particles dispersed

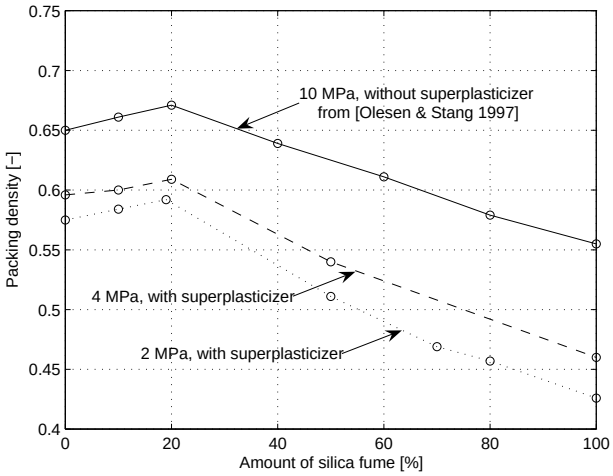

Figure 12: Current consolidation experiments with superplasticizer and results from (Olesen & Stang 1997) without superplasticizer.

- The electrostatic repulsion is negligible in cement-interactions. Instead, the van der Waals force causes agglomeration of the particles. The addition of superplasticizers reduces the attractive force, but the resulting action is still attractive.
- Calculations show attractive interaction between silica fume and cement. However, the addition of superplasticizer, combined with the gravitational force may be enough to keep the particles dispersed and caused the packing characteristics to resemble that of larger grain size populations, where inter-particle forces are negligible
- Applying a high enough consolidation force will overrule the inter-particle force actions and compress the mix to a characteristic maximum packing density

4.2 Pore size characteristics

As is well known, a cement-based material comprises a variety of different pore sizes. This is initially due to the constituent particle size distributions being very wide, and later also due to hydration products being formed. However; the assumption of one characteristic pore size, determining for the resulting flow through the material, still seems valid. In figure 13 the calculated mean characteristic pore sizes as a function of silica fume content, are shown for the mixes with and without superplasticizer addition. In the calculations, the following constant were used: the viscosity of water at 20°C is $1.002 \cdot 10^{-3}$ Pa·s and

the constant load applied at the top of the piston corresponded to a uniformly distributed pressure, p, of 2 and 4 MPa. Furthermore, an arbitrarily chosen tortuosity factor, $\tau = 2$, is used.

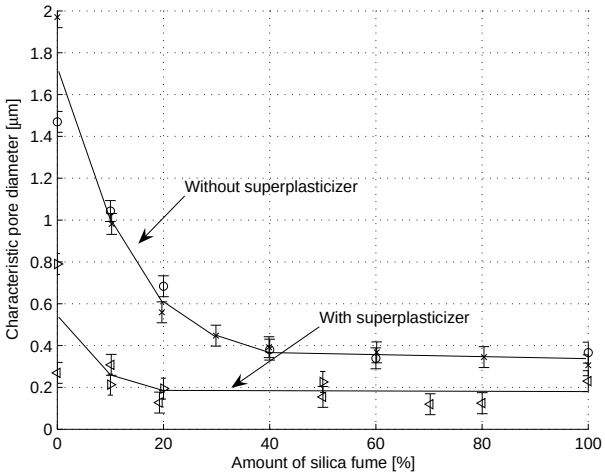

Figure 13: Calculated characteristic pore diameters. Results from both 2 MPa ($\triangleleft$, $\times$) and 4 MPa ($\circ$, $\triangleright$) pressure measurements are shown. Errorbars indicate an estimated standard deviation of 0.03 μm

The validity of this size range of the calculated pore diameters is estimated by taking the mean particle diameters, d, obtained from figure 7 and assuming simple cubic lattice packing. The measured mean cement diameter is about 10 μm, while the mean silica fume diameter is about 0.8 μm. In a simple cubic lattice, the smallest pore diameter that can be obtained is $0.414 \cdot d$. Thus, the pore sizes between the cement grains may be around $0.414 \cdot 10\mu\text{m} \approx 4\ \mu\text{m}$ while they may be around 0.3μm between the silica fume grains. These size ranges seem to correlate well to the calculated pore sizes.

Figure 13 shows that cement alone will yield the more coarse pore structure. For the suspensions without superplasticizer addition, the addition of silica fume decreases the characteristic pore size up to about 40% silica fume addition. After this point, the characteristic pore size keeps almost constant. This means, that beyond 40% silica fume addition, the silica fume is determining for the characteristic permeable pore size in a cement-based material. For the suspensions with superplasticizer addition, the tendency is similar, but silica fume is already determining for the characteristic pore size after about 20% addition.

The increased pressure should cause a slight decrease in pore size. This is not seen

in the results, but it is expected that this may be due to the somewhat large variability on the pore size results. Considering the applied consolidation pressure and the packing results, it was assumed that the characteristic pore size in the pure cement suspensions with and without superplasticizer be the same. Furthermore, the overall decrease in pore size when adding superplasticizer, can at present not be explained as preliminary measurements showed no significant change in viscosity due to superplasticizer addition.

Sub conclusions
From the flow experiments and subsequent modelling, the following can be deducted:

- The proposed pore size model correlated in general with the calculated characteristic mean pore sizes
- Estimates of pore sizes from the measured particle size distributions correlate well with the calculated characteristic pore size $\overline{x_c}$
- When no superplasticizer is used, increasing the amount of silica fume up to about 40% caused a decrease in the characteristic pore diameter of the consolidated material. Beyond this, no change in characteristic pore size was observed. This is assumed caused by the silica fume being the determining pore size factor in this region
- When superplasticizer was used, increasing the amount of silica fume up to about 20% caused a decrease in the characteristic pore diameter of the consolidated material. Beyond this point, no change was found
- The addition of superplasticizer unexpectedly caused a decrease in the overall characteristic pore size that could not be explained.

5 Summary and conclusions

Calculations of inter-particle forces acting between the particles in cement/silica fume suspensions showed a large electrostatic repulsion in silica fume-silica fume interaction at close separation distances, whereas cement-cement and cement-silica fume interactions are governed by highly attractive forces. Adding the superplasticizer, attractive forces between cement and silica fume were reduced to a point where they had no influence. Attractive forces between cement grains were reduced by the addition of superplasticizer, but remained attractive. Based on considerations on particle packing and the effect of inter-particle forces, a conceptual model for particle packing and pore sizes was proposed.

Cement-based systems a Danish Portland BASIS cement, with varying additions of silica fume, both with and without an anionic superplasticizer were studied by compressive consolidation. Modelling the consolidation process and using the Hagen-Poiseuille equation made it possible to determine a characteristic mean pore diameter in the studied systems.

The results correlated well to the proposed model.

The results show the importance of implementing inter-particle forces in packing and pore size models, in order to accurately describe the initial microstructure of a cement-based material. Furthermore, the flow modelling approach offers an elegant way of determining transport properties in fresh cement-based materials.

6 Acknowledgements

Sika Technology AG are kindly thanked for providing the PC4 polymer used in the study.

References

Bergström, L. (1997), 'Hamaker constants in inorganic materials', *Advances in Colloid and Interface Science* **70**, 125–169.

Bergström, L., Schilling, C. & Aksay, I. (1992), 'Consolidation behavior of flocculated alumina suspensions', *J.Am.Ceram.Soc.* **75**(12), 3305–3314.

Butt, H.-J. (1991), 'Measuring electrostatic, van der waals, and hydration forces in electrolyte solutions with an atomic force microscopy', *Biophys.* **60**, 1438–1444.

de Larrard, F. (1999), *Concrete Mixture Proportioning - A Scientific Approach*, Modern Concrete Technology, E&FN SPON.

Diamond, S. (2003), Densified silica fume - it is what you think it is?, *in* 'Proceedings of Advances in Cement and Concrete', Copper Mountain, Colerado, USA, pp. 233–248.

D.P.Bentz, O.M.Jensen, A.M.Coats & F.P.Glasser (2000), 'Influence of silica fume on diffusivity in cement-based materials', *Cement and Concrete Research* **30**.

Flatt, R., Houst, Y., Bowen, P., Hofmann, H., Widmer, J., Sulser, U., Maeder, U. & Burge, T. (1998), Effects of superplasticizers in highly alkaline model suspensions containing silica fume, *in* 'Sixth CANMET/ACI international conference on Fly ash, Silica fume, slag and natural pozzolans in concrete', Vol. 2, American Concrete Institute, Farmington Hill, Mi, USA, pp. 911–930.

Flatt, R. J. (1999), Interparticle Forces and Superplastisizers in Cement Suspensions, PhD thesis, Ecole Polytechnique Federale Lausanne.

Flatt, R. J. (2001), *Polymers in Particulate Systems - Properties and Applications*, Marcel Dekker, Inc., chapter Polymeric Dispersions in Concrete, pp. 247–294.

Flatt, R. J. (2004*a*), 'Dispersion forces in cement suspensions', *Cem Concr Research* **34**, 399–408.

Flatt, R. J. (2004*b*), 'Towards a prediction of superplasticized concrete rheology', *Materials and Structures* **37**, 289–300.

Garboczi, E. & Bentz, D. (1996), 'Modelling the microstructure and transport properties of concrete', *Concrete and Construction Materials* **10**(5), 293–300.

Geankoplis, C. J. (2003), *Transport Processes and Separation Process Principles (Includes Unit Operations)*, fourth edition edn, Prentice Hall.

Hogg, R., Healy, T. & Fuerstenau, D. (1966), 'Mutual coagulation of colloidal dispersions', *Transactions of the Faraday Society* **62**, 1638–1651.

Hunter, R. (1993), *Introduction to Modern Colloid Science*, Oxford University Press.

Kauppi, A., Banfill, P., Bowen, P., Galmiche, L., Houst, Y., Lafuma, F., Mäder, U., Perche, F., Petersen, B., Reknes, K., Schober, I., Siebold, A. & Swift, D. (2003), Improved superplasticizers for high performance concrete, *in* 'Proc. 11th ICCC', Tech book International, New Delhi, India, Durban, pp. 528–537.

Kjeldsen, A., Bergstrom, L. & Geiker, M. (2004), Centrifugal consolidation of mgo-suspensions - the influence of superplasticizers on particle packing, *in* S. Mason, ed., 'Annual Transactions - The Nordic Rheology Society', Vol. 12, pp. 31–39.

Kjeldsen, A., Flatt, R. & Bergstrom, L. (2006), 'Relating the molecular structure of comb-type superplasticizers to the compression rheology of mgo suspensions', *Accepted for publication in Cement and Concrete Research* .

Nägele, E. (1985), 'The zeta-potential of cement', *Cement and Concrete Research* **15**, 453–462.

Olesen, J. F. & Stang, H. (1997), Improved quality assurance and methods of grouting post-tensioned tendons, S 96II.I, Dept. of Structural Engineering and Materials, Technical University of Denmark.

Perche, F. (2004), Adsorption de polycarboxylates et de lignosulfonates sur poudre modèle et ciments, Phd-thesis no 3041, EPFL, Lausanne, Switzerland.

Perche, F., Houst, Y., Bowen, P. & Hofmann, H. (2003), Adsorption of lignosulfonates and polycarboxylates - depletion and electroacoustic methods, *in* V. Malhotra, ed., 'Proc. 7th CANMET/ACI International Conference on Superplasticizers and Other Chemical Admixtures in Concrete', Vol. Supplementary papers, Berlin, Germany, pp. 1–15.

Ramachandran, V. S., Malhotra, V. M., Jolicoeur, C. & Spiratos, N. (1998), Superplasticizers: Properties and applications in concrete, Technical report, Ministry of public works and government services, Ottawa, Ontario, Canada.

Raviv, U. & Klein, J. (2002), 'Fluidity of bound hydration layers', *Science* (297), 1540–1543.

Russel, W., Saville, D. & Schowalter, W. (1989), *Colloidal Dispersions*, Cambridge University Press.

Schober, I. & Mäder, U. (2003), Compatibility of polycarboxylate superplasticizers with cement and cementitious blends, *in* V. Malhotra, ed., 'Proc. 7th Canmet/ACI Int. Conf. on Superplasticizers and Other Chemical Admixtures in Concrete', number SP-217, American Concrete Institute, Farmington Hills, pp. 453–448.

Stang, H., Fredslund-Hansen, H. & Puclin, T. (2006), 'Method of extrusion of particulate pastes or suspensions', Patent: WO 2006/034557 A1. International Application Published under the Patent Coorporation Treaty (PCT).

Stovall, T., De Larrard, F. & Buil, M. (1986), 'Linear packing density model for grain mixtures', *Powder Technology* **48**(1-12).

Uchikawa, H., Hanehara, S. & Sawaki, D. (1997), 'The role of steric repulsive force in the dispersion of cement particles in fresh paste prepared with organic admixtures', *Cem and Concr Res* **27**(1), 37–50.

Appendix 1

In the following, the basis for calculating inter-particle forces between two spheres is reviewed. The inter-particle forces considered correspond to those considered in the article. Finally, the properties of cement and silica fume, necessary for a calculation, are listed.

van der Waals force
The van der Waals force between two spheres $(_1)$ and $(_2)$, across a medium $(_3)$ can be approximated by (see e.g. (Flatt 2004*a*), (Flatt 1999)):

$$F_{vdW} \approx -A_{132} f_{retardation} \frac{dH}{dh} \tag{33}$$

where A_{132} is the Hamaker constant (see (Bergström 1997)), $f_{retardation}$ is a retardation factor that incorporates the retardation of the dipole interaction over large distances, H is a geometrical factor dependant on the shape of the interacting particles (see (Bergström et al. 1992)) and h is the separation distance.
The retardation factor can be calculated according to (Russel et al. 1989):

$$f_{retardation}(h) = \left(1 + \left(\frac{n_{water}\sqrt{n_{particle}^2 + n_{water}^2}}{4\sqrt{2}} \frac{h\pi\omega_{UV}}{c} \right)^{\frac{3}{2}} \right)^{-\frac{2}{3}} \tag{34}$$

where,

c is the speed of light, $3.0 \cdot 10^8 m/s$
ω_{UV} is a characteristic frequency in the ultra violet range,
$\omega_{UV,C} = 1.71 \cdot 10^{16} rad/s$ and $\omega_{UV,SF} = 2.03 \cdot 10^{16} rad/s$
n are the refractive indices, $n_C = 1.735$, $n_{SF} = 1.448$, $n_{water} = 1.325$

For spheres, the derivative of the geometrical factor can be expressed as (Russel et al. 1989), (Flatt 1999):

$$\begin{aligned} \frac{dH}{dh} &= -\frac{1}{6}\left(\frac{-4a_1a_2\left[a_1+a_2+h\right]}{\left[2(a_1+a_2)h+h^2\right]^2} + \frac{-4a_1a_2\left[a_1+a_2+h\right]}{\left[4a_1a_2+2(a_1+a_2)h+h^2\right]^2} \right) \\ &\quad -\frac{1}{6}\left(\frac{8a_1a_2\left[a_1+a_2+h\right]}{\left[4a_1a_2+2(a_1+a_2)h+h^2\right]\left[2(a_1+a_2)h+h^2)\right]} \right) \end{aligned} \tag{35}$$

Between most materials, the van der Waals force is highly attractive and is thereby the primary source of agglomeration between particles.

Electrostatic force

The electrostatic force between particles of similar low zeta-potentials can be calculated by (Flatt 1999):

$$F_{El} = -2\varepsilon_0\varepsilon_r\overline{a}\pi\psi_0^2 \cdot \frac{\kappa e^{-\kappa h}}{1+e^{-\kappa h}} \tag{36}$$

where,

ε_0 is the permittivity in vacuum, $8.854 \cdot 10^{-12} C^2/Nm^2$
ε_r is the relative permittivity of water, 80
$\frac{2a_1a_2}{a_1+a_2}$ is the harmonic average radius of the interacting particles with radii a_1, a_2.
κ is the so-called Debye-length
ψ_0 is the electrostatic potential, usually replaced by the measurable zeta-potential.

The Debye-length can be calculated by (see e.g.(Flatt 2001)):

$$1/\kappa = \sqrt{\frac{\varepsilon_0\varepsilon_r k_B T}{2e^2 N_A I}} \tag{37}$$

e is the charge on an electron, $1.60 \cdot 10^{-19}$ C
N_A is Avogadros constant, $6.03 \cdot 10^{23}$ molecules/mole
I is the ionic strength of the solution
k_B is the Boltzmann constant, $1.38 \cdot 10^{-23}$ J/° K
T is the temperature, 293° K

Electrostatic interactions between spherical particles with different or oppositely signed zeta-potentials at close separation distance are attractive and can be approximated by equation (38) (Hogg et al. 1966). The expression is only exact for potentials below 25 mV, but gives good approximations below 50-60 mV as well.

$$F_{El,uneven} \approx K_1K_2\left(\frac{-\kappa \cdot e^{-\kappa h}}{1+e^{-\kappa h}} - \frac{\kappa \cdot e^{-\kappa h}}{1-e^{-\kappa h}}\right) + K_1\left(\frac{2\kappa \cdot e^{-2\kappa h}}{1-e^{-2\kappa h}}\right) \tag{38}$$

$$K_1 = \frac{\varepsilon_r\varepsilon_0 a_1 a_2(\psi_{0,1}^2 + \psi_{0,2}^2)}{4(a_1+a_2)} \tag{39}$$

$$K_2 = \frac{2\psi_{0,1}\psi_{0,2}}{\psi_{0,1}^2 + \psi_{0,2}^2} \tag{40}$$

Brownian motion
Brownian motion can be approximated by (Flatt 2004*b*), (Hunter 1993):

$$F_B \approx \frac{3}{2} \cdot \frac{k_B T}{a} \tag{41}$$

Gravity
The gravitational force acting on the particles can be calculated by (Flatt 2004*b*):

$$F_g = \frac{4}{3}\pi a^3 \Delta\rho g \tag{42}$$

where,

$\Delta\rho$ is the density difference between particle and fluid
g is the gravitational acceleration, $9.82 m/s^2$

Material properties
The material property values used in the calculations are given in table 3.

Table 3: Material properties used in the inter-particle force calculations. **The static part of the Hamaker constant is screened by electrolytes and is not included. ** As determined in (Kjeldsen et al. 2006)*

		SF-SF	C-C	C-SF
A_{132}*	10^{-20} J	0.16	2.01	0.55
a_1	nm	50	5000	5000
a_2	nm	50	5000	50
$h_{solvation}$	nm	2×0.3	2×0.3	2×0.3
$h_{superplast}$**	nm	2×0.3	2×6.0	$0.3 + 6.0$
$\zeta_0 \sim \psi_0$	mV	-50	+5	-50/+5

Paper V

On the Interpretation of Low Temperature Calorimetry Data

Paper submitted to Journal of Materials and Structures
Kjeldsen, A.M. and Geiker, M.

On the Interpretation of Low Temperature Calorimetry Data

Ane M. Kjeldsen* and Mette Geiker

Department of Civil Engineering, Technical University of Denmark DK-2800 Kgs. Lyngby, Denmark, e-mail: amk@byg.dtu.dk

Paper submitted to Journal of Materials and Structures

Abstract

The effect of selected factors and phenomena on Low Temperature Calorimetry (LTC) results has been investigated, in order to determine the possibilities and limitations of using LTC for characterization of the porosity of cement-based materials. LTC was carried out on a model material with mono-sized pores of approximately 14 nm saturated with either distilled water or a sodium chloride solution, as well as on water, the salt solution, and an artificial pore solution, alone.

It was found that supercooling is unavoidable during the liquid-solid phase transition, and that even at low temperature gradients equilibrium cannot be obtained with the sample size used (1 g liquid). Correcting for non-equilibrium between reference block and sample, the Gibbs-Thomson equation seems applicable for estimation of pore sizes of the investigated size. The estimate may be further improved by taking the effect of ions on freezing point depression into account.

It is proposed that the connectivity of pores, e.g. in cement-based materials, may be characterized based on cooling curves, whereas the pore size distribution may be characterized based on the heating curve. Cooling should be undertaken at a high rate to limit transport of liquid, whereas heating should be undertaken at a low rate to limit the effect of non-equilibrium.

Résumé

L'effet de certains paramètres et phénomènes particuliers sur les résultats de calorimetrie à basse température (LTC pour Low Temperature Calorimetry) a été étudié afin de déterminer les potentialités et les limitations d'utilisation de cette méthode pour la caractérisation de la porosité des matériaux cimentaires.

Des mesures de LTC ont été réalisées d'une part sur un matériau modèle à distribution de taille de pores unique d'environ 14 nm, saturé soit avec de l'eau distillée soit avec une solution de chlorure de sodium, et d'autre part sur l'eau seule, sur la solution saline, et sur une solution de pore artificielle.

Il a été observé que les phénomènes de surfusion sont inévitables pendant la transition de phase liquide-solide, et que même en utilisant des gradients de température faible, l'équilibre ne peut être atteint avec la taille d'échantillon utilisée dans le cas présent (1g). En apportant les corrections nécessaires de non-équilibre entre le bloc référence et

l'échantillon, l'équation de Gibbs-Thomson est toutefois applicable pour l'évaluation de la taille des pores. L'évaluation peut être encore améliorée en tenant compte de l'effet des ions sur l'abaissement du point de solidification. Il est propose que la connectivité des pores, dans le cas des matrices cimentaires, soit caractérisée sur la base des courbes de refroidissement, tandis que la distribution de taille des pores soit estimée à partir des courbes de chauffage.
Le refroidissement doit être rapide afin de limiter le transport du liquide; le chauffage doit en revanche être relativement long afin de prévenir les effets de non-équilibre.

1 Introduction

The pore structure of cement-based materials affects many engineering properties, e.g. permeability, shrinkage, and strength. Thus, characterization of the porosity is an important tool in connection with both design and investigation of such materials. A number of methods, both direct and indirect, have been developed for this purpose.
Low temperature (micro) calorimetry (LTC) (also called differential scanning calorimetry (DSC), cryoporometry, and thermoporometry) is one of the indirect methods. The method has been used since the late 1970'ties. A thorough description of the thermodynamics governing the solidification process is given in (Brun et al. 1977). Reasons for using LTC are, among others, that the method can be performed on virgin (not dried) samples and compared to water desorption is fast, i.e. can be used on young samples.
The principle of LTC is based on 1) the freezing of liquid is an exothermic process (and melting of ice is an endothermic process) and 2) at subfreezing temperatures a solid meniscus exists, whose curvature lowers the free energy of the pore liquid and induces a freezing point depression. Determination of pore size distribution from freezing point depression has been dealt with by e.g. Fagerlund (Fagerlund 1973). The author described, among others, the effect of supercooling on ice formation down to about -40°C, where homogeneous nucleation can take place in isolated pores.
Based on work by Winslow and Diamond, Fagerlund furthermore discussed the existence of threshold diameters ("bottle necks"), causing ice formation to take place at intervals. Fontenay and Sellevold (Fontenay & Sellevold 1980) observed during cooling three well-defined peaks and claimed LTC to have a great potential for characterization of pore water and pore structure due to the consistency and reproducibility of measurements. The presence of threshold diameters has been further indicated by correlated LTC and mercury intrusion porosimetry (MIP) on cement mortar, which showed comparable results (Sellevold & Bager 1980). The appearance and disappearance of these peaks have recently been used by Snyder, Bentz, and Stutzman for characterization of the effect of curing conditions and alkalis on microstructure development of cement-based materials ((Snyder & Bentz 2004), (Bentz & Stutzman Submitted 2005), (Bentz Submitted 2005)).
The well-defined peaks observed on cooling curves for cement-based materials may not only be due to the existence of threshold diameters. Recent investigations by proton NMR (McDonald et al. 2005) have indicated that in some cement-based systems the porosity seems to consist of a series of pores of discrete sizes. To investigate this further, correlated

studies of proton NMR and other methods for characterization of porosity are in progress within the framework of Nanocem (Nanocem n.d.).
To avoid the effect of supercooling and hysteresis between cooling and heating curves, Fagerlund (Fagerlund 1973) recommended, in accordance with (Powers & Brownyard 1947), specimens be frozen to at least -50°C before test, and that the test is performed as a thawing test.
When performing LTC, heat flow to and from a (partly) saturated porous material is measured during controlled cooling and heating, typically between 20°C and -55°C. From the resulting heat flow curves the amount of ice formed or melted at a given temperature can be calculated. This information may be used to estimate threshold pore sizes or the pore size distribution in the material by means of the Gibbs-Thomson equation, see e.g. (Fagerlund 1973), (Villadsen 1992), (Valkenborg et al. 2002). However, the use of LTC and the Gibbs-Thomson equation for quantification of pore size (distribution) is based on several questionable assumptions, see e.g. (Fagerlund 1973), (Sellevold & Bager 1980)

1. Pores are cylindrical
2. Interfacial energy of the liquid-ice interface can be used to quantify the chemical energy of the solution
3. No liquid transport to the surface or larger pores takes place during freezing
4. The freezing point depression caused by dissolved ions is negligible
5. Temperature equilibrium is obtained between reference block and sample

   and for pore size distribution estimations from cooling curves also:

6. Supercooling (including the so-called ink-bottle effect) does not take place

The purpose of the present paper is to investigate the effect on LTC results of selected factors and phenomena. These factors and phenomena are super-cooling, transport of liquid, dissolved ions, and thermal non-equilibrium between reference block and sample. For this purpose LTC has been undertaken on simple model materials; water, a salt solution for which a phase diagram is available, and an artificial pore solution, as well as on a solid with mono-sized pores saturated with water or the salt solution.
The possible effect of cracking of the porous material, see e.g. (Scherer & Valenza II 2004), (Sellevold & Radjy 1976), on LTC results is not treated in the present paper. However, especially when investigating the connectivity of pores, possible effects of cracking during freezing should be considered.

2 Experimental

SilicaV432 from Grace Davison, Germany, was selected for the present study. According to the producer, the silica contains pores with a diameter of 14 nm and has a pore volume

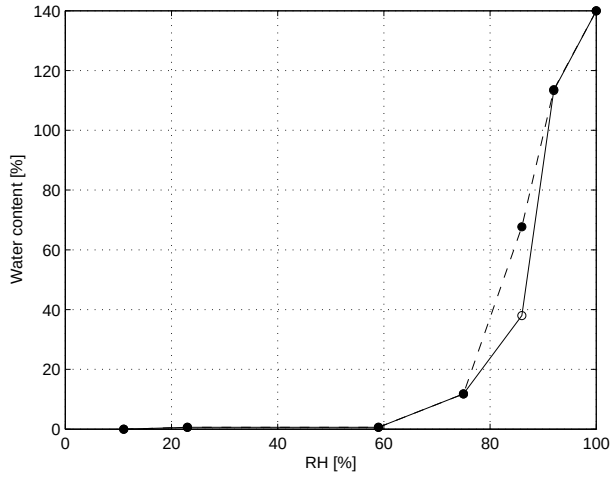

Figure 1: Water absorption (○) and desorption (●) isotherm for the porous model material, SilicaV432

Table 1: Salt concentrations in the artificial pore solution (Kjeldsen et al. 2004)

Salt	$CaSO_4{\cdot}2H_2O$	Na_2SO_4	NaOH
g/L	2.07	12.50	2.92

of 1.05 cm^3/g, a specific surface area between 285 and 355 m^2/g (determined by N_2-sorption and BET analysis), and a particle size of approximately 1 mm. Distilled water sorption isotherms were measured at 20°C to further characterize the material, see figure 1.

Three liquids were used; distilled water, distilled water with 10 weight-% NaCl (99% pure from Baker), and an artificial pore solution made from distilled water and salts in the concentrations given in table 1. Dr. Yves Houst (EPFL) proposed to replace potassium ions by sodium, minimizing the risk of supersaturation and following precipitation, without affecting the ionic strength of the solution. An overview of the experiments is given in table 2. When the porous model material was used, the dry sample size was between 0.4 and 1.2 g, containing about 250% water. When liquids only were tested, about 1 g was used, except for the artificial pore solution where 11 g were used. All experiments were made in doublets, except the measurements at high freezing rate and with the artificial pore solution, where only one experiment was carried out of each. No doublet experiments showed deviation from each other.

Table 2: Material combinations and cooling/heating rates

	H_2O			H_2O+ 10% NaCl	Artificial pore solution, see table 1
Rate	-1.2°C/h +1.2°C/h	-3.3°C/h +4.1°C/h	-15°C/h +15°C/h	-3.3°C/h +4.1°C/h	-3.3°C/h +4.1°C/h
pure liquid	x	x	-	x	x
saturated silica	x	x	x	x	

The silica was saturated prior to testing by applying 33 mbar for four hours to the silica covered by the liquid followed by 18 hours at atmospheric pressure. Excess liquid was removed by filtering at atmospheric pressure. As can be seen from the heat flow curves in e.g. figure 8, a measurable amount of bulk water was present after this process, indicating that the silica carried excess water.
LTC was undertaken in a Low Temperature Calvet Micro Calorimeter, model "-196°C to 200°C", from Setaram. The calorimeter is described in e.g. (Fontenay & Sellevold 1980), (Bager 1984). Temperature cycles were made between +20°C and -50°C. According to (Fontenay & Sellevold 1980) little ice forms below -55°C. The cooling and heating rates are given in table 2. As nucleation agent, approximately 0.005 g silver iodide was sprinkled onto each sample prior to cooling.

3 Results and discussion

All data given in the following are for single experiments, as repetitions showed no significant variability in the results. The heat flow is given as apparent heat capacity; the method of calculation of ice formation and melting from heat flow curves is described in e.g. (Fontenay & Sellevold 1980). The measured temperatures are temperatures registered in the reference block. Testing samples of cement paste and mortar samples with a size of ø15 mm × 70 mm Fontenay and Sellevold (Fontenay & Sellevold 1980) and Sellevold and Bager (Sellevold & Bager 1980) found that the difference between sample temperature and reference block is typically between 0.4°C and 0.8°C during heating at 4.1°C/h and cooling at -3.3°C/h, but can be up to several degrees when concentrated freezing and thawing takes place.

3.1 Freezing of bulk water

When the temperature rises just above 0°C, melting of ice will occur. However, for ice to form from pure water, the temperature must drop to about -30°C (Weeks & Ackley 1986). This phenomenon is called supercooling and is caused by the lack of nucleation sites. In most cases, the supercooling of water is fairly small due to the presence of impurities. Substrates that mimic the structure of ice facilitate the initiation of ice growth and limit

supercooling. Silver iodide or any biological material are well functioning nucleation agents for ice growth (Weeks & Ackley 1986), (Scherer 2003).
The measured heat flow from bulk water as a function of temperature is shown in figure 2. An increased cooling rate caused a slightly larger supercooling, even though a nucleation agent was used. Melting began between 0.3°C and 1.5°C from the freezing point of bulk water. Furthermore, as melting takes time and the temperature continuously changes in the calorimeter, equilibrium is not obtained and some of the ice apparently melts at higher temperatures. As found by Bager and Sellevold (Bager & Sellevold 1986) lower rates decrease the width of the peak. If equilibrium between the reference block and the water sample was obtained and no supercooling took place, each peak should be a vertical line at 0°C.

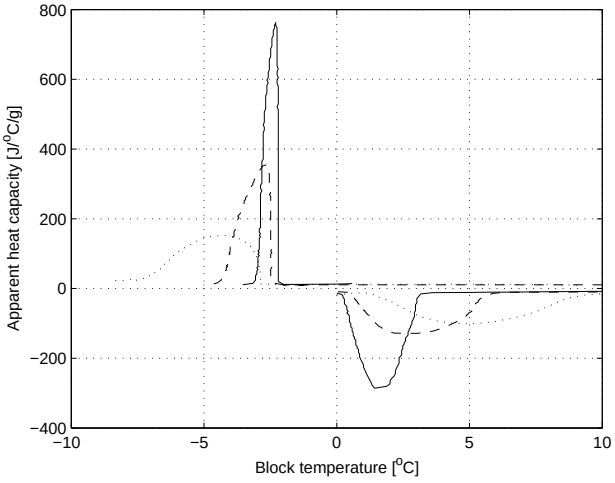

Figure 2: Heat flow from bulk water (given as apparent heat capacity) as a function of block temperature. Cooling and heating rates:- ± 1.2°C/h, - - ± 3.3°C/h, · · ± 15°C/h

The effect of heating rate on the temperature at peak start and peak maximum is illustrated in figure 3 for all three melting rates investigated. Assuming the temperature at peak maximum to be 0°C for a melting rate of 0°C/h, the temperature at peak maximum seems have a power function variation with melting rate. This is not observed for the temperature at peak start. At present the temperature dependency has not been explained but could be due to kinetics of ice growth (Bentz Submitted 2005).

Sub conclusions
Based on the above, the following can be concluded;

A Bulk water supercooling is in practice unavoidable, even with the addition of a nucle-

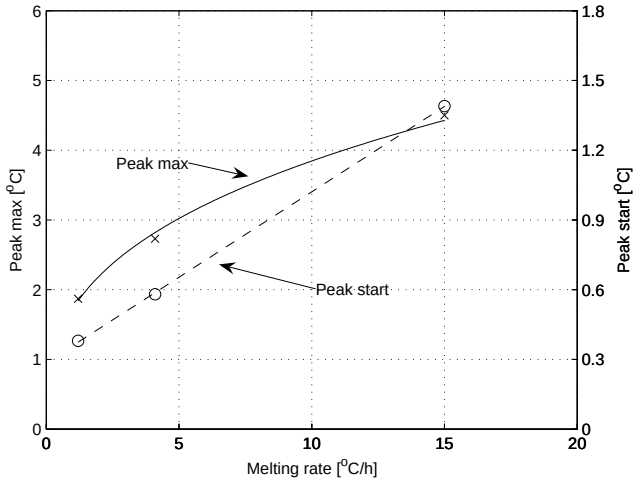

Figure 3: Temperature at peak start (∘ - right ordinate) and at peak maximum (× - left ordinate) of the bulk ice melting as a function of heating rate (approximately 1-3 g water)

ation agent.

B Due to a constant rate of temperature change, equilibrium between reference block and sample is for the investigated sample size (1 g liquid) not obtained during cooling and heating, indicated by a certain width of the peaks for pure water. The lower the cooling and heating rate, the more narrow peaks are obtained.

3.2 Effect of dissolved salts

If ions are present in the water, the freezing point is depressed below that of pure water. The freezing point depression can be estimated based on a combination of Raoults law and the Clapeyron equation (Castellan 1970). Furthermore, during freezing of a salt solution, ice formation will cause an increased salinity of the remaining solution due to ions being expelled from the ice front, see e.g. (Weeks & Ackley 1986), (Wang et al. 1996). The amount of ice to be formed as a function of temperature can be estimated based on phase diagrams, if available.
In figure 4, the phase diagram for the sodium chloride and water system is shown. For a 10% aqueous sodium chloride solution freezing will start around -8°C. It is seen that with decreasing temperature the salinity increases in the remaining solution from 10% to about 22%, when the temperature reaches -21°C. If the temperature is decreased beyond this point $NaCl{\cdot}2H_2O$ will precipitate (Weeks & Ackley 1986).
For bulk solutions it has been found that when sufficient ice has formed, small pockets

of brine will be encapsulated in the pure ice. The size of these pockets will gradually decrease with temperature until precipitated salt is trapped in the pure water ice (Weeks & Ackley 1986).

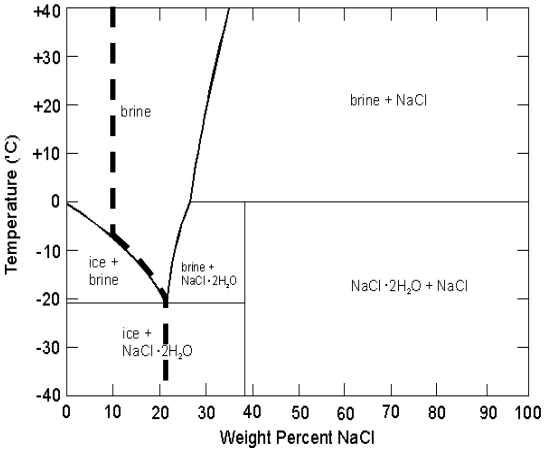

Figure 4: Phase diagram for the sodium chloride and water system. The thick line is explained in the text. (Weeks and Ackley 1986)

The heat flow curves for the 10 weight-% NaCl solution are shown in figure 5. For comparison, the heat flow curves for pure water are also shown. It should be recalled that the temperature given is the temperature of the reference block, and that the temperature of the sample should be expected to be up to 2°C behind. From the cooling curve it is observed that initial freezing of the salt solution starts around -8°C. The temperature at peak start indicates that supercooling does not occur. However, the shape of the peak indicates super-cooling. A second peak starts at -26°C. The discrepancy between the -21°C given in the phase diagram and the -26°C found experimentally may be explained by either 1) a form of supercooling; in this case due to the fact that a nucleus resembling the shape of the salt crystal is missing, or 2) the small pockets of brine encapsulated in the pure water ice (mentioned previously) acting as small pores and causing an additional freezing point depression (Nestle 2005). During heating, melting begins at -22°C and finalizes at -4°C. The latter can be explained by a combination of gradual melting of ice and non-equilibrium.
The amounts of ice formed during cooling and melted during heating are in figure 6 compared to amounts estimated from the phase diagram in figure 4. Except for the differences in temperatures discussed above, the measured data correlate well with data obtained from the phase diagram.
Measurements of the less concentrated solution, the artificial pore solution, which resembles a fresh paste pore liquid, are shown in figure 7. During freezing, three peaks are

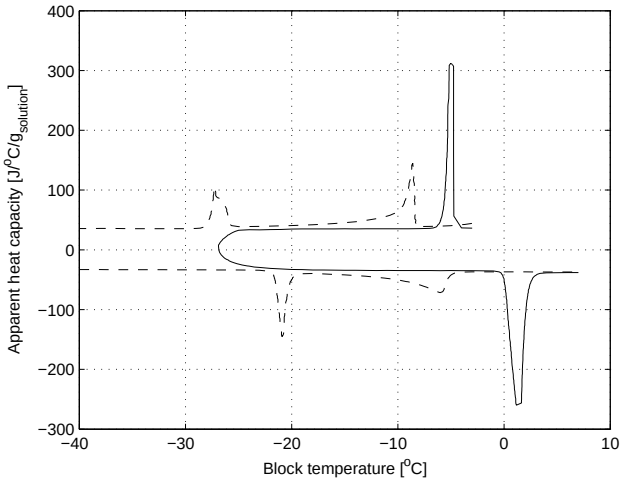

Figure 5: Heat flow (given as apparent heat capacity) as a function of block temperature. − Bulk water and −− 10 weight-% NaCl solution. Cooling and heating rates -3.3°C/h and +4.1°C/h.

observed, two of which are superimposed around -7°C. The third freezing peak occurs at -47°C. As no phase diagram exists for this solution, it is not possible to calculate the expected phase transformation temperatures. During melting only two peaks are observed. This is probably because two of the peaks are fully superimposed by one another. Furthermore, the melting begins around -3°C, indicating that even in this rather dilute solution the ions cause a measurable melting point depression of the ice in the vicinity of the deposits of ions. Due to a larger sample size (10 g vs. approximately 1 g) the heat flow curves for the artificial pore solution should not be directly compared to the heat flow of the other samples tested. A larger sample size is likely to decrease the amount of supercooling due to higher risk of impurities facilitating heterogeneous nucleation, as well as increase the equilibrium time.

Sub conclusions

Based on the above the following can be concluded;

C During cooling ice is gradually formed from a salt solution. This is explained by ions being expelled from the ice front causing an increased ion concentration and freezing point depression of the remaining solution.

D Even a relatively low ion concentration, resembling that of the pore liquid in fresh cement-paste, affects the position and the width of the peaks as well as introduces

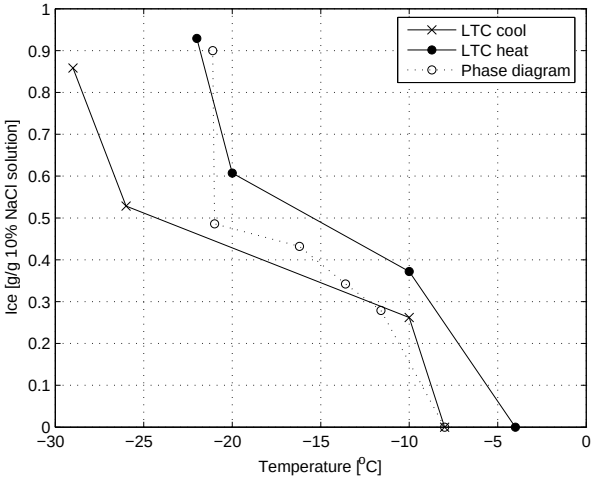

Figure 6: Estimated (from phase diagram, figure 4) and measured (from LTC, figure 5) ice formation during cooling and heating of the 10 weight-% NaCl solution.

additional peaks.

E The amount of ice formed can be estimated from phase diagrams, if available.

3.3 Effect of pores

According to Feldman (Feldman 1970) a solid meniscus exists between liquid and ice in capillary condensed liquids at subfreezing temperatures. The curvature of the meniscus lowers the free energy of the pore liquid and induces a freezing point depression.
This effect can be quantified by use of the Gibbs-Thomson equation (see e.g. (Tombari et al. 2005)). The equation describes the connection between the so-called Kelvin radius of the pore, r_K [m], and the freezing point depression, $T = T - T_0$;

$$r_K = -\frac{2 \cdot M \cdot \sigma_{l-s}}{\Delta H_{fus} \cdot \rho_l \cdot ln\left(\frac{T}{T_0}\right)} \tag{1}$$

where M is molar mass of the liquid [kg/mole], σ_{l-s} is the interfacial energy between liquid and solid [N/m], ΔH_{fus} is the heat of fusion [J/mole], ρ_l is the density of the liquid [kg/m^3], and T_0 and T are the freezing temperature of the bulk liquid and the pore liquid [K].

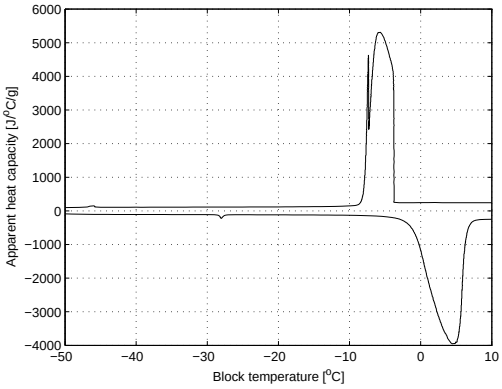

(a)

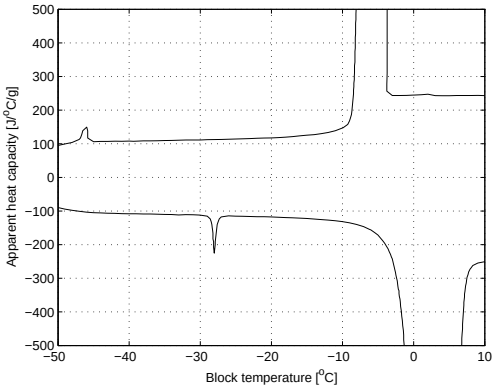

(b) Zoomed section of figure 7a

Figure 7: Heat flow from the artificial pore solution (given as apparent heat capacity) as a function of block temperature.

The heat of fusion of water is temperature dependent and e.g. given by (Fontenay & Sellevold 1980) as:

$$\Delta H_{fus} = 6012 + 40(T - T_0) \qquad [J/mole] \tag{2}$$

The temperature dependency of the density of water and the interfacial energy of water and ice have been given in (Fagerlund 1973) as;

$$\rho_l = 1000 - 0.26 \cdot \Delta T \qquad [kg/m^3] \tag{3}$$

$$\sigma_{s-l} = 30.5(1 - 0.93 \cdot 10^{-2}\Delta T) \cdot 10^{-3} \qquad [N/m] \tag{4}$$

The Gibbs-Thomson equation is based on the assumptions of ice in contact with water, cylindrical pores (which is usually the case in indirect pore size characterization), and an even freezing front. Experiments using a directional solidification technique indicate the assumption of an even meniscus between the solid and liquid in the pore being reasonable for a pure water/ice interface (Wang et al. 1996). However, in the same paper it was also shown that when the liquid is a salt solution the interface is not smooth, but highly spiked, and the ice crystals grow, side by side, separated by small non-frozen areas. The altered freezing front shape might induce a change of the chemical energy of the solution. As mentioned in Section 3.1, the rate of cooling and heating affects the measured heat flow. Figure 8 shows the effect of cooling and heating rate on the heat flow during cooling and heating for the porous model material saturated with distilled water.

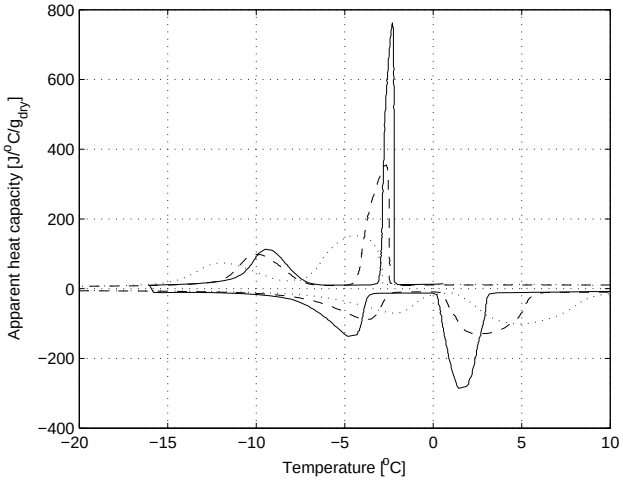

Figure 8: Heat flow (given as apparent heat capacity) as a function of temperature. Silica and water. - ± 1.2°C/h, —— -3.3°C/h, +4.1°C/h, and · · ± 15°C/h.

Two peaks are present in each curve. The first peak is due to freezing of the bulk water, which is present between the particles. The second represents freezing of the water in the pores. In the literature (e.g. (Sellevold & Bager 1980), (Snyder & Bentz 2004)) the

Table 3: Temperature at peak maximum of melting peak (Corrected = Measured - ΔT_B)

	Rate	1.2°C/h	4.1°C/h	15.0°C/h
Bulk	ΔT_B (from fig.8)	1.9°C	2.7°C	4.5°C
Pore	Measured (from fig.8)	-4.8°C	-4.0°C	-2.1°C
Pore	Corrected	-6.7°C	-6.7°C	-6.6°C

peak value has been used to estimate pore size. However, it may be argued that the temperatures where freezing and melting begin most accurately reflect the maximum and minimum pore size, respectively.

As previously mentioned, there is a discrepancy between the block temperature measured and the temperature the sample freezes and melts at; the larger the rate of freezing and melting, the larger is the discrepancy, see figure 3 and figure 8. Based on the observed difference between the melting temperature of bulk water in equilibrium (0°C) and the measured melting peak maximum, ΔT_B, the melting temperature at peak maximum of the pore water can be corrected. Measured and corrected temperatures at the maximum of the melting peaks are given in table 3. The applied correction seems to be valid, as the corrected temperature at peak maximum is not affected by the rate of heating. The correlation will of course only reflect samples where the water content is similar to the current (i.e. about 1 g), and the heat capacity and thermal conductivity of the sample are similar. A larger amount of water will facilitate greater discrepancy than recorded here, due to increasing equilibration times.

Using the procedure described above for correction for non-equilibrium during melting, the estimated amount of ice melting as given in figure 6, has also been corrected. The results are shown in figure 9, where an improved correlation between cooling, heating, and the calculated curve can be observed.

The temperature at peak maximum is assumed to reflect the mean pore size, whereas the initial melting temperature is assumed to reflect the minimum pore size (maximum if cooling curve). Based on the equations (1)-(4), the pore sizes have been calculated from the corrected temperature at peak maximum and for the temperature at pore peak starting around -11°C. The same procedure should not be carried out on the cooling results, however, as supercooling strongly influences the initial freezing temperature and the amount of supercooling is random and thus unquantifiable. The properties of water used are: $T_0 = 273.2$°K, and M=0.018 kg/mole. Furthermore, a non- freezable adsorbed layer thickness of 6 Å (2 layers of water molecules of 3Å each) is assumed (Schreiber et al. 2001). The results of the calculations are shown in table 4;

Measurements of dilatation of saturated porous materials during freezing have been reported in several papers (see e.g. (Scherer & Valenza II 2004), (Sellevold & Radjy 1976), (Litvan 1972)). The investigations showed a volume decrease during freezing, which was interpreted as desorption of water from the pores to the bulk. Higher cooling rates should thus produce higher amounts of water remaining in the pores due to limitations of transport.

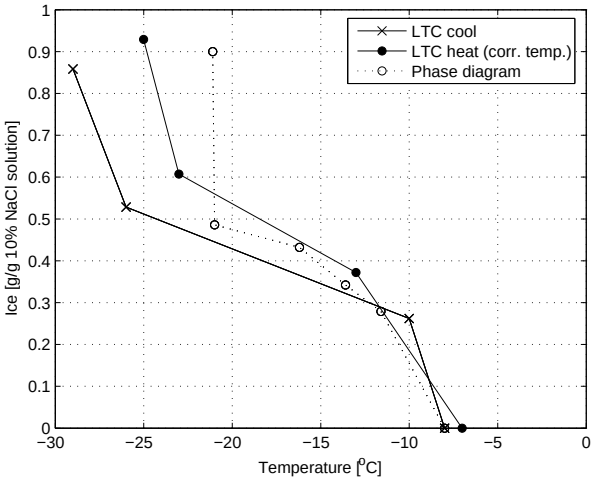

Figure 9: Estimated amount of ice melted, data from Fig. 6 corrected according to table 3.

Table 4: Calculated pore sizes of the porous model material

	Temperature °C	Pore size nm
Peak start (not corrected)	-11.0	10
Peak maximum (corrected value from table 3)	-6.7	16

To investigate the effect of cooling rate on water transport, the amount of ice formed in the bulk liquid and the pore liquid, respectively, has been calculated for the three cooling and heating rates, using the data given in figure 8. The amount of non-freezable water has been estimated by subtracting the measured amount of frozen water in the pores (w_{fp}) and bulk water (w_b) from the measured total amount of water as well as by multiplying an adsorption layer thickness (t) with the specific surface area (S_{BET}). The equations are shown below, and the results are given in table 5 nd table 6.

$$w_{nf} = w_{tot} - w_{fp} - w_b \tag{5}$$

$$w_{nf} = S_{BET} \cdot t \tag{6}$$

Table 5: Amounts of freezable and non-freezable water [g/g_{dry}] based on heat flow curves given in figure 8

		(i) Measured (LTC) amount of bulk water, w_b	(ii) Measured (LTC) amount of freezable pore water, w_{fp}	(iii) Measured total amount of water, w_{tot}	(iv) Non-freezable water, w_{nf} (from eq.(5))
Cooling	-15°C/h	1.43	0.92	2.49	0.14
	-3.3°C/h	1.39	0.87	2.43	0.17
	-1.2°C/h	1.40	0.88	2.50	0.22
Heating	+15°C/h	1.37	0.98	2.49	0.14
	+4.1°C/h	1.34	0.97	2.43	0.12
	+1.2°C/h	1.38	0.88	2.50	0.23

Table 6: Amounts of freezable and non-freezable water [g/g_{dry}] based on heat flow curves given in figure 8

		(v) Estimated non-freezable water, w_{nf} from (eq.(6))	(vi) Total pore volume $w_{pt} = w_{fp} + w_{nf}$	(vii) Total pore volume given by supplier, ml/g
Cooling	-15°C/h	0.17-0.32	1.06	1.05
	-3.3°C/h		1.04	
	-1.2°C/h		1.10	
Heating	+15°C/h	0.17-0.32	1.12	1.05
	+4.1°C/h		1.09	
	+1.2°C/h		1.11	

The total amount of water in the samples (column iii) was not constant, probably due to varying amounts of excess water. Accordingly, the measured amount of bulk water (column i) should not be compared.
Column ii shows the measured amount of freezable pore water. Only limited differences are observed between data obtained during cooling and heating.
The estimated amount of non-freezable water is given in column v. The minimum and a maximum value correspond to two water molecule layers and a specific surface area at 285 m^2/g and three water molecule layers and a specific surface area at 355 m^2/g, respectively. The measured amounts of non-freezable water (column iv) are slightly lower than estimated values for the high cooling and heating rates indicating some water transport, but not for the low cooling rate, assumed to facilitate transport.
The sum of columns ii and iv is the measured total pore volume (column vi). As the measured values show no major deviation from the pore volume given by the supplier (1.05 ml/g, column vii), it is assumed that only minor water transport takes place during any of the cooling rates tested. Fontenay and Sellevold (Fontenay & Sellevold 1980) obtained similar conclusions based on LTC on cement pastes.

Sub conclusions
Based on the above the following can be concluded;

F Freezing of a water-saturated monosized porous material, results in two peaks; a bulk liquid peak and a pore liquid peak.

G The temperature at peak maximum is assumed to reflect the mean pore size, whereas the initial melting temperature is assumed to reflect the minimum pore size (maximum pore size if cooling curve is used)

H Only limited water transport seems to take place in the investigated material at the cooling and heating rates applied.

3.4 Combined effect of pores and ions

Combining the above-described effects of pores and ions should give four peaks on the heat flow curves for the silica saturated with the aqueous 10% NaCl solution; 1) a peak for the bulk liquid, 2) a peak for the precipitation of $NaCl \cdot 2H_2O$ in the bulk liquid, 3) a peak for the initiation of freezing within the pores, and finally 4) a peak for the precipitation of salt within the pores. The experimental results are shown in figure 10. Contrary to expectations only three peaks are seen. However, the peaks are not well defined and the expected 2nd and 3rd peaks are presumably both contributing to the middle peak.
The first freezing peak starts at around -8°C, as anticipated from the phase diagram. The second peak is the combination of the bulk precipitation at around -21°C, and the initial freezing of the pore liquid. The latter is assumed to occur around -15°C (sum of freezing point depression of 8°C from the phase diagram (figure 4) and approximately 7°C from the pore size (table 3). Assuming -15°C as the freezing point of the pore liquid, the

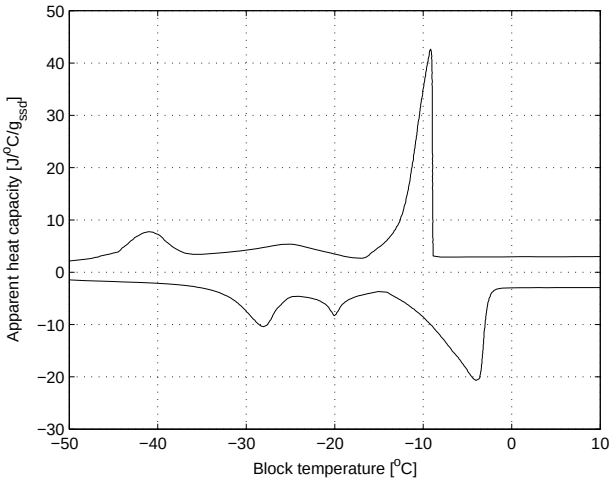

Figure 10: Heat flow (given as apparent heat capacity) as a function of temperature. Silica with an aqueous 10% NaCl solution.

precipitation within the pore should begin around -36°C, which corresponds well to the experimental results. A similar conclusion can be made for peak at the lowest temperature on the melting curve.
For saturated systems cracking is to be expected (Fontenay & Sellevold 1980). The mechanism has been treated in e.g. (Scherer & Valenza II 2004) and (Sellevold & Radjy 1976). Cracking during freezing may change the connectivity of the pore system and may thus affect the position of heat flow peaks observed during cooling. This effect has, however, not been dealt with in this paper.

Sub conclusions
Based on the above the following can be concluded;

I The combination of pores and ions results in complicated heat flow curves.

J For a mono-sized porous material, the resulting peaks can be explained and the pore size may be estimated taking into account the freezing point depression induced by the liquid used.

3.5 Cement-based materials

When cement reacts with water, the resulting pore sizes are manifold and the pore liquid contains a number of different ions. In addition, bulk liquid may be present on the surface

of the sample.
Dissolved ions present in a cement paste pore liquid will in general cause an initial freezing point depression at 1 to 2°C. However, as mentioned in Section 3.2, the concentration of ions, and thus the freezing point depression, increases with ice formation. This effect complicates the assessment of results from LTC on porous materials with ill-defined pore liquids.
As cement in itself does not act as a nucleation agent, such should be added, e.g. silver iodide. Freezing will initiate where the nucleation agent has been placed on the surface of the sample and propagate through the sample. For cement-based materials, where larger pores are likely to be connected to the surface through smaller pores, the propagation of ice from the surface causes, as mentioned in the introduction, ice formation to take place at intervals. Upon reaching the temperature corresponding to the freezing point of the liquid in the small pore, ice will almost simultaneously form throughout all the larger pores connected through this pore. This is reflected in the heat flow curves, obtained during cooling of cement paste, see figure 11. For the actual sample, three peaks characterizing the sample and a fourth peak at approximately −4°C corresponding to bulk liquid were obtained.

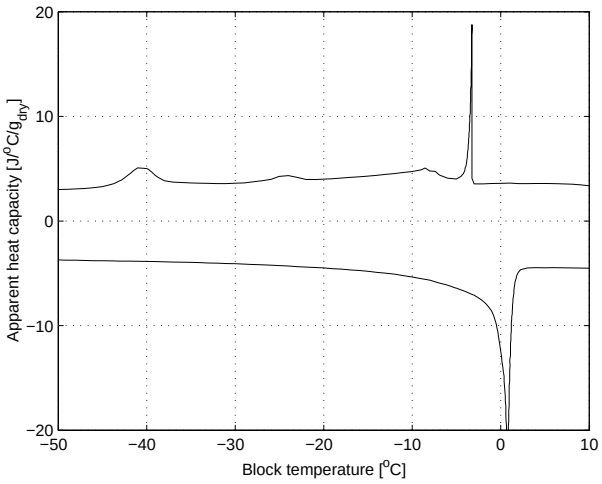

Figure 11: Heat flow (Heat flow (given as apparent heat capacity) as a function of temperature. Cement paste, w/c=0.5 after 75 days of hydration at 15°C (Kjeldsen 2003).

Compared to the heating curve for the (almost) monosized model material saturated with the salt solution (figure 10) the heat flow curve for cement paste (figure 11) seems to represent the manifold pore sizes in cement-based materials. During heating, the effect of threshold pores ("bottle necks") vanishes, as melting can occur, irrespective of the

connectivity. However, the ions in the pores will cause some melting in their vicinity prior to the melting point dictated by the pore size. According to (Kirkpatrick 2005) it is likely that ions accumulate in the structured layers of water on the tobormorite-like hydrates (C-S-H); the ions will thus be well distributed in the paste. Thus, the melting of the liquid is expected gradually to take place. Finally, lack of thermal equilibrium causes the apparent melting temperature to be higher then the actual.

3.6 Recommendations for LTC on cement-based materials

Based on the above it is proposed LTC might be used for characterization of porosity of cement-based materials. A nucleation agent, e.g. silver iodide, should be added to limit supercooling. The connectivity of pores may be characterized based on cooling curves (initiation of peak), whereas the pore size distribution may be characterized based on the heating curve. In the latter case cooling should be undertaken at a high rate to limit migration of water, whereas heating should be undertaken at a low rate to limit the effect of non-equilibrium.
The Gibbs-Thomson equation might be used to describe the correlation between melting point and pore size. However, the measured temperature should be corrected for non-equilibrium between the sample and the reference block. For approximately 1 g ice and heating rates between 1.2 and 15°C/h the peak temperature at melting can be corrected according to the empirical equation;

$$T_{Corr} = 1.7 \left(\frac{\Delta T}{\Delta t} \right)^{0.35} \tag{7}$$

Due to the varying pore size distribution as well as accumulated ions in cement-based materials the ice will melt gradually. Thus, the correction given in equation (7) corresponds to the worst case.
Furthermore, corrections are recommended for the effect on the freezing (melting) point depression of the varying ion concentration in the non-frozen part of the pore solution.
Finally, LTC results should always be supported by measurement of total evaporable water content, and especially when investigating the connectivity of pores, possible effects of cracking during freezing should be considered.

4 Conclusions

Supercooling, general lack of equilibrium, bottle neck pores, and ions being expelled during freezing make assessment of heat flow curves from heating and cooling of cement-based materials a delicate matter.
Nevertheless, it is proposed LTC be used more for characterization of porosity of cement-based materials. The connectivity of pores may be characterized based on cooling curves, whereas the pore size distribution may be characterized based on the heating curve. The

Gibbs-Thomson equation might be used to describe the correlation between freezing (or melting) point and the (capillary) pore size. The measured temperature is proposed corrected for non-equilibrium between the sample and the reference block. Furthermore, corrections should be made for the effect on the freezing point depression of the varying ion concentration in the non-frozen part of the pore solution.

5 Acknowledgements

The authors would like to than Lizzy, Alfred og Valdemar Taumose's Foundation for their financial support. Dale Bentz (NIST) is kindly thanked for his valuable comments to this paper. Graduate student Martin N. Olsen is thanked for his assistance undertaking LTC. Emmanuel Gallucci (EPFL, Switzerland) is thanked for translation of the abstract.

References

Bager, D. (1984), Ice formation in hardened cement paste, Technical Report 141/84, Technical University of Denmark.

Bager, D. & Sellevold, E. (1986), 'Ice formation in hardened cement paste, part i - room temperature cured pastes', *Cement and Concrete Research* **16**.

Bentz, D. (Submitted 2005), 'Lithium, potassium, and sodium additions to cement pastes', *Advances in Cement Research* .

Bentz, D. & Stutzman, P. E. (Submitted 2005), 'Curing, hydration, and microstructure of cement paste', *ACI Materials Journal* .

Brun, M., Lallemand, A., Quinson, J.-F., & Eyroud, C. (1977), 'A new method for the simultanious determination of the size and the shape of pores: the thermoporometry', *Thermochimica Acta* **21**, 59–88.

Castellan, G. (1970), *Physical Chemistry*, Addison-Wesley Publishing Company.

Fagerlund, G. (1973), 'Determination of pore-size distribution from freezing-point depression', *Materials and Structures* **33**(6), 215–225.

Feldman, R. (1970), 'Length change-adsorption relations for the water-porous glass system to $-40°c$', *Canad. J. of Chem.* **48**, 287–297.

Fontenay, le sage de, C. & Sellevold, E. (1980), Ice formation in hardened cement pastes - i. mature water-saturated pastes, *in* 'Durability of Building Materials and Components', ASTM STP 691, pp. 425–454.

Kirkpatrick, J. (2005), Private discussion.

Litvan, G. (1972), 'Phase transitions of adsorbates. iii. heat effects and dimensional changes in nonequilibrium temperature cycles', *Colloid and Interface Science* **38**, 75–83.

McDonald, P., Mitchell, J., Mulheron, M., Aptaker, P., Korb, J.-P. & Monteilhet, L. (2005), 2-d correlation relaxomatry experiments of cement pastes performed using a new one-sided nmr magnet, *in* 'Proceedings, Cementitious materials as model porous media: Nanostructure and transport processes', Switzerland.

Nanocem (n.d.), 'webpage'.

Nestle, N. (2005), Private communication. TU Damstadt, Germany.

Powers, T. & Brownyard, T. (1947), 'Studies of the physical properties of hardened portland cement paste', *American Concrete Institute* **8**(18).

Scherer, G. (2003), Private communication. Princeton University.

Scherer, G. & Valenza II, J. (2004), *Materials Science of Concrete*, Vol. VII, American Ceramic Society, chapter Mechanisms of Frost Damage.

Schreiber, A., Ketelsen, I. & Findenegg, G. (2001), 'Melting and freezing of water in ordered mesoporous silica materials', *Phys. Chem. Chem. Phys.* **3**, 1185–1195.

Sellevold, E. & Bager, D. (1980), Low temperature calorimetry as a pore structure probe, *in* '7th International Congress on the Chemistry of Cement', Vol. 4, Paris.

Sellevold, E. & Radjy, F. (1976), 'Low temperature dynamic mechanical response of porous vycor glass as a function of moisture content - part 1: The capillary transition', *Materials Science* pp. 1927–1938.

Snyder, K. & Bentz, D. (2004), 'Suspended hydration and loss of freezable water in cement pastes exposed to 90% relative humidity', *Cement and Concrete Research* **34**, 2045–2056.

Tombari, E., Salvetti, G., Farrari, G., & Johari, G. (2005), 'Thermodynamic functions of water and ice confined to 2 nm radius pores', *Chemical Physics* **122**.

Valkenborg, R., Pel, L., & Kopinga, K. (2002), 'Combined nmr cryoporometry and relaxometry', *Phys.D: Appl. Phys.* **35**, 249–256.

Villadsen, J. (1992), Pore structure in cement-based materials, Technical Report 277, Technical University of Denmark.

Wang, K., Monteiro, P., Rubinsky, B. & Arav, A. (1996), 'Microscopic study of ice propagation in concrete', *ACI Matr. Jour.* **4**(93), 370–377.

Weeks, W. & Ackley, S. (1986), *The Geophysics of Sea Ice*, NATO ASI Series, New York, chapter The growth structure and properties of sea ice, pp. 9–164.

Report no R-136
ISSN 1601-2917
ISBN 978-87-7877-207-7